An Investigation of the Running Coupling and Meson Masses in Lattice QCD

Thesis submitted in accordance with the requirements of the University of Liverpool for the degree of Doctor in Philosophy by Kieran James Sharkey

November 27, 2000

Declaration

I hereby declare that all the work described in this thesis is the result of my own research activities unless reference is given to others. None of this material has been previously submitted to this or any other University. All work was carried out in the Department of Theoretical Physics during the period October 1997 to November 2000.

Contributions from this work have been published elsewhere in:

- P. Boucaud *et al.*JHEP 0004 (2000) 006

Acknowledgements

Primarily, I would like to thank my supervisor Chris Michael for making what at one time appeared to be an impossible task into a fun and rewarding experience for me. I am indebted to him for his endless patience and genuine enthusiasm for helping me.

I would also like to thank the other members of the theoretical physics department at Liverpool, each of whom has helped me in some way or another during my time here and who have made this a pleasant place to work. In particular, thanks go to Tim Jones.

Of my fellow students, I particularly thank Simon for putting up with me for so long and for his support and friendship. Thanks also go to Chris, Jude, David and Roz for more of the same.

Outside of the department, I mostly wish to thank my parents for their unconditional love help and support in everything I do and have ever done. I also thank my sister Sarah and grandparents for more of the same. I only wish they had all lived to see me complete this.

I thank my friends outside of university, particularly Paul and Steven(Stoat) for reminding me that there is more to life than physics, and for being there over the years.

Finally, I thank Liz for her love and support and for not giving up on me.

Abstract

We investigate a lattice determination of the running coupling defined in the $\widetilde{MOM}$ scheme to see if it is consistent with a power correction to the perturbative formula.

We attempt a lattice determination of the masses of the a_0, a_1 and b_1 flavour nonsinglet mesons.

We then consider the mass differences between flavour singlet and nonsinglet mesons in the cases of the π, ρ, a_1 and b_1 mesons.

Finally, we investigate the pion decay constant f_π using both quenched and unquenched lattice data.

Contents

Chapter 1

Introduction

1.1 A Brief Summary of QCD

Quantum chromodynamics (QCD) arose as a result of efforts to explain the strong nuclear interactions by analogy with the very successful quantum field theory of electrodynamics (QED). The strong nuclear force is not, as was first thought, fundamentally a force between nucleons, but rather a force between quarks that go to make up nucleons.

It was found necessary[1] to assign to quarks a new quantum number. This quantum number is known as "colour". The colour quantum number can take three values, which are conventionally called "red"(r), "green"(g) and "blue"(b). Antiquarks contain anti-colour which we denote by a bar, ie $\bar{r}, \bar{g}, \bar{b}$.

Colour is never observed directly. Any particle that we can observe which is composed of quarks is therefore a colour singlet. In the quark model of hadrons[2], particles are either made up of a red, blue and a green quark (called baryons), or are composed of a quark and an anti-quark (which has anti-colour) called mesons. In the quark model, we describe the change from one colour to another as an exchange of a "gluon". For example a red quark can change to a green quark by exchange of a $\bar{r}g$ gluon. The anti-red part $\bar{r}$ cancels the red quark's colour and the g part gives it the green colour. There are eight gluons, each one corresponding to the way in which a quark colour can be changed to another (eg red to blue , or green to red etc). The quark model was quite successful in classifying the multitude of hadrons, but is too simplistic. A proper understanding of hadrons requires QCD.

Since colour is not observed, transforming the colours into each other in a unitary fashion will cause no alteration to observed quantities. This transformation corresponds to an $SU(3)$ colour symmetry. To be compatible with observation, the QCD Lagrangian must be symmetric under this group transformation. By analogy with QED, we can build up the QCD Lagrangian by requiring that it be invariant under a local $SU(3)$ gauge transformation. We require that the Lagrangian remains unchanged when the colour fields are transformed into each other under $SU(3)$ in a space and time dependent manner.

In QCD the colour transformation properties of gluons are represented by the Gell-Mann matrices, which are generators of $SU(3)$. Gluons always carry a colour charge (ie there is no colour singlet gluon). This comes from the fact that QCD is built upon an $SU(3)$ gauge group which has eight generators as opposed to $U(3)$ which has nine. We choose $SU(3)$ over $U(3)$ for the simple fact that if a colour singlet gluon existed it would have been observed.

The QCD Lagrangian is:

$$L_{QCD} = -\frac{1}{4}F_a^{\mu\nu}F^a_{\mu\nu} + \sum_{i=1}^{6}\bar{\psi}_i(i\gamma^\mu D_\mu - m_i)\psi_i \tag{1.1}$$

Here, ψ_i denotes quark fields, and m_i denotes the quark masses. The i index is summed over the six quark flavours which are the up, down, strange, charm, bottom, and top. $F_a^{\mu\nu}$ is defined by:

$$F_a^{\mu\nu} = \partial^\mu A_a^\nu - \partial^\nu A_a^\mu - g f_{abc} A_b^\mu A_c^\nu \tag{1.2}$$

where A_a^ν are the gauge (or gluon) fields, f^{abc} is the totally antisymmetric tensor of rank 3 and g is the coupling constant of the interaction. The covariant derivative D_μ is designed to leave the quark fields invariant under a local $SU(3)$ gauge transformation and is defined by:

$$D_\mu\psi = (\partial_\mu + igT \cdot A_\mu)\psi \tag{1.3}$$

where T is a generator of the gauge group $SU(3)$.

In order to calculate with the theory perturbatively, it is necessary to add to the Lagrangian (Eq 1.1) the Faddeev-Popov ghost fields η_a. These are not physical particles, but they allow the integrals in the generating functional to be performed. The conventional Lagrangian used to determine the Feynman diagrams of QCD uses covariant gauge fixing and is given by[3]:

$$L = L_{QCD} - \frac{1}{2\xi}(\partial_\mu A_a^\mu)^2 + \partial_\mu \eta_a^*(\partial^\mu \eta_a + g f_{abc}\eta_b A_c^\mu) \tag{1.4}$$

Here ξ is the gauge parameter defined such that $\xi = 0$ ($\partial_\mu A^\mu_a = 0$) is the Landau gauge.

The Lagrangian contains the symmetries of the fields in the theory. To calculate physical quantities in quantum field theory, we need a method of determining the Greens functions of the theory, since these contain the information about the probabilities of events or interactions taking place. In QED, a perturbation theory was developed in which the Greens functions could be written as a power expansion in the coupling constant g. This was possible because at low energies, g is small. Unfortunately in QCD, g is large at low energies as we shall see in chapter 2. This means that the low energy behaviour of the theory is out of bounds for a perturbative analysis. This is unfortunate, because we live in the low energy region. If we want to try to predict the masses of the hadrons and mesons which we observe in our experiments, we need to find an alternative to perturbation theory.

1.2 QCD on the Lattice

In the absence of any analytical procedure for solving low energy QCD, our only hope is in some kind of computational method. Such a method was proposed by K. G. Wilson in 1974[4] and is known as lattice gauge theory. Lattice QCD is a way of regularising[1] QCD in a non-perturbative way.

[1] Regularisation is a way of making a field theory finite in a consistent fashion so that we can calculate with it. Most methods of regularisation are based in perturbation theory, and so are of no use for studying non-perturbative aspects of QCD.

The basic observation behind lattice gauge theory is the fact that since spacetime is a continuum, the Feynman path integral in a quantum field theory requires the sum of an infinite number of terms. Wilson proposed calculating the path integral on a regular lattice of points separated by a lattice spacing a. This makes the computational procedure finite and therefore potentially achievable. The amount of computation needed even on a small lattice (typically about 16^4 points) is still immense, and it is only recently that computers have become powerful enough to make this kind of calculation relevant to real QCD.

Problems with lattice QCD are numerous and awkward. Firstly, the fact that we restrict our lattice to some finite size removes any low frequency signals from existing. This leads to what are termed "finite volume effects". Also, the lattice spacing a is always going to be bigger than zero, so we can never directly calculate continuum QCD with lattice methods. This leads to worries about order a and a^2 corrections to any quantity that we calculate. A further problem is that the lattice does not possess the spherical symmetry of the continuum. This manifestly breaks the $O(3)$ rotational invariance which QCD has.

In spite of its significant problems, lattice QCD produces relevant results. Lattice theorists have found ways to quantify and deal with the apparently significant problems that arise. With ever increasing computational power, it increasingly seems to be the way forward not only for QCD but also for other field theories.

1.3 The Wilson Lattice Gauge Action

We consider a four dimensional regular lattice. This is composed of a collection of points or sites which are connected together by links. This is illustrated for a two dimensional lattice in Fig 1.1.

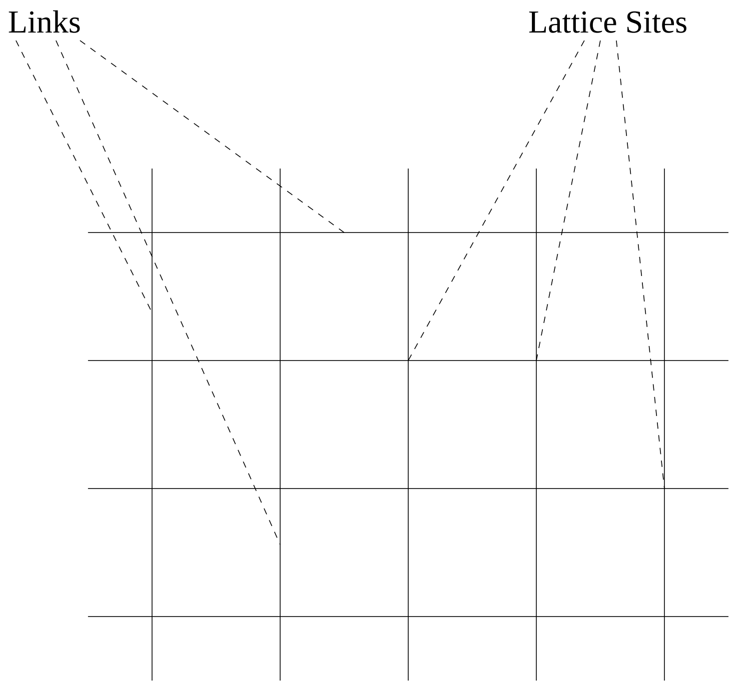

Figure 1.1: A two dimensional lattice illustrating the lattice sites and links.

In QCD, the gauge fields are defined at each point in the continuum and denoted by A_μ. Wilson recognised that in lattice gauge theory, it is necessary to associate the gauge fields with the links between lattice sites instead of with the sites themselves. We construct the parallel transporter $U_{\mu,x} \equiv U(x, x+\mu)$ which transports a vector field A from site x to a neighbouring site $x+\mu$:

$$U_{\mu,x} = P \exp ig_0 \int_x^{x+\mu} A_\mu^a(z) T_a dz^\mu \tag{1.5}$$

where P denotes a path ordered integral along the gauge link.

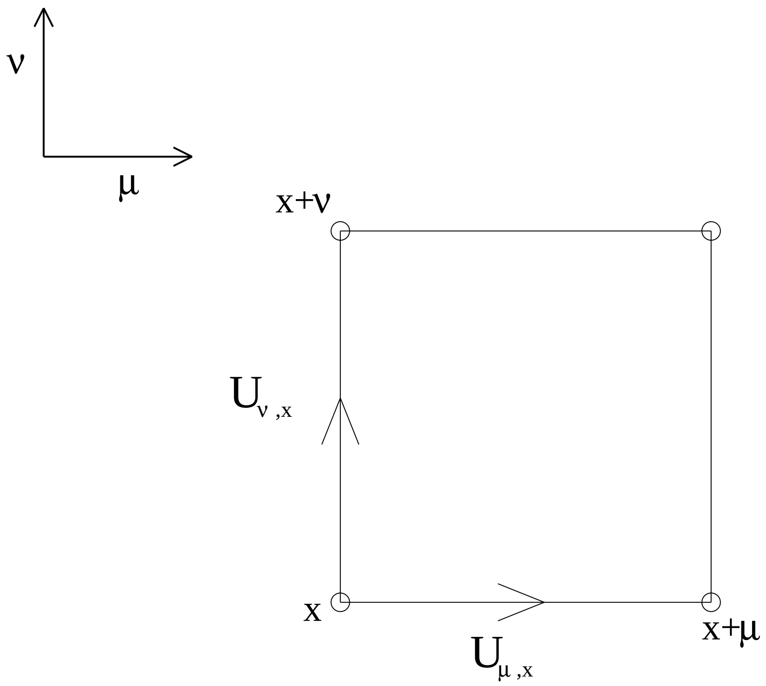

Figure 1.2: For the Wilson action, we parallel transport the gauge field A_μ around the plaquette shown. The parallel transporters U are shown for both link directions on the lattice.

We define the plaquette $\Box_{\mu\nu}$ to be the path ordered integral of the field A around an elementary square of the lattice (see Fig 1.2):

$$\Box_{\mu\nu} = U_{\mu,x} U_{\nu,x+\mu} U^\dagger_{\mu,x+\nu} U^\dagger_{\nu,x} \tag{1.6}$$

where:

$$U^\dagger_{\nu,x} \equiv U^\dagger(x, x+\nu) = U(x+\nu, x) \tag{1.7}$$

The trace of the plaquette is gauge invariant. From this we define the gauge field part of the lattice action:

$$S_G = -\frac{\beta}{3} \sum_{x,\mu>\nu} \mathrm{ReTr}\Box_{\mu\nu} \tag{1.8}$$

This action is constructed to be real and gauge invariant. It satisfies the requirement that on approaching the continuum limit ($a \to 0$), it becomes the continuum SU(3) Yang-Mills action if we define $\beta \equiv 6/g^2$ where g is the coupling constant. The gauge part of continuum QCD is recovered in the continuum limit. In fact it can be shown that the gauge part of the lattice action S_G is related to the gauge part of the continuum action (first term in Eq 1.1) S_{cont} by:

$$S_G = S_{cont} + \mathcal{O}(a^2) \tag{1.9}$$

We see that corrections to the gauge part of the continuum action go as the square of the lattice spacing.

This action is used in chapters 2 to 4 to generate data on the running coupling α_s in pure gauge QCD.

1.4 Wilson Fermions

We now need to consider how to put fermions on the lattice so as to produce a lattice version of full QCD.

The fermionic part of the continuum action is (See Eq 1.1):

$$S_F = \bar{\psi}(i\gamma^\mu D_\mu - m)\psi \tag{1.10}$$

with $D_\mu\psi$ defined as in Eq 1.3.

We define the lattice analogy of the differential $\partial\psi$ on a given lattice link as the difference between the fermion field at one end of the link ψ_x and the field at its nearest neighbour along that link $\psi_{x+\mu}$ divided by the distance a:

$$\partial_\mu \to \frac{1}{a}(\psi_{x+\mu} - \psi_x) \tag{1.11}$$

Using this in Eq 1.10 we obtain:

$$S_F(\mathrm{Latt}) = \sum_x \left(\frac{a^3}{2} \sum_{\mu=1}^{4} \bar{\psi}_x \gamma^\mu (\psi_{x+\mu} - \psi_{x-\mu}) + ma^4 \bar{\psi}_x \psi_x \right) \tag{1.12}$$

Taking the Fourier transform of the ψ field we obtain:

$$S_F(\mathrm{Latt}) = \int \frac{d^4k}{(2\pi)^4} \bar{\psi}(-k) \left(i \sum_\mu \gamma^\mu \frac{\sin(ak_\mu)}{a} + m \right) \psi(k) \tag{1.13}$$

This results in the following fermion propagator:

$$G(p) = (i\gamma_\mu \sin(p_\mu a) + ma)^{-1} = \frac{-i\gamma_\mu \sin(p_\mu a) + ma}{\sum_\mu \sin^2(p_\mu a) + m^2 a^2} \tag{1.14}$$

We associate particles with poles in the propagator at $p_0 = iE$. For the continuum propagator we have a single pole at $pa = (0,0,0,0)$, $E = \pm m$. With the lattice propagator, we not only have this pole, but also poles at $p_\mu a = \pi$. For four dimensions we have sixteen poles: $pa = (0,0,0,0)$, $(\pi,0,0,0)$, $(0,\pi,0,0)$, ..., (π,π,π,π) giving sixteen fermions. This is known as the fermion doubling problem. There are a few solutions to this problem. The one used in this thesis is Wilson's original solution. This is to add to the fermionic lattice action (Eq 1.12) the Wilson term:

$$S^W = -\frac{r}{2a} \sum_{x,\mu} \bar{\psi}_x (\psi_{x+\mu} - 2\psi_x + \psi_{x-\mu}) \tag{1.15}$$

where we are at liberty to choose what we want for r provided that $0 < r \leq 1$. The value we choose for r has no physical consequences and it is usual to set $r = 1$[5].

We can add the Wilson term because in the continuum limit ($a \to 0$), the QCD continuum action is returned. Eq 1.13 now becomes:

$$S_F(\text{Latt}) = \int \frac{d^4k}{(2\pi)^4} \bar{\psi}(-k) \left(i \sum_\mu \gamma^\mu \frac{\sin(ak_\mu)}{a} + m - \sum_\mu \frac{\cos(ak_\mu - 1)}{a} \right) \psi(k) \tag{1.16}$$

This action removes the unwanted poles in the propagator, but retains the one we want at $k = 0$. We now have a lattice gauge theory of a single fermion instead of sixteen fermions.

Unfortunately, when the quark masses are set equal to zero, the Wilson term is not chirally symmetric unlike QCD. This means that the gauge theory only regains the chiral symmetry of QCD in the continuum limit when the Wilson term disappears. Further, the new term adds $\mathcal{O}(a)$ discretisation errors to the action, whereas previously we had $\mathcal{O}(a^2)$ errors. The lattice errors are therefore more significant, and the approach to the continuum limit with decreasing a is much slower.

The $\mathcal{O}(a)$ errors can be removed by adding the term:

$$S_{SW} = -C_{SW} \frac{i\kappa}{2} \sum_{x,\mu,\nu} \bar{\psi}(x) \sigma_{\mu\nu} F_{\mu\nu} \psi(x) \tag{1.17}$$

where κ is related to the fermion (quark) mass m_q by:

$$\kappa = \frac{1}{8r + 2m_q} \tag{1.18}$$

This results in the "Sheikholeslami-Wohlert" or "clover" action[6, 7]. The coefficient C_{SW} can be tuned such that the $\mathcal{O}(a)$ lattice artifacts are completely removed. This action is used in chapters 5 to 8 to generate the data from which the ground state masses of various mesons are found.

1.5 Greens Functions on the Lattice

The expectation value $\langle O \rangle$ of an observable O in a theory with an action S is defined in terms of a Greens function. On the lattice, this is given by:

$$\langle O \rangle = \frac{1}{Z} \int \mathcal{D}U \mathcal{D}\bar{\psi} \mathcal{D}\psi O(U, \bar{\psi}, \psi) e^{-S} \tag{1.19}$$

where Z is known as the partition function by analogy with statistical mechanics and is defined by:

$$Z = \int \mathcal{D}U \mathcal{D}\bar{\psi} \mathcal{D}\psi e^{-S} \tag{1.20}$$

where $\mathcal{D}$ denotes the Feynman path integral[3, 8]. In general, Greens functions cannot be calculated by analytic methods, and so a computational procedure is employed. The fermionic fields are Grassmann variables which makes numerical integration techniques difficult to apply. We get around this problem by defining the fermionic part of the action via the Wilson fermion determinant M:

$$\int \mathcal{D}\bar{\psi} \mathcal{D}\psi e^{-\bar{\psi} M \psi} = \det M \tag{1.21}$$

This allows us to write Eq 1.19 as:

$$\langle O \rangle = \frac{1}{Z} \int \mathcal{D}U O(U) \det M(U) e^{S_G} \tag{1.22}$$

where S_G is the pure gauge part of the Wilson action. This Integration is now only over the gauge fields U. The integration can be performed using Monte-Carlo integration[9].

We still need to evaluate the fermion determinant det M. This is very computer intensive. The computer time of the simulations is significantly cut if we set det M equal to a constant. This is called the quenched approximation. The quenched approximation can be shown to be equivalent to ignoring fermionic loops in the vacuum of QCD.

1.6 Comment

In this chapter, we have briefly reviewed some of the important aspects of lattice QCD. In particular we have focussed on the parts which are relevant to the rest of this thesis. Further details of Lattice QCD can be found in several texts[10, 11, 12]. Also see the review article [13].

Chapter 2

The Running Coupling

2.1 Introduction

In this chapter, we firstly consider the renormalisation of QCD. We then derive the renormalisation group equation, from which we derive the perturbative running coupling.

We derive the tree-level three-gluon vertex, and then consider the generalised three-gluon vertex. From the generalised three-gluon vertex, we proceed to define the running coupling in the $\widetilde{MOM}$ scheme. At the end of the chapter, we review a non-perturbative lattice calculation of the running coupling defined in the $\widetilde{MOM}$ scheme.

2.2 Renormalisation of QCD

The quantities in the QCD Lagrangian Eq 1.4 are not observed by us directly. We are therefore at liberty to redefine them provided that the overall Lagrangian is not altered. If we call the quantities in Eq 1.4 the "bare" quantities and give them a suffix B, then we can redefine the quantities by [3, page 132]:

$$\begin{aligned}
(A_a^\mu)_B &= Z_A^{\frac{1}{2}} A_a^\mu \\
(\eta_a)_B &= Z_\eta^{\frac{1}{2}} \eta_a \\
\psi_B &= Z_\psi^{\frac{1}{2}} \psi \\
\xi_B^{-1} &= \xi^{-1} Z_\xi Z_A^{-1} \\
m_B &= m Z_m Z_\psi^{-1}
\end{aligned} \tag{2.1}$$

The Lagrangian defines four different vertices which gives us four ways of defining the renormalised coupling:

$$\begin{aligned}
\text{Ghost-Gluon:} \qquad g_B &= g Z_1 Z_\eta^{-1} Z_A^{-\frac{1}{2}} \\
\text{Gluon-Fermion:} \qquad g_B &= g Z_2 Z_\psi^{-1} Z_A^{-\frac{1}{2}} \\
\text{Three-Gluon:} \qquad g_B &= g Z_3 Z_A^{-\frac{3}{2}} \\
\text{Four-Gluon:} \qquad g_B^2 &= g^2 Z_4 Z_A^{-2}
\end{aligned} \tag{2.2}$$

The Z_i, $i = 1...4$ renormalise the vertex, while the other factors renormalise the vertex legs. To make the theory consistent, all of these definitions of g must be equal. This gives rise to the Ward identities:

$$Z_1 Z_\eta^{-1} = Z_2 Z_\psi^{-1} = Z_3 Z_A^{-1} = Z_4^{-\frac{1}{2}} Z_A^{-\frac{1}{2}} \tag{2.3}$$

Of particular interest to us in this work is purely gluonic QCD where any fermionic part has been removed. Looking at Eq 1.4 we have the Lagrangian:

$$L = -\frac{1}{4} F_a^{\mu\nu} F_{\mu\nu}^a - \frac{1}{2\xi} (\partial_\mu A_a^\mu)^2 \tag{2.4}$$

From Eq 2.1, the renormalised variables are given by:

$$(A_a^\mu)_B = Z_A^{\frac{1}{2}} A_a^\mu \tag{2.5}$$

$$\xi_B^{-1} = \xi^{-1} Z_\xi Z_A^{-1} \tag{2.6}$$

We now have only the three-point and four-point gluon vertices with which to define the renormalised coupling:

$$g_B = g Z_3 Z_A^{-\frac{3}{2}} \tag{2.7}$$

$$g_B^2 = g^2 Z_4 Z_A^{-2} \tag{2.8}$$

which gives the Ward identity:

$$Z_3^2 = Z_4 Z_A \tag{2.9}$$

2.3 Renormalisation Group Equation

Provided that the Ward identities are satisfied, we can in principle choose whatever we want for the Z numbers.

It is well known that quantum field theory gives rise more often than not to infinities whenever a calculation is made. Due to this, it is usual to choose the Z numbers so that they cancel these infinities and make the theory return finite results. There is still a lot of freedom in how we go about this, and the precise way in which it is done in a given calculation is known as the "Renormalisation Scheme".

One point in common to all schemes is that they have to define the theory at a given momentum μ where μ is arbitrary. Therefore we can alter the scheme by changing μ. A given scheme is then one of a set of schemes which are connected by varying the parameter μ.

Renormalisation follows from a freedom to redefine parameters in the theory. It is not a physical process and we do not expect any physical quantity to depend on the scheme in which it is calculated. It is therefore surprising that the freedom to renormalise leads to an important physical consequence called "asymptotic freedom" as we shall see in section 2.5.

In field theory, the objects we are interested in are Greens functions. These describe particle interactions. In pure gauge QCD there are no fermions so we just deal with the Greens functions of vertices where the legs are gluons. If the Greens function G has n legs, then the function can depend on the various external gluon leg momenta $p_1.....p_n$, the coupling constant g and the gauge parameter ξ:

$$G_B^{(n)}(p_1.....p_n, g_B, \xi_B) \tag{2.10}$$

where the subscript B indicates that it is the unrenormalised or bare Greens function.

This is related to the renormalised Greens function by:

$$G_B^{(n)}(p_1.....p_n, g_B, \xi_B) = Z_A^{-\frac{n}{2}} G^{(n)}(p_1.....p_n, g, \xi, \mu) \tag{2.11}$$

where the factor $Z_A^{-\frac{n}{2}}$ accounts for the renormalisation of the external gluon leg propagators Eq 2.5. Here we have parametrised the renormalisation scheme by μ and allowed for the Greens function to have a direct functional dependence on μ as well as indirectly via the other renormalised quantities g and ξ.

By definition, the unrenormalised bare Greens function $G_B^{(n)}$ is independent of the parameter μ. So applying the dimensionless derivative $\mu\partial/\partial\mu$ to the above, we get:

$$\begin{aligned} 0 &= \mu G^{(n)} \frac{\partial}{\partial\mu} Z_A^{-\frac{n}{2}} + \mu Z_A^{-\frac{n}{2}} \frac{\partial}{\partial\mu} G^{(n)} \\ &= -\frac{n}{2} G^{(n)} \mu Z_A^{-\frac{n}{2}} Z_A^{-1} \frac{\partial}{\partial\mu} Z_A + Z_A^{-\frac{n}{2}} \left(\mu \frac{\partial G^{(n)}}{\partial\mu} + \mu \frac{\partial g}{\partial\mu} \frac{\partial G^{(n)}}{\partial g} + \mu \frac{\partial\xi}{\partial\mu} \frac{\partial G^{(n)}}{\partial\xi} \right) \end{aligned} \tag{2.12}$$

If we remove the common factor of $Z_A^{-\frac{n}{2}}$ then we have:

$$\left(\mu \frac{\partial}{\partial\mu} + \beta_g \frac{\partial}{\partial g} + \beta_\xi \frac{\partial}{\partial\xi} - n\gamma \right) G^{(n)} = 0 \tag{2.13}$$

where we have defined the following dimensionless coefficients:

$$\beta_g = \mu \frac{\partial g}{\partial\mu} \tag{2.14}$$

and

$$\beta_\xi = \mu \frac{\partial\xi}{\partial\mu} \tag{2.15}$$

$$\gamma \; = \; \frac{1}{2}\mu Z_A^{-1}\frac{\partial}{\partial\mu}Z_A \tag{2.16}$$

Eq 2.13 is known as the renormalisation group equation. The importance of this equation is that it tells us how how renormalised functions change with a change in the mass scale μ. From this there follows important consequences for the QCD coupling as we shall now show.

2.4 Scaling of External Momenta

If the renormalised n point bosonic Greens function $G^{(n)}$ has mass dimension D, then we can factor this out to leave a dimensionless quantity f:

$$G^{(n)}(p_i, g, \mu, \xi) = \mu^D f(p_i, g, \mu, \xi) \tag{2.17}$$

Now consider scaling the momenta of the external legs of the vertex by an arbitrary factor $\lambda = e^t$ so $p_i \to \lambda p_i = e^t p_i$. We have:

$$G^{(n)}(\lambda p_i, g, \mu, \xi) = \mu^D f(\lambda p_i, g, \mu, \xi) \tag{2.18}$$

Since the Greens function must be Lorentz invariant, we can write f as a function of dimensionless Lorentz scalars so:

$$G^{(n)}(\lambda p_i, g, \mu, \xi) = \mu^D f\left(\frac{\lambda^2 p_i \cdot p_j}{\mu}, g, \xi\right) \tag{2.19}$$

which satisfies the equation:

$$\left(\mu\frac{\partial}{\partial\mu} + \frac{\partial}{\partial t} - D\right) G^{(n)} = 0 \tag{2.20}$$

If we apply the scaling $p_i \to \lambda p_i$ to the renormalisation group equation Eq 2.13, then we can use this to eliminate the term $\mu\frac{\partial}{\partial\mu}$ from Eq 2.20. This gives:

$$\left(-\frac{\partial}{\partial t} + \beta_g \frac{\partial}{\partial g} + \beta_\xi \frac{\partial}{\partial \xi} - n\gamma + D\right) G^{(n)}(\lambda p_i, g, \xi) = 0 \tag{2.21}$$

Physical quantities cannot be gauge dependent, so for any real, on shell vertex, there cannot be any dependence on the gauge parameter ξ. Ignoring ξ dependence[1], this equation has solution:

$$G^{(n)}(\lambda p_i, g) = G^{(n)}(p_i, \bar{g}) exp\left(\int_g^{\bar{g}} dg' \frac{\tilde{\gamma}(g')}{\beta(g')}\right) \tag{2.22}$$

where:

$$\frac{d\bar{g}(g,t)}{dt} = \beta(\bar{g}) \equiv \mu \frac{\partial \bar{g}(g,t)}{\partial \mu} \tag{2.23}$$

which can be seen by inserting back into Eq 2.21.

From Eq 2.22 we see that the Greens function at the scaled momenta λp_i is identical to the function at p_i except that we require a redefined coupling constant $\bar{g}$ instead of g. The Greens function is also ambiguous by a multiplicative exponential factor. This factor makes no difference to the physics since the Greens functions must be normalised to calculate S matrix elements. Any multiplicative factor gets removed by the normalisation.

It follows from Eq 2.23 that:

$$\bar{g}(t) = g(e^t \mu) \tag{2.24}$$

So we see that a scaling by λ in external momenta of a Greens function results

[1] It is not necessary to ignore ξ dependence, see[3, Section 12.1]

in the same Greens function, but with the coupling constant defined at an energy given by $\lambda\mu$ instead of μ.

2.5 Perturbative Running Coupling

If the coupling g is small, we may try expanding the β function in Eq 2.23 as a power series in α_s. This gives us the corresponding power series in g:

$$\beta_g = -g^3 \left\{ b_0 + b_1 g^2 + b_2 g^4 + ... \right\} \tag{2.25}$$

The b coefficients can be determined from calculating the Z numbers in Eq 2.7 or Eq 2.8 perturbatively.

From one loop perturbation theory, it can be shown that for purely gluonic QCD we have $b_0 = 11/(16\pi^2)$[14]. So for the coupling $\bar{g}$, we have from Eq 2.23:

$$\frac{d\bar{g}(g,t)}{dt} = -b_0 \bar{g}^3 \tag{2.26}$$

which is valid up to one loop.

From Eq 2.24, we have the boundary condition that when $t = 0$, $\bar{g} = g$. We can use this to write Eq 2.26 as:

$$\int_g^{\bar{g}} \frac{d\bar{g}}{\bar{g}^3} = -b_0 \int_0^t dt \tag{2.27}$$

ie:

$$\bar{g}^{-2}(\mu) = g^{-2}(\mu) + 2b_0 \ln \lambda = g^{-2}(\lambda\mu) \tag{2.28}$$

where the last equality comes from applying Eq 2.24. We write:

$$\alpha_s(\lambda\mu) = \frac{\alpha_s(\mu)}{1 + 8\pi b_0 \alpha_s(\mu) \ln \lambda} \tag{2.29}$$

where $\alpha_s \equiv g^2/4\pi$. For convenience, we define the momentum Q by $\lambda^2 = Q^2/\mu^2$ or $t = \frac{1}{2} \ln Q^2/\mu^2$, so we can write:

$$\alpha_s(Q^2) = \frac{\alpha_s(\mu^2)}{1 + 4\pi b_0 \alpha_s(\mu^2) \ln Q^2/\mu^2} \tag{2.30}$$

By defining the constant Λ by:

$$\ln \Lambda^2 = \ln \mu^2 - \frac{1}{\alpha_s(\mu^2) 4\pi b_0} \tag{2.31}$$

we can write:

$$\alpha_s(Q^2) = \frac{1}{4\pi b_0 \ln Q^2/\Lambda^2} \tag{2.32}$$

Λ is known as the QCD scale parameter and sets the momentum scale of the theory.

Eq 2.32 tells us how the strong coupling varies with a scaling of the momenta of a vertex. It is a remarkable result to come from something as apparently trivial as the redefining of unmeasurable quantities.

Eq 2.32 is only valid insofar as Eq 2.26 is applicable. This requires g to be small enough for higher powers in g to be safely neglected. We see that in its range of validity, Eq 2.32 tells us that the coupling decreases with increasing vertex leg momenta.

Provided that we start with a value of α_s small enough for Eq 2.26 to be valid, then we can predict that the coupling will decrease according to Eq 2.32

with increasing momenta. At high enough momenta, α_s becomes effectively zero, and the theory becomes a free theory. This is known as "asymptotic freedom".

If instead of calculating β to one loop in Eq 2.26 we calculated it to two loops, then we would have the following two loop formula for α_s:

$$\alpha_s(p) = \frac{4\pi}{b_0 \ln(p^2/\Lambda^2)} - \frac{b_1}{b_0} \frac{\ln(\ln(p^2/\Lambda^2))}{(b_0 \ln(p^2/\Lambda^2))^2} \tag{2.33}$$

with $b_1 = 102/(4\pi^4)$[15].

Since b_0, b_1 are scheme independent, Eq's 2.32 and 2.33 are valid in any scheme.

2.6 Tree-Level Three-Gluon Vertex

From the pure gauge Lagrangian Eq 2.4 we see that the gluonic fields A only occur at higher than second order in the Yang-Mills term:

$$L_{YM} = -\frac{1}{4} F_a^{\mu\nu} F_{\mu\nu}^a \tag{2.34}$$

where:

$$F_a^{\mu\nu} = \partial^\mu A_a^\nu - \partial^\nu A_a^\mu - g f_{abc} A_b^\mu A_c^\nu \tag{2.35}$$

There are four terms which are trilinear in A. These contribute:

$$\begin{aligned} -\frac{g}{4} \Big[& -\partial^\mu A_a^\nu f_{abc} A_\mu^b A_\nu^c \\ & +\partial^\nu A_a^\mu f_{abc} A_\mu^b A_\nu^c \\ & -f_{abc} A_b^\mu A_c^\nu \partial_\mu A_\nu^a \end{aligned}$$

$$+f_{abc}A_b^\mu A_c^\nu \partial_\nu A_\mu^a\Big] \tag{2.36}$$

Swapping the dummy indices $\mu \leftrightarrow \nu$ and $b \leftrightarrow c$ in the second and fourth terms we pick up a $-$ sign due to the antisymmetric tensor f_{abc}. The above then becomes:

$$g f_{abc} A_b^\mu A_c^\nu \partial_\mu A_\nu^a = -ig f_{abc} g_{\lambda\nu} p_\mu A_a^\lambda A_b^\mu A_c^\nu \tag{2.37}$$

where we have put $\partial_\mu \to -ip_\mu$.

We now Fourier transform the fields:

$$\begin{aligned} A_a^\lambda(x) &= \int \frac{d^4p}{(2\pi)^4} e^{ip\cdot x} \tilde{A}_a^\lambda(p) \\ A_b^\nu(x) &= \int \frac{d^4q}{(2\pi)^4} e^{iq\cdot x} \tilde{A}_b^\nu(q) \\ A_c^\mu(x) &= \int \frac{d^4r}{(2\pi)^4} e^{ir\cdot x} \tilde{A}_c^\mu(r) \end{aligned} \tag{2.38}$$

which gives:

$$-ig f_{abc} \int \frac{d^4p}{(2\pi)^4} \frac{d^4q}{(2\pi)^4} \frac{d^4r}{(2\pi)^4} e^{-i(p+q+r)\cdot x} g_{\lambda\nu} p_\mu \tilde{A}_a^\lambda \tilde{A}_b^\mu \tilde{A}_c^\nu \tag{2.39}$$

This is the tree-level vertex function depicted in Fig 2.1.

f_{abc} is antisymmetric under interchange of any two colours eg $a \leftrightarrow b$. From the symmetry of the vertex, if we then interchange $(\lambda, p) \leftrightarrow (\nu, q)$ we must end up where we started. Therefore the vertex must also be antisymmetric under the interchange of any two of $(\lambda, p), (\nu, q), (\mu, r)$. This antisymmetry becomes

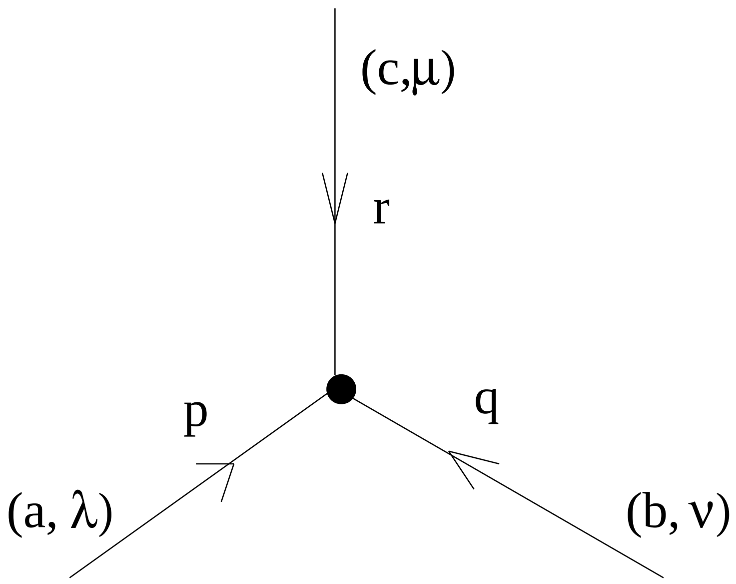

Figure 2.1: Tree-Level Three-Gluon Vertex

explicit once we notice that:

$$p_\mu g_{\lambda\nu} = \frac{1}{6}\left[(q-r)_\lambda g_{\nu\mu} + (p-q)_\mu g_{\lambda\nu} + (r-p)_\nu g_{\mu\lambda}\right] \tag{2.40}$$

The tree level three-gluon vertex is then:

$$f_{abc}\Gamma^{tree}_{\lambda\mu\nu} = -igf_{abc}\left[(q-r)_\lambda g_{\nu\mu} + (p-q)_\mu g_{\lambda\nu} + (r-p)_\nu g_{\mu\lambda}\right] \tag{2.41}$$

2.7 General Three-Gluon Vertex

We now consider the most general form of the three-gluon vertex function. We denote the three-gluon vertex function by:

$$\Gamma^{abc}_{\lambda\mu\nu}(p,q,r) \tag{2.42}$$

where we have the colour indices a, b, c, Lorentz indices λ, μ, ν and momenta p, q, r as in Fig 2.2.

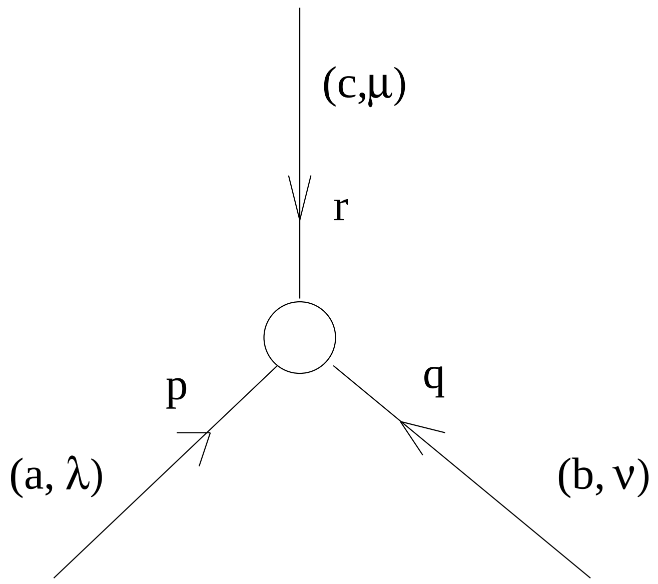

Figure 2.2: General Three-Gluon Vertex

The three-gluon vertex only depends on terms involving an antisymmetric factor f_{abc}. Since the vertex must have no net colour dependence, we can factor it out:

$$\Gamma^{abc}_{\lambda\mu\nu}(p,q,r) = -igf_{abc}\Gamma_{\lambda\mu\nu}(p,q,r) \tag{2.43}$$

As in the tree-level case, the function $\Gamma_{\lambda\mu\nu}(p,q,r)$ must be antisymmetric under the interchange of any two of $(\lambda,p),(\nu,q),(\mu,r)$. We need the most general function we can write which has this property[16, 17]. We preserve symmetry by making the expression invariant under cyclic permutations. The transverse component of Γ is given by:

$$\begin{aligned}\Gamma^{(T)}_{\lambda\mu\nu}(p,q,r) &= F(p^2,q^2;r^2)\left(g_{\lambda\mu}p\cdot q - p_\mu q_\lambda\right)B^3_\nu \\ &+ H\left[-g_{\lambda\mu}B^3_\nu + \frac{1}{3}\left(p_\nu q_\lambda r_\mu - p_\mu q_\nu r_\lambda\right)\right] + \text{Cyclic Permutations}\end{aligned} \tag{2.44}$$

where

$$B^3_\nu = (p_\nu q \cdot r - q_\nu p \cdot r) \tag{2.45}$$

and F is symmetric in its first two arguments and H is totally symmetric in p^2, q^2, r^2.

The longitudinal part is:

$$\begin{aligned}
\Gamma^{(L)}_{\lambda\mu\nu}(p,q,r) &= A(p^2,q^2;r^2)g_{\lambda\mu}(p_\nu - q_\nu) + B(p^2,q^2;r^2)g_{\lambda\nu}(p_\nu + q_\nu) \\
&+ C(p^2,q^2;r^2)(p_\mu q_\lambda - g_{\lambda\mu} p \cdot q)(p-q)_\nu \\
&+ \frac{1}{3}S(p_\nu q_\lambda r_\mu + p_\mu q_\nu r_\lambda) + \text{Cyclic Permutations}
\end{aligned} \tag{2.46}$$

where A and C are symmetric in their first two arguments, B is antisymmetric in its first two arguments, and S is totally symmetric in all arguments.

2.8 Asymmetric Three-Gluon Vertex in the Landau Gauge

We now make some specifications[18, 19, 20, 21] which considerably simplify the above expressions for Γ. We define the antisymmetric point by requiring that the vertex momenta satisfy:

$$r = 0 \tag{2.47}$$

and from the requirement of conservation of momentum at a vertex, we have:

$$p = -q \tag{2.48}$$

We immediately see that $\Gamma^{(T)} = 0$ and that we have left:

$$\begin{aligned}
\Gamma_{\lambda\mu\nu}(p, -p, 0) &= \Gamma^{(L)}_{\lambda\mu\nu}(p, -p, 0) \\
&= 2A(p^2, p^2; 0) g_{\lambda\mu} p_\nu - 2C(p^2, p^2; 0) \left[p_\mu p_\lambda p_\nu - p^2 g_{\lambda\mu} p_\nu \right] \\
&- (g_{\lambda\nu} p_\mu + g_{\mu\nu} p_\lambda) \left[A(0, p^2; p^2) - B(0, p^2; p^2) \right]
\end{aligned} \tag{2.49}$$

We now choose to work in the Landau gauge because this significantly reduced the number of tensors in the vertex function. We project transversely to the momenta. This is equivalent to putting $\lambda = \mu \neq \nu$. For the purposes of a lattice calculation, we also need to define the function in Euclidean space which means $g_{\mu\nu} \to \delta_{\mu\nu}$. We get:

$$\Gamma_{\lambda\lambda\nu}(p, -p, 0) = 2A(p^2, p^2; 0) \delta_{\lambda\lambda} p_\nu \tag{2.50}$$

where we may suppose that there is a summation over λ if we wish. Comparing with the Euclidean version of Eq 2.41 we see that we obtain the tensor that multiplies the tree-level vertex.

2.9 Non-perturbative Running Coupling in the $\widetilde{MOM}$ Scheme

We now consider a method of defining the running coupling in a non-perturbative way. In pure gauge QCD, there are two definitions of the running coupling from vertices. We choose to use the one from the three-gluon vertex Eq 2.7. We see that we must calculate Z_3 and Z_A non-perturbatively to give us the non-perturbative running coupling. We shall define the Z numbers using the $\widetilde{MOM}$ scheme[22] which is a variant on the MOM scheme[23]. First we shall define Z_A.

Consider the unrenormalised gluon propagator $G_U^{(2)}(p^2)$. In the Landau gauge, this becomes:

$$G_{\mu\nu}^{(2)}(p) = T_{\mu\nu}(p) G_U(p^2) \tag{2.51}$$

where T is the transverse projection operator defined by:

$$T_{\mu\nu}(p) \equiv \delta_{\mu\nu} - \frac{p_\mu p_\nu}{p^2} \tag{2.52}$$

At some sufficiently high momenta, the tree-level gluon propagator becomes valid. We renormalise our gluon propagator by equating it with the tree-level value at momentum $p^2 = \mu^2$:

$$G_R^{(2)}(p^2)\Big|_{p^2=\mu^2} = Z_A^{-1} G_U^{(2)}(p^2)\Big|_{p^2=\mu^2} = \frac{1}{\mu^2} \tag{2.53}$$

Hence:

$$Z_A = \mu^2 G^{(2)}(\mu) \tag{2.54}$$

To define Z_3 we first note that the unrenormalised three-point Greens function $G_U^{(3)}$ is related to the unrenormalised vertex function Eq 2.43 by adding on the three-gluon leg propagators:

$$G_{U\,\alpha\beta\gamma}^{(3)\,abc}(p,q,r) = -igf_{abc}\Gamma_{U\,\lambda\mu\nu}(p,q,r) T_{\lambda\alpha} G_U^{(2)}(p^2) T_{\mu\beta} G_U^{(2)}(q^2) T_{\nu\gamma} G_U^{(2)}(r^2) \tag{2.55}$$

If we now apply our previous prescription $p = -q$, $r = 0$, $\lambda = \mu \neq \nu$ we get:

$$\sum_{\alpha} G^{(3)}_{U\,\alpha\alpha\gamma}(p, -p, 0) = -ig \sum_{\alpha} \Gamma_{U\,\alpha\alpha\gamma}(p, -p, 0) \left[G^{(2)}(p)\right]^2 G^{(2)}(0) \tag{2.56}$$

where we have ignored the colour factor.

We have shown with Eq 2.50 that Γ is composed of a tensor multiplied by the tree-level vertex. We can therefore renormalise the three-point Greens function in a similar way to the gluon propagator. At momentum μ we specify that the renormalised vertex is equal to the tree-level vertex, so:

$$-ig\Gamma_{R\,\lambda\lambda\nu}(p, -p, 0)\big|_{p^2=\mu^2} = -igZ_3\Gamma_{U\,\lambda\lambda\nu}(p, -p, 0)\big|_{p^2=\mu^2} = \Gamma^{tree} \tag{2.57}$$

So using Eq 2.56 we get:

$$\frac{\sum_{\alpha} G^{(3)}_{U\,\alpha\alpha\gamma}}{\left[G^{(2)}(p)\right]^2 G^{(2)}(0)} = 6iZ_3^{-1} g_B p_\gamma \tag{2.58}$$

So, finally, from Eq's 2.7,2.54 and 2.58, we get:

$$g = \frac{G^{(3)}_U Z_A^{3/2}(\mu^2)}{\left[G^{(2)}(p)\right]^2 G^{(2)}(0)} \tag{2.59}$$

where:

$$Z_A^{3/2}(\mu^2) = p^2 G^{(2)}(p^2)\Big|_{p^2=\mu^2} \tag{2.60}$$

By evaluating these quantities on the lattice, we obtain the running coupling at the antisymmetric point in the Landau gauge.

2.10 Lattice Calculation

We define the gluon field on the lattice by[21]:

$$A_\mu(x + \hat{\mu}/2) = \frac{U_\mu(x) - U^\dagger_\mu(x)}{2iag_0} - \frac{1}{3} Tr \left(\frac{U_\mu(x) - U^\dagger_\mu(x)}{2iag_0} \right) \tag{2.61}$$

where $\hat{\mu}$ is the unit lattice vector in the direction μ and g_0 is the bare coupling constant.

The two and three-point Greens functions can be evaluated from the following expression for an n-point Greens function:

$$G^{(n)a_1 a_2 \cdots a_n}_{\mu_1 \mu_2 \cdots \mu_n}(p_1, p_2, \cdots p_n) = \langle A^{a_1}_{\mu_1}(p_1) A^{a_2}_{\mu_2}(p_2) \cdots A^{a_n}_{\mu_n}(p_n) \rangle \tag{2.62}$$

where $\langle\ \rangle$ represents the Monte-Carlo average and:

$$A^a_\mu(p) = \frac{1}{2} Tr \left[\sum_x A_\mu(x + \hat{\mu}/2) exp(ip(x + \hat{\mu}/2)) \lambda^a \right] \tag{2.63}$$

where the trace is over the colour index.

By evaluating the two and three-point Greens functions as defined on the lattice by Eq 2.62, the running coupling can be calculated in the $\widetilde{MOM}$ scheme using the formulae in section 2.9.

The running coupling is defined in the Landau gauge. By definition, the Landau gauge requires that $p_\mu A^a_\mu(p) = 0$. This does not happen in the lattice calculation on account of $O(a^2)$ effects. We can get around this problem by using the "sinus correction" which is a method of accounting for the $O(a^2)$ effects.

We first note that the quantity $\tilde{p}_\mu A^a_\mu(p)$ is zero on the lattice when we define $\tilde{p}$ by:

$$\tilde{p}_\mu = \frac{2}{a} sin \left(\frac{ap_\mu}{2} \right) \tag{2.64}$$

This gives us $\tilde{p}_\mu \simeq p_\mu(1 - \frac{1}{24} a^2 p_\mu^2)$. The rescaling of momenta $p \to \tilde{p}$ is known as the sinus correction[21].

By performing fits to the results of lattice simulations, the best χ^2 is found when the momenta are scaled by $1 - ca^2p^2$ and $c \sim 1/24$[21]. This gives support to the sinus improvement definition of momenta in Eq 2.64.

α_s has been calculated[20] on 16^4 and 24^4 lattices at $\beta = 6.2$ with 1000 configurations. It has also been calculated on a 32^4 lattice with 100 configurations. The running coupling data are plotted in Figs 2.3 to 2.7. The data has been scaled with the sinus correction. Apart from the case of $\beta = 6.0$ on the 32^4 lattice, data for a given value of β are plotted on the same graph so that any obvious volume dependence can be seen.

The lattice at $\beta = 6.2$ is calibrated by using results from a fit to the K^* mass in [24]. This gives $a^{-1}(\beta = 6.2) = 2.75(17)\mathrm{GeV}$. For the other values of β, [20] uses the results for the string tension in lattice units ($a\sqrt{\sigma}$) given in [25]. By taking the ratios of the string tension in different lattice units, the factor $\sqrt{\sigma}$ cancels and we can determine the lattice spacing by a ratio with $a^{-1}(\beta = 6.2)$. We obtain $a^{-1}(\beta = 6.0) = 1.97\mathrm{GeV}$, $a^{-1}(\beta = 6.0) = 2.75\mathrm{GeV}$, $a^{-1}(\beta = 6.4) = 3.66\mathrm{GeV}$ and $a^{-1}(\beta = 6.8) = 6.10\mathrm{GeV}$.

The important point about the running coupling data presented here is that it was determined from a first principles pure gauge QCD lattice calculation. This potentially gives us access to studying some non-perturbative aspects of the running coupling. In the paper [26], this data was used to study the possibility of a non-perturbative correction to the perturbative running coupling of the form c/p^2 where c is some constant and p is the momentum dependence.

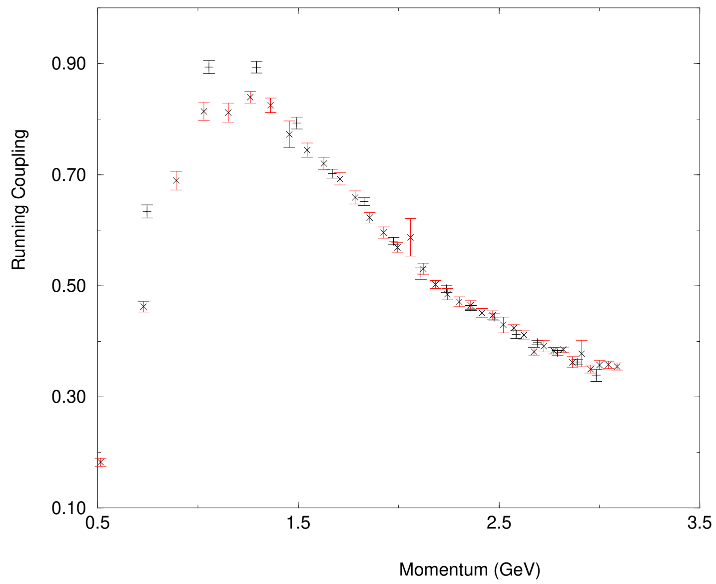

Figure 2.3: The Running Coupling calculated on 16^4(symbol "$-$") and 24^4(symbol "$\times$") lattices with $\beta = 6.0$.

We shall return to this in chapter 4. In the next chapter we show how to relate Λ in the $\widetilde{MOM}$ scheme to Λ in the more commonly used minimal subtraction scheme ($\overline{MS}$).

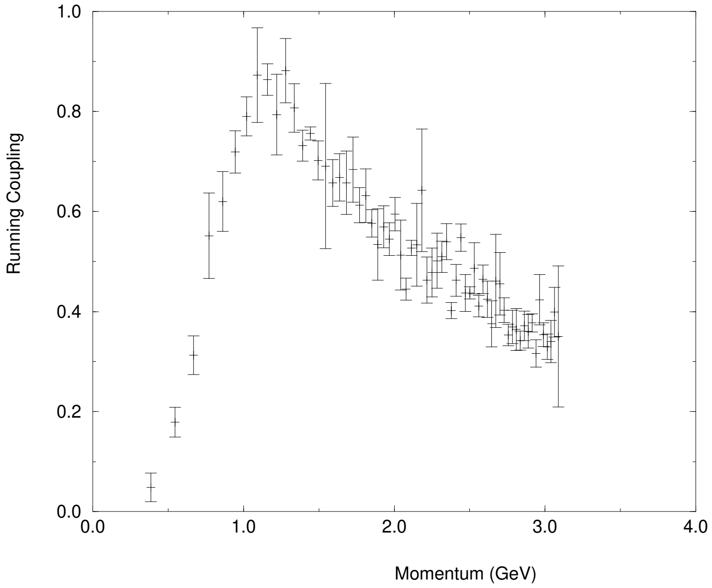

Figure 2.4: The Running Coupling calculated on a 32^4(symbol "$-$") lattice with $\beta = 6.0$.

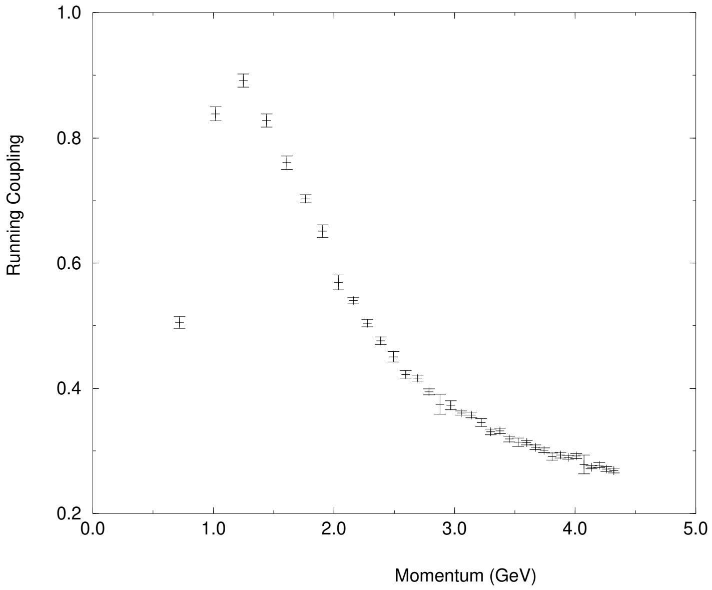

Figure 2.5: The Running Coupling calculated on a 24^4(symbol "$-$") lattice with $\beta = 6.2$.

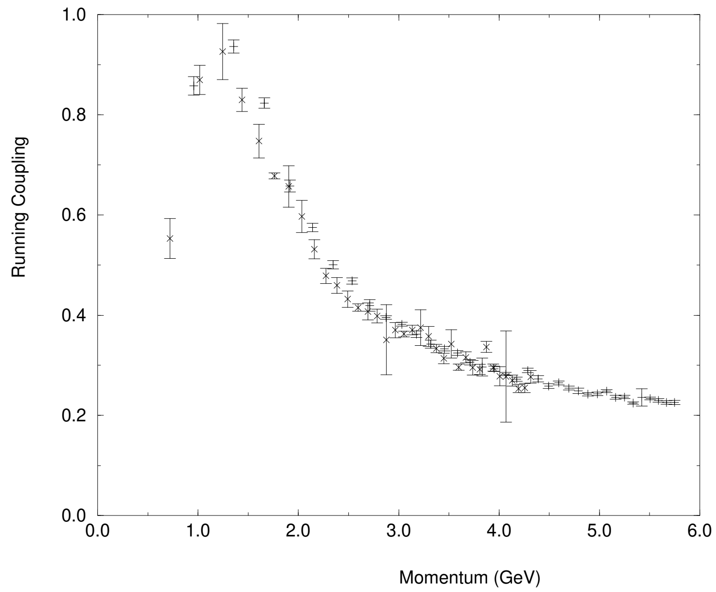

Figure 2.6: The Running Coupling calculated on 24^4(symbol "$-$") and 32^4(symbol "$\times$") lattices with $\beta = 6.4$.

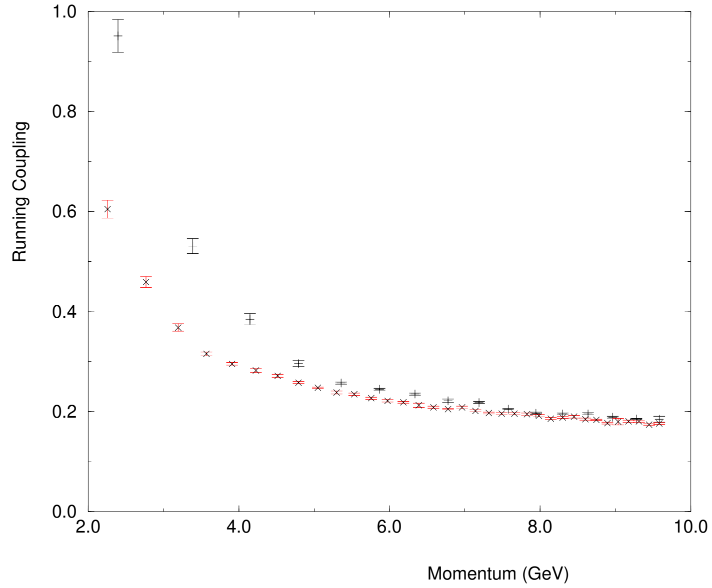

Figure 2.7: The Running Coupling calculated on 16^4(symbol "$-$") and 24^4(symbol "$\times$") lattices with $\beta = 6.8$.

Chapter 3

Perturbative Matching

In Chapter 2 we defined the running coupling in the $\widetilde{MOM}$ scheme. Since most results are quoted in the $\overline{MS}$ scheme, we now show how to relate a perturbative quantity in the $\widetilde{MOM}$ to the $\overline{MS}$ scheme.

3.1 Introduction

If we have two schemes A and B, then we can write the running coupling α_A in scheme A as a power expansion of the coupling in scheme B:

$$\alpha_A = \alpha_B + C_{AB}(\alpha_B)^2 + ... \tag{3.1}$$

By using $\alpha_s = g^2/4\pi$ we have:

$$g_A^2 = g_B^2 \left(1 + C_{AB}\frac{g_B^2}{4\pi} + O(g_B^4)\right) \tag{3.2}$$

From the expression for the running coupling to one loop (Eq 2.32), we have:

$$\frac{\Lambda_A}{\Lambda_B} = exp\left[\frac{1}{2b_0}\left(\frac{1}{g_B^2} - \frac{1}{g_A^2}\right)\right] \tag{3.3}$$

Using the expression for g_A^2 in Eq 3.2 we have:

$$\frac{\Lambda_A}{\Lambda_B} = exp\left(\frac{C_{AB}}{8b_0\pi}\right) \tag{3.4}$$

So evaluating the constant C_{AB} will enable us to relate Λ in different schemes to one loop order in perturbation theory. Most particularly we would like to relate $\Lambda_{\widetilde{MOM}}$ to $\Lambda_{\overline{MS}}$.

Consider the three-gluon vertex definition of the running coupling Eq 2.7:

$$g^2(\mu) = Z_A^3 Z_3^{-2} g_B^2 \tag{3.5}$$

If we define the running coupling in this way for the $\overline{MS}$ and the $\widetilde{MOM}$ schemes, we get:

$$\frac{g^2_{\overline{MS}}}{g^2_{\widetilde{MOM}}} = \left(\frac{Z_A^{\overline{MS}}}{Z_A^{\widetilde{MOM}}}\right)^3 \cdot \left(\frac{Z_3^{\widetilde{MOM}}}{Z_3^{\overline{MS}}}\right)^2 \tag{3.6}$$

So if we can define these Z numbers then we have a way of relating the couplings to each other.

3.2 Z_3

Z_3 is defined by renormalising the three-gluon vertex function. Eq 2.58 defines Z_3 in the $\widetilde{MOM}$ scheme:

$$\frac{\sum_\alpha G_{U\,\alpha\alpha\gamma}}{[G(p)]^2\,G(0)} = 6i\left(Z_3^{\widetilde{MOM}}\right)^{-1} g_B p_\gamma \tag{3.7}$$

Z_3 in the $\overline{MS}$ scheme is defined by the three gluon vertex in the $\overline{MS}$ scheme:

$$\Gamma_U = (Z_3^{\overline{MS}})^{-1}\Gamma_{\overline{MS}} \tag{3.8}$$

The asymmetric three-gluon vertex is given by Eq 2.49. It can be shown[27, Eq 4.35] that to one loop order in perturbation theory the following relation holds:

$$A(p^2, p^2; 0) - A(0, p^2; p^2) + B(0, p^2; p^2) = 0 \tag{3.9}$$

So at one loop, Eq 2.49 becomes:

$$\Gamma_{\lambda\mu\nu}(p, -p, 0) = (2g_{\lambda\mu}p_\nu - g_{\lambda\nu}p_\mu - g_{\mu\nu}p_\lambda)\, T_1(p^2) - p_\nu \left(g_{\lambda\mu} - \frac{p_\lambda p_\mu}{p^2} \right) T_2(p^2) \tag{3.10}$$

where we have defined:

$$\begin{aligned} T_1(p^2) &= A(p^2, p^2; 0) \\ T_2(p^2) &= -2p^2 C(p^2, p^2; 0) \end{aligned} \tag{3.11}$$

to be consistent with [27].

Recalling the tree-level vertex function Eq 2.41, we have, ignoring the colour dependence:

$$\Gamma^{tree}_{\lambda\mu\nu}(p, -p, 0) = -ig\,(2g_{\lambda\mu}p_\nu - g_{\lambda\nu}p_\mu - g_{\mu\nu}p_\lambda) \tag{3.12}$$

We can now write Eq 3.10 to one loop order as:

$$-ig\Gamma_{\lambda\mu\nu}(p, -p, 0) = \Gamma^{tree}\left(1 + T_1^{1loop}\right) + igp_\nu \left(g_{\lambda\mu} - \frac{p_\lambda p_\mu}{p^2} \right) T_2^{1loop} \tag{3.13}$$

where we have reintroduced the factor $-ig$ which we removed in Eq 2.43. T_1^{1loop} and T_2^{1loop} are the one loop perturbative contributions to T_1 and T_2 respectively.

The pure gauge T_1^{1loop}, T_2^{1loop} calculated using dimensional regularisation are given in [28]. I have reproduced these below:

$$T_1^{(1loop,\alpha)}(p^2) = C_A \frac{g^2\eta}{(4\pi)^{n/2}}(-p^2)^{-\varepsilon} \qquad \left[\frac{1}{\varepsilon}\left(-\frac{2}{3}-\frac{3}{4}\alpha\right) - \frac{35}{18} + \frac{1}{2}\alpha - \frac{1}{4}\alpha^2 \right.$$
$$\left. +\varepsilon\left(-\frac{107}{27}+\alpha-\frac{1}{2}\alpha^2\right)\right] + O(\varepsilon^2) \tag{3.14}$$

$$T_2^{(1loop,\alpha)}(p^2) = C_A \frac{g^2\eta}{(4\pi)^{n/2}}(-p^2)\left[-\frac{4}{3} - 2\alpha + \frac{1}{4}\alpha^2 + \varepsilon\left(-\frac{26}{9} - \alpha + \frac{1}{4}\alpha^2\right)\right] + O(\varepsilon^2) \tag{3.15}$$

Here, C_A is defined by $C_A = N$ for an $SU(N)$ gauge theory, so for us, $C_A = 3$. n is the space-time dimension $n = 4 - 2\varepsilon$.

η is defined by:

$$\eta = e^{-\gamma\varepsilon}\left(1 - \frac{1}{12}\pi^2\varepsilon^2 + O(\varepsilon^3)\right) \tag{3.16}$$

where $\gamma = 0.577215....$ is the Euler constant. As $n \to 4$, $\eta \to 1$.

α is the gauge parameter, and is related to ξ in section 1.1 by $\alpha \equiv 1 - \xi$. In the Landau gauge, $\alpha = 1$. If we renormalise the expressions in the $\overline{MS}$ scheme, we get (when $\varepsilon \to 0$):

$$T_1^{1loop} = \frac{3g^2_{\overline{MS}}}{(4\pi)^2}\left[-\frac{35}{18} + \frac{1}{2} - \frac{1}{4}\right] = -\frac{g^2_{\overline{MS}}}{(4\pi)^2}C_V \tag{3.17}$$

$$T_2^{1loop} = \frac{3g^2_{\overline{MS}}}{(4\pi)^2}\left[-\frac{4}{3} - 2 + \frac{1}{4}\right] = -\frac{g^2_{\overline{MS}}}{(4\pi)^2}C_E \tag{3.18}$$

where we have defined:

$$\begin{aligned} C_V &= \tfrac{61}{12} \\ C_E &= \tfrac{37}{4} \end{aligned} \tag{3.19}$$

So, from Eq 3.13 we have:

$$-ig\Gamma_{\lambda\mu\nu} = \Gamma^{tree}\left(1 + C_V\frac{g^2_{\overline{MS}}}{(4\pi)^2}\right) - igp_\nu\left(g_{\lambda\mu} - \frac{p_\lambda p_\mu}{p^2}\right)\frac{g^2_{\overline{MS}}}{(4\pi)^2}C_E \tag{3.20}$$

but for the Landau gauge, we need $\lambda = \mu$, so:

$$\begin{aligned} -ig\sum_\lambda \Gamma_{\lambda\lambda\nu} &= 6igp_\nu\left(1 + C_V\frac{g^2_{\overline{MS}}}{(4\pi)^2}\right) - 3igp_\nu\frac{g^2_{\overline{MS}}}{(4\pi)^2}C_E \\ &= 6igp_\nu\left(1 + \frac{g_{\overline{MS}^2}}{(4\pi)^2}\left(C_V - \frac{C_E}{2}\right)\right) \end{aligned} \tag{3.21}$$

where we have put $g_{\lambda\lambda} = \delta_{\lambda\lambda}$.

We now equate the two expressions for the unrenormalised three-gluon vertex (Eq's 3.7 and 3.21):

$$\Gamma_U = -6\left(Z_3^{\widetilde{MOM}}\right)^{-1} p_\gamma = -6\left(Z_3^{\overline{MS}}\right)^{-1} p_\nu\left(1 + \frac{g_{\overline{MS}^2}}{(4\pi)^2}\left(C_V - \frac{C_E}{2}\right)\right) \tag{3.22}$$

So:

$$\frac{Z_3^{\widetilde{mom}}}{Z_3^{\overline{MS}}} = \left[1 + \frac{g^2_{\overline{MS}}}{16\pi^2}\left(C_V - \frac{C_E}{2}\right)\right]^{-1} \tag{3.23}$$

3.3 $Z_A^{\overline{MS}}$

The Z_A numbers are defined via the gluon propagator. To one loop order, the gluon propagator is given by [23, Eq's 9 and 10]:

$$\Pi_{ab}^{\mu\nu}(p) = -i\delta_{ab}\left\{\left[\left(g^{\mu\nu} - \frac{p^\mu p^\nu}{p^2}\right)\frac{1}{p^2}\right]h(p^2) + \xi\frac{p^\mu p^\nu}{p^2} + O(\varepsilon)\right\}\mu^\varepsilon \tag{3.24}$$

where,

$$\begin{aligned} h(p^2) = 1 + \frac{g^2 C_2(G)}{16\pi^2} \quad & \left\{-\frac{13}{6}\left[\frac{2}{\varepsilon} + \gamma_E - \ln(4\pi) + \ln\left(\frac{-p^2}{\mu^2}\right)\right] + \frac{97}{36}\right. \\ & \left. +\xi\left(\frac{1}{2}\left[\frac{2}{\varepsilon} + \gamma_E - \ln(4\pi) + \ln\left(\frac{-p^2}{\mu^2}\right)\right] + \frac{1}{2}\right) + \xi^2\left(\frac{1}{4}\right)\right\} \end{aligned}$$

$$+\frac{g^2}{16\pi^2}T(R)n_F \quad \left\{\frac{4}{3}\left[\frac{2}{\varepsilon}+\gamma_E-\ln(4\pi)+\ln\left(\frac{-p^2}{\mu^2}\right)\right]-\frac{20}{9}\right\}-(Z_A\mu^{-\varepsilon}-1) \tag{3.25}$$

Here, $C_2(G)$ is the same as the C_A in Eq's 3.14 and 3.15 and is 3 for SU(3). γ is the Euler constant.

In the Landau gauge we have $\xi = 0$. We are interested in flavourless QCD, so the number of flavours n_f is zero. In the notation of Eq 2.51 we are left with:

$$G^{(2)\,\overline{MS}}_{\mu\nu} = T_{\mu\nu}\cdot\frac{1}{p^2}\cdot h^{\overline{MS}}(p^2) \tag{3.26}$$

where:

$$T_{\mu\nu} = \delta_{\mu\nu} - \frac{p_\mu p_\nu}{p^2} \tag{3.27}$$

and:

$$h(p^2) = 1+\frac{g^2C_2(G)}{16\pi^2}\left\{-\frac{13}{6}\left[\frac{2}{\varepsilon}+\gamma_E-\ln(4\pi)+\ln\left(\frac{-p^2}{\mu^2}\right)\right]+\frac{97}{36}\right\}-(Z_A\mu^{-\varepsilon}-1) \tag{3.28}$$

In the $\overline{MS}$ scheme, we renormalise the propagator by defining Z_A to remove the poles in ε and also the associated terms with logs and γ's. This gives us:

$$h^{\overline{MS}}(p^2) = 1+\frac{3g^2_{\overline{MS}}}{16\pi^2}\left\{-\frac{13}{6}\ln\left(\frac{-p^2}{\mu^2}\right)+\frac{97}{36}\right\} \tag{3.29}$$

3.4 $Z_A^{\widetilde{MOM}}$

The MOM scheme differs from the $\widetilde{MOM}$ scheme only in the leg momenta of the three-gluon vertex. The renormalisation of the gluon propagator is defined in the same way. From [23, Eq 12] we have:

$$h^{\widetilde{MOM}}(p^2) = 1 + g^2_{\widetilde{MOM}} K \ln\left(\frac{-p^2}{M^2}\right) \tag{3.30}$$

where K is some arbitrary factor and M is the momentum scale at which we renormalise.

We relate the unrenormalised propagator $G_U^{(2)}$ to the renormalised ones by:

$$G_U^{(2)} = (Z_A^{\overline{MS}})^{-1} G^{(2)\,\overline{MS}} = (Z_A^{\widetilde{MOM}})^{-1} G^{(2)\,\widetilde{MOM}} \tag{3.31}$$

So:

$$\begin{aligned} \frac{Z_A^{\overline{MS}}}{Z_A^{\widetilde{MOM}}} &= \frac{G^{(2)\,\overline{MS}}}{G^{(2)\,\widetilde{MOM}}} = \frac{h^{\overline{MS}}}{h^{\widetilde{MOM}}} \\ &= \frac{1 + \frac{3g^2_{\overline{MS}}}{16\pi^2}\left\{-\frac{13}{6}\ln\left(\frac{-p^2}{\mu^2}\right) + \frac{97}{36}\right\}}{1 + g^2_{\widetilde{MOM}} K \ln\left(\frac{-p^2}{M^2}\right)} \end{aligned} \tag{3.32}$$

We choose to renormalise at the same energy in the $\overline{MS}$ and $\widetilde{MOM}$ schemes, so we put $M = \mu$. After expanding the denominator using Eq 3.2, Eq 3.32 becomes:

$$\frac{Z_3^{\overline{MS}}}{Z_3^{\widetilde{MOM}}} = 1 + \frac{3g^2_{\overline{MS}}}{16\pi^2} . \frac{97}{36} + (g^4) = 1 + \frac{C_A g^2_{\overline{MS}}}{16\pi^2} + (g^4) \tag{3.33}$$

where:

$$C_A = 3\frac{97}{36} \tag{3.34}$$

3.5 Perturbative Matching of $\Lambda_{\overline{MS}}$ and $\Lambda_{\widetilde{MOM}}$

From Eq's 3.6,3.23 and 3.33 we get:

$$\frac{g^2_{\overline{MS}}}{g^2_{\widetilde{MOM}}} = \left(1 + \frac{C_A g^2_{\overline{MS}}}{16\pi^2}\right)^3 \left[1 + \frac{g^2_{\overline{MS}}}{16\pi^2}\left(C_V - \frac{C_E}{2}\right)\right]^{-2}$$

$$
\begin{aligned}
&= \left(1+\frac{3C_A g^2_{\overline{MS}}}{16\pi^2}\right)\left(1-\frac{2g^2_{\overline{MS}}}{16\pi^2}\left(C_V-\frac{C_E}{2}\right)\right) \\
&= 1+g^2_{\overline{MS}}\left[\frac{3C_A}{16\pi^2}-\frac{2}{16\pi^2}\left(C_V-\frac{C_E}{2}\right)\right]
\end{aligned}
\tag{3.35}
$$

If we compare with Eq 3.2 we see that:

$$
C_{AB} = -\left[\frac{3}{4\pi}C_A - \frac{2}{4\pi}\left(C_V-\frac{C_E}{2}\right)\right] = -1.856807.... \tag{3.36}
$$

From Eq 3.4 with $b_0 = 11/16\pi^2$ for quenched QCD, we get:

$$
\frac{\Lambda_{\overline{MS}}}{\Lambda_{\widetilde{MOM}}} = \exp\left[\frac{C_{AB}}{8\pi b_0}\right] = 0.34625 \tag{3.37}
$$

which is quoted in [19].

3.6 Comment

Eq 3.37 is an important result for us. In the next chapter, we shall perform fits to the data in section 2.10. These fits will give us Λ in the $\widetilde{MOM}$ scheme. Results are normally quoted in the $\overline{MS}$ scheme. It is therefore important for us to be able to convert our fit result to $\overline{MS}$ so as to compare with other determinations of Λ.

As an example, in [29], $\Lambda_{\overline{MS}}$ has been calculated on the lattice to give:

$$
\Lambda_{\overline{MS}} = 0.238(19)\text{GeV} \tag{3.38}
$$

Using Eq 3.37 we can give $\Lambda_{\widetilde{MOM}}$:

$$
\Lambda_{\widetilde{MOM}} = 0.687(55)\text{GeV} \tag{3.39}
$$

We shall make frequent use of this result in the next chapter.

Chapter 4

Search for Power Corrections to α_S

4.1 Introduction

We now make an analysis of the running coupling data in section 2.10. We try and determine whether the data supports the notion that the running coupling contains power corrections to the perturbative expressions. The method employed is to fit expressions to the data to determine which provides the best model for the coupling. This chapter covers research which was first presented in [26].

4.2 Why do we Expect Power Corrections?

The running coupling is defined by Eq 2.23. We have shown how to calculate this perturbatively by writing the beta function as a power expansion in α_s. However, it is possible that the beta function contains contributions which would not show up in such a power expansion. For example, if the running coupling had a term like $\exp(-b_0/\alpha_s)$, then this could not show up in any finite expansion in α_s. We must allow for the idea that the perturbative running coupling is ambiguous due to non-perturbative contributions α_N. ie:

$$\alpha_s(p^2) = \alpha_P(p^2) + \alpha_N(p^2) \tag{4.1}$$

where α_P is the perturbative part.

We parameterise the non-perturbative contribution as a power expansion:

$$\alpha_N(p^2) = \sum_{n=1}^{\infty} \frac{c_n}{p^{2n}} \tag{4.2}$$

So we expect that the first non-perturbative contribution to show up as we approach small momenta is c_1/p^2. To a first approximation we expect:

$$\alpha_s = \alpha_P + \frac{c}{p^2} \tag{4.3}$$

We shall now consider several theoretical arguments as to why such a term might be expected. None of these are conclusive, but they are suggestive and motivate us to further study.

4.2.1 The Potential Argument

We consider a definition of the coupling by analogy with the coulomb potential in electrostatics:

$$\alpha(p) = \frac{3}{4} R^2 \frac{dV(R)}{dR} \tag{4.4}$$

where V is the static inter-quark potential and R is the separation which is related to the characteristic momentum by $p = 1/R$. In the one gluon approximation, it is found that:

$$V(r) \propto \alpha_s \int d^3k \frac{exp(ik \cdot r)}{|k|^2} \tag{4.5}$$

We now generalise this and assume its validity when α is a running coupling:

$$V(r) \propto \int d^3k \alpha_s \frac{exp(ik \cdot r)}{|k|^2} \tag{4.6}$$

If we suppose that α_s contains a c/p^2 term then this would contribute to the potential a linear term Kr. This is of interest since such a term is confining (ie increasing the potential with distance). A term like this would be necessary to explain confinement in QCD[30, 31].

It is also interesting that the non-perturbative string tension term Kr leads to ambiguity when we define the running coupling on the lattice from the "force" definition (Eq 4.4)[32].

4.2.2 The Gluon Condensate

The standard way of parameterising non-perturbative corrections is using the operator product expansion[33]. This can be proven perturbatively, and its validity was extended for use beyond perturbation theory by [34].

A potential problem with the OPE has arisen through a lattice calculation of the gluon condensate[35] which we now describe.

The gluon condensate is defined by:

$$W = \frac{\langle TrG^2 \rangle}{Q^4} \tag{4.7}$$

where G is the gluon propagator and Q is momentum scale with respect to which the coupling α_s runs (see section 2.5). The operator product expansion tells us that:

$$W = W_0 + (\Lambda^4/Q^4)W_4 + ... \tag{4.8}$$

There is no term with Λ^2/Q^2 because there are no gauge invariant operators of order two in the theory.

Λ has no power expansion in terms of α_s, which tells us that the perturbative contribution to the condensate must be in the term W_0. It can be shown that the term W_0 is made up of the perturbative part of the gluon condensate plus a contribution from a renormalon[1][36] which goes as Λ^4/p^4. It follows from this and Eq 4.8 that we expect:

$$W - W^{Pert} \sim \frac{\Lambda^4}{p^4} \tag{4.9}$$

W can be determined by Monte Carlo simulations on the lattice. W^{Pert} can be determined up to ten loops on the lattice[37]. It is found[35] that

[1]A renormalon is a non perturbative term which arises due to performing an infinite sum of perturbative diagrams

$W - W^{pert} \sim \Lambda^2/p^2$ which seems to dramatically contradict the predictions of the operator product expansion.

It has been pointed out[30, 36, 38] that this problem can be solved while still maintaining the validity of the OPE. The gluon condensate can be written in the general form[39]:

$$W = \int_0^{Q^2} \frac{k^2 dk^2}{Q^4} f(k^2/\Lambda^2) \tag{4.10}$$

where Q is the ultraviolet cutoff which is π/a on a lattice with lattice spacing a. We have assumed an infinite lattice, so there is no infrared cutoff. If we consider $f(k^2/\Lambda^2)$ as a power expansion in α_s, then the condensate has a contribution:

$$W = \int_0^{Q^2} \frac{k^2 dk^2}{Q^4} \alpha_s(k^2) \tag{4.11}$$

which becomes a valid expression for the condensate at large k^2. Now, if α_s has a non-perturbative contribution of the type we have been considering, we get the following non-perturbative correction to W:

$$W = \int_0^{Q^2} \frac{k^2 dk^2}{Q^4} \frac{c}{k^2} = \frac{c}{Q^2} \tag{4.12}$$

We see that the unexpected power correction may have arisen from a power correction to the running coupling. This would leave the validity of the OPE intact.

4.2.3 The Landau Pole

This argument[40, 41, 42] concerns the poles that occur in perturbative expressions for the coupling. These expressions are not valid in the regions where the poles exist because perturbation theory is not relevant when the coupling is large. Since we expect that the "true" running coupling has no poles, we can consider adding non-perturbative corrections to the perturbative coupling with a view to removing them.

For example, at the one loop level, the analytic pole in Eq 2.32 is cancelled by the addition of a non-perturbative term:

$$\alpha_s = \frac{1}{4\pi b_0 \ln(p^2/\Lambda^2)} + \frac{\Lambda^2}{4\pi b_0(\Lambda^2 - p^2)} \tag{4.13}$$

The non perturbative term contains a power correction of the form Λ^2/p^2. Here the sign of the power correction is opposite to what we expect from the results of section 4.2.2. However, we may consider a more general kind of correction such as:

$$\alpha_s = \frac{1}{4\pi b_0 \ln(p^2/\Lambda^2)} + \frac{\Lambda^2}{4\pi b_0(\Lambda^2 - p^2)} + c\frac{\Lambda^2}{p^2} \tag{4.14}$$

4.3 The Perturbative Part

Our objective now is to use the data presented in Section 2.10 to look for power corrections. The general idea is to fit Eq 4.3 to the data to determine c.

We expect that if Eq 4.3 contains the major non-perturbative correction, then it should be valid to lower momenta than perturbation theory on its own. We expect it to produce a good fit to the data provided that:

- The perturbative part α_P is known accurately enough.
- c^2/p^2 is the only significant non-perturbative contribution.

The first point is the requirement that α_s is small enough for the perturbative formulae to be meaningful. The second point is the obvious statement that other terms come into play at even lower momenta and mess up our ansatz. Establishing evidence for Eq 4.3 means finding a region where it holds in between where α_s is purely perturbative, and where perturbation theory breaks down completely.

The perturbative part of Eq 4.3 is given to one loop and two loop orders by Eq 2.32 and Eq 2.33 respectively. At three loops, it is necessary to solve the following equation[20, 21] for α_s:

$$\Lambda_{\widetilde{MOM}} = \Lambda^{(c)}(\alpha_s)\left(1+\frac{\beta_1\alpha_s}{2\pi\beta_0}+\frac{\beta_2^{\widetilde{MOM}}\alpha_s^2}{32\pi^2\beta_0}\right)^{\beta_1/2\beta_0^2}$$
$$\times\exp\left\{\frac{\beta_0\beta_2^{\widetilde{MOM}}-4\beta_1^2}{2\beta_0^2\Delta}\left[\arctan\left(\frac{\Delta}{2\beta_1+\beta_2^{\widetilde{MOM}}\alpha_s/4\pi}\right)-\arctan\left(\frac{\Delta}{2\beta_1}\right)\right]\right\} \tag{4.15}$$

where $\Lambda^{(c)}$ is the two loops formula:

$$\Lambda^{(c)} \equiv p\exp\left(\frac{-2\pi}{\beta_0\alpha_s}\right)\times\left(\frac{\beta_0\alpha_s}{4\pi}\right)^{-\beta_1\beta_0^2} \tag{4.16}$$

and $\Delta \equiv \sqrt{2\beta_0\beta_2^{\widetilde{MOM}}-4\beta_1^2}$

Here $\beta_0 = 11$ and $\beta_1 = 51$. $\beta_2^{\widetilde{MOM}}$ is not universal and so is dependent on the scheme in which it is calculated, hence the superscript $\widetilde{MOM}$. It is given by[20]:

$$\beta_2^{\widetilde{MOM}} = 4824.31 \tag{4.17}$$

An exact analytical solution to Eq 4.15 does not exist, however an approximate solution which is correct to three loops is[26]:

$$\alpha_s(p^2) = \frac{4\pi}{\beta_0 t} - \frac{8\pi\beta_1}{\beta_0}\frac{\ln(t)}{(\beta_0 t)^2} + \frac{1}{(\beta_0 t)^3}\left(\frac{2\pi\widetilde{\beta}_2}{\beta_0} + \frac{16\pi\beta_1^2}{\beta_0^2}(\ln^2(t) - \ln(t) - 1)\right) \tag{4.18}$$

where $t = \ln(p^2/\Lambda^2)$.

Alternatively, we can solve Eq 4.15 exactly on a computer using numerical methods.

We refer to Eq 4.18 as the formula solution and to the numerical method as the numerical inversion. Both methods are equally valid to three loops, so we cannot really choose one over the other as a prefered method. However, the most common procedure is to use the numerical inversion. This was used in determining Eq 3.38[29] to which we make significant comparison when making the fits in Section 4.8.

4.4 Fitting Procedure

The standard way in which we determine how well an equation for a curve is a good fit to a given set of data is by calculating the statistical quantity $\chi^2_{d.o.f.}$. If the data varies with parameter p and the function to match the data is $\alpha_s(p)$, then χ^2 is defined by:

$$\chi^2 = \sum_t \left[\frac{(\alpha_s(p) - \mathrm{Data}(p))}{\mathrm{DataError}(p)}\right]^2 \tag{4.19}$$

where DataError(p) is the error on the data point defined at p.

The best fit is determined by minimising χ^2 with respect to the variables in the expression for $\alpha_s(p)$.

To decide how well a given fit matches to the data, we need to divide χ^2 by the degree of freedom (d.o.f.) to give $\chi^2_{d.o.f.}$. The degree of freedom is calculated by subtracting the number of fit parameters from the number of data points. A good fit is when $\chi^2_{d.o.f.}$ is approximately one or less.

We require that the fits include a reasonably large section of the data. We also require that the fit parameters are stable with respect to changing initial and final points.

We define two sorts of fits. We perform fits to Eq 4.18 and to the numerical inversion of Eq 4.15. We call these "pure" fits. We also perform fits to our ansatz Eq 4.3 with the perturbative part α_P coming either from Eq 4.18 or the numerical inversion of Eq 4.15. We call these "corrected" fits. The fits would support our ansatz if the corrected fits were better than the pure ones, particularly when low momenta are included.

4.5 Note on some Preliminary Fits

As a preliminary analysis, we fit to each of the data sets in section 2.10 independently. The hope is to obtain good fits to each set and then compare the fit parameters to determine the volume dependence of $\Lambda_{\widetilde{MOM}}$ and c. We choose to ignore the data in Fig 2.4 because the errors on this data set are much greater than on any of the others. We also ignore the data at $\beta = 6.8$ since this had not been generated at the time this analysis was carried out. We consider fits

Data Set		Pure Fits	
Lattice	β	$\Lambda_{\widetilde{MOM}}$	$\chi^2_{d.o.f.}$
16^4	6.0	0.776^{4}_{30}	1.05
24^4	6.0	0.782^{0}_{78}	1.08
24^4	6.2	0.790^{7}_{2}	0.96
24^4	6.4	0.755^{34}_{3}	2.00
32^4	6.4	0.806^{0}_{32}	1.91

Table 4.1: Results of pure fits to Eq 4.18 for some of the data in section 2.10. $\Lambda_{\widetilde{MOM}}$ is in GeV.

that cover a momentum range of at least 0.7GeV. We use the formula Eq 4.18 for the perturbative part, and do not make any fits with Eq 4.15 at this stage.

The pure perturbative fits turned out to be reasonably stable and consistent. The results are given in Table 4.1. The values presented were selected on the basis that they had the lowest $\chi^2_{d.o.f.}$. The errors quoted are the fit errors determined by the variation in Λ within the region of stability of the fits, and so are somewhat less than they should be and heavily dependent on what we choose to be the region of stability. Nevertheless, it is clear that the results are somewhat higher than those of Eq 3.39[29].

The corrected fits showed no real sign of stability or consistency.

4.6 Feasibility of Determining a Power correction by Fitting to the Data

We now attempt a more careful study of the data to look for a power correction. In what follows, we systematically convert all results for $\Lambda_{\widetilde{MOM}}$ into $\Lambda_{\overline{MS}}$ using Eq 3.37.

Before performing any more fits, we can ask whether it is reasonable to expect to determine a power correction from data at the energies that we are working. This question divides into two parts:

- Is the power correction big enough at the energies we are working to be detected over the errors of the data?
- Do we know the perturbative part of the running coupling well enough at these energies so that the non-perturbative part can be distinguished?

The first question is answered by studying the quality and stability of fits to a correction term. We shall return to this in Section 4.8. We now address the second question.

We note that the perturbative contribution is known down to some momentum where perturbation theory breaks down. The perturbative equations can be used with the value of $\Lambda_{\overline{MS}}$ in Eq 3.38. Since Λ is known, we do not have to obtain it from a fit to the data.

In Fig 4.1 we plot the perturbative results Eq's 2.32,2.33,4.18 and the numerical inversion of Eq 4.15 with $\Lambda_{\overline{MS}} = 0.238\text{GeV}$ from Eq 3.38.

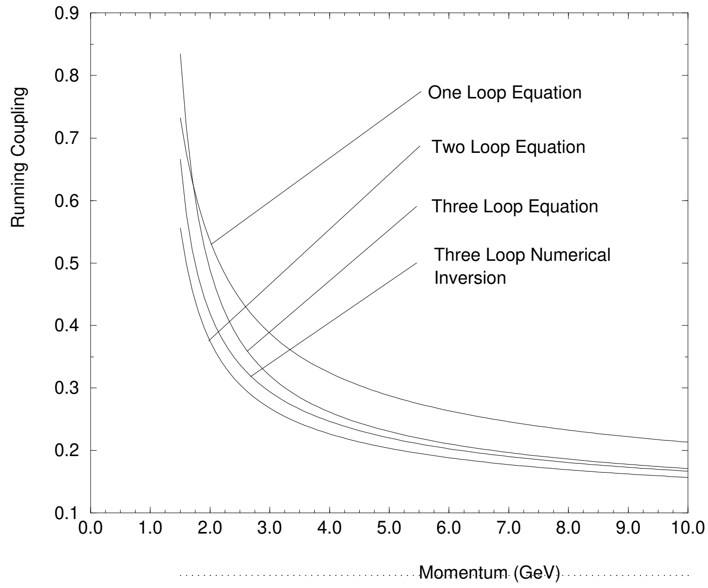

Figure 4.1: Plot of the running coupling as a function of momentum in GeV in our region of interest. It is calculated to one, two and three loops using Eq 2.32, Eq 2.33 and Eq 4.18 respectively. It is also calculated using the numerical inversion of Eq 4.15. In each, $\Lambda_{\overline{MS}} = 0.238\text{GeV}$ was used (from Eq 3.38).

These clearly differ significantly in our region of interest which is $2 \to 10$ GeV. However, the two three-loop estimates are quite similar.

As we have noted, Eq 4.18 and the numerical inversion of Eq 4.15 only differ from each other at the higher than three loop level. We can therefore interpret their difference as an uncertainty in the perturbative part of the running coupling due to higher than three loop effects. I have plotted this difference as a percentage of the numerical inversion of Eq 4.15 in Fig 4.2. The question is whether this perturbative uncertainty would make it unlikely for the power correction in our ansatz to show up.

If we imagine that we have a power correction with $c = 0.6\text{GeV}^2$, then we can plot this as a percentage of the numerical inversion. This is also plotted in Fig 4.2.

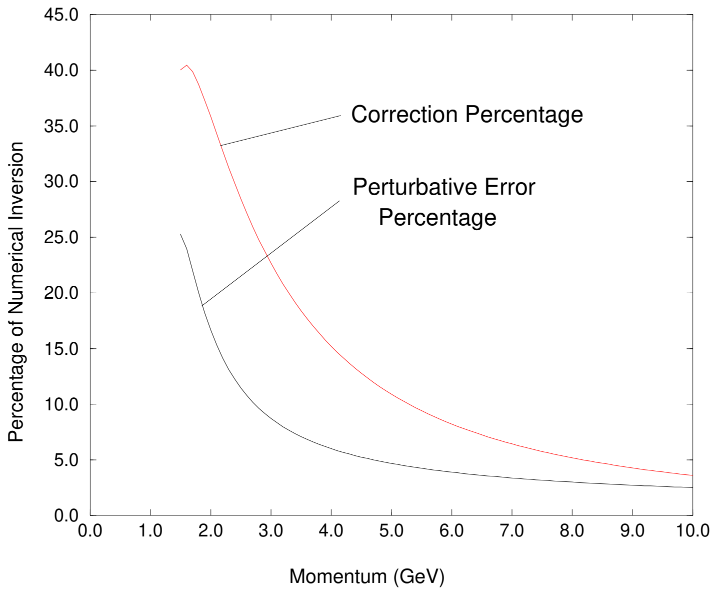

Figure 4.2: Plot of the perturbative error as a percentage of the numerical inversion with $\Lambda_{\overline{MS}} = 0.238\text{GeV}$. The perturbative error is defined to be the difference between the 3 loop formula (Eq 4.18) and the numerical inversion. Also plotted is c/p^2 as a percentage of the numerical inversion with $c = 0.6\text{GeV}^2$ and $\Lambda_{\overline{MS}} = 0.238\text{GeV}$.

This clearly shows us that we should be able to distinguish a power correction of this magnitude from the perturbative part provided that the data is not too noisy.

4.7 Construction of the Data Set

Instead of fitting to the data sets separately, I shall perform fits to a data set formed from an aggregate of the data sets in section 2.10. The advantage of this is that the high momenta results of Fig 2.7 will fix the perturbative part. Also with more data to fit to, we should expect more stable fits if our ansatz is correct.

Here we construct an aggregated data set on a 24^4 lattice by putting together data for various β values. In restricting to the 24^4 lattice, we do not loose much data since most of the other lattice data is ruled out by other criteria.

We see from Fig 2.7 that there is a significant finite volume effect for quite high energies at $\beta = 6.8$. The effect is not so pronounced for the other values of β. We have only one $\beta = 6.2$ and so cannot make a direct volume effect comparison.

Our method for producing the aggregated 24^4 data set is the following. We include the large momenta points of each data sets since these are least likely to suffer from finite volume effects and perturbative errors. The lower momenta cut off P_{min} is defined such that adding data lower than this momentum causes the $\chi^2_{d.o.f.}$ in fits to increase notably. This gives:

- $P_{min}(\beta = 6.0) = 2.0$ GeV
- $P_{min}(\beta = 6.2) = 2.5$ GeV
- $P_{min}(\beta = 6.4) = 4.0$ GeV

- $P_{min}(\beta = 6.8) = 6.0$ GeV

The resulting data set is plotted in Fig 4.3.

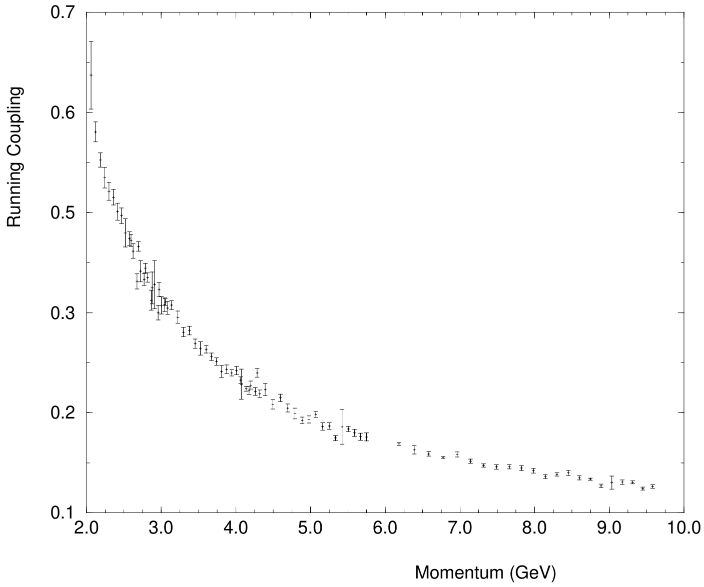

Figure 4.3: This graph shows the data for the running coupling which we analyse in the rest of this chapter. It is formed from aggregating data from 24^4 lattices with $\beta = (6.0, 6.2, 6.4, 6.8)$ (see Figs 2.3,2.5,2.6,2.7).

In the next section we focus our efforts on an analysis of this data set to determine the existence or otherwise of a power correction to the running coupling.

A further demonstration that a three loop analysis contains the perturbative part quite well comes from subtracting the three loop formula and the three loop numerical inversion from the aggregated data set. In doing this, we gain a direct estimate of the non-perturbative part of the data. This is plotted in Fig 4.4 where we have ignored error-bars. The one and two loop subtractions are also plotted for comparison.

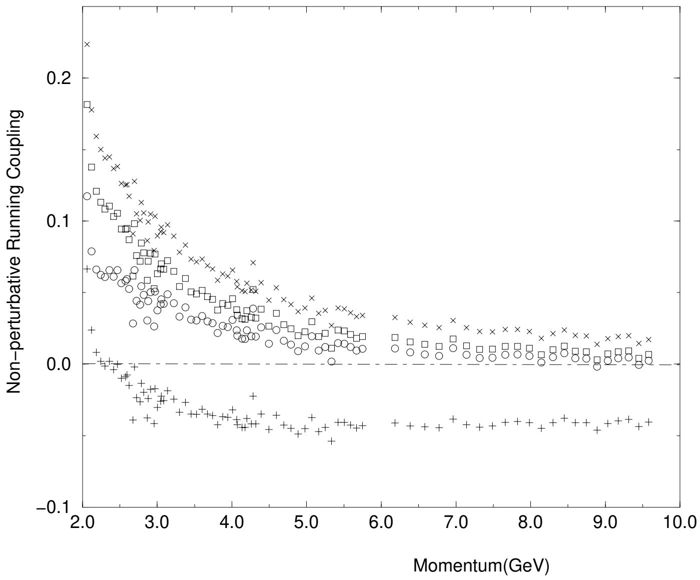

Figure 4.4: This is an estimate of the non-perturbative running coupling obtained from subtracting the various perturbative estimates (Fig 4.1) from the running coupling data in Fig 4.3. There are four determinations of the perturbative coupling which we have subtracted. These are the one loop equation (symbol "+"), two loop equation (symbol "×"), three loop equation (symbol "∘") and the three loop numerical inversion (symbol "□"). The error-bars on the points are point for point the same as in Fig 4.3, but have been omitted here for clarity.

We see that both the three loop estimates become similar and are close to zero at 10GeV indicating that perturbative scaling has been reached.

4.8 Fits to the Aggregated Data Set

In this section we perform fits to the running coupling data set in Fig 4.3. We include all the high momentum points since these are least likely to suffer from finite lattice size effects. Further to this, the high momenta points provide a fix on the perturbative tail which is very useful for us. In any case, each fit was found to be stable with respect to removing high momentum points. We consider the stability of fits with respect to varying the lowest momentum points. The fits for every fourth lowest momentum point are presented.

4.8.1 Determination of c From one Parameter Fits

We first consider fits of the non-perturbative correction term c/p^2 directly to the non-perturbative data in Fig 4.4 (with the error-bars given in Fig 4.3).

We perform fits of c/p^2 for the non-perturbative data generated with the three loop formula. The results for c and the $\chi^2_{d.o.f.}$ for each fit are given in Table 4.2. We do the same thing for the data generated using the three loop numerical inversion. These results are in Table 4.3. The errors in these tables come the errors in Eq 3.38 as we now describe.

The non-perturbative graphs were obtained by subtracting the perturbative formulae calculated with $\Lambda_{\overline{MS}} = 0.238$GeV from Eq 3.38. This has errors on it of ± 0.019GeV. We therefore calculate the non-perturbative again, but using $\Lambda_{\overline{MS}} = 0.219$GeV and $\Lambda_{\overline{MS}} = 0.257$GeV. We fit c/p^2 to the non-perturbative data calculated with $\Lambda_{\overline{MS}} = 0.219$GeV to obtain the upper bound on c. We then subtract the central value of c given in the Tables 4.2 and 4.3 to obtain the upper error. A similar procedure applies to determining the lower error using $\Lambda_{\overline{MS}} = 0.257$GeV. The upper and lower errors are similar, so we only quote the upper one.

We see that we obtain a better $\chi^2_{d.o.f.}$ from the numerical inversion fits. The $\chi^2_{d.o.f.}$ and stability of c indicate that the non-perturbative data are fitted quite well by a power correction of the type postulated. We can see this visually by plotting c/p^2 against the non-perturbative data. For the numerical inversion we get Fig 4.5.

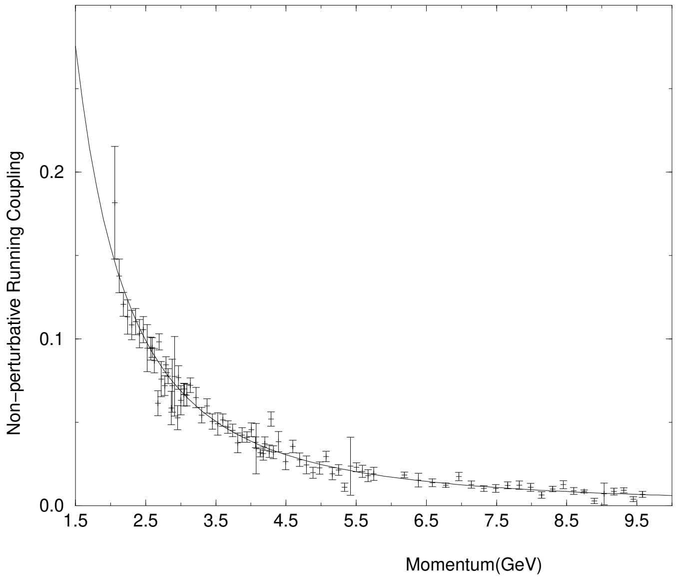

Figure 4.5: Plot of the non-perturbative correction term c/p^2 (with $c = 0.62$ taken from the fits in Table 4.3) against the non-perturbative data. The non-perturbative data is generated by subtracting the numerical inversion from the full running coupling of Fig 4.3 (see Fig 4.4).

The fits in Tables 4.2 and 4.3 agree within errors. The difference comes from

Initial Momentum(GeV)	$c(\mathrm{GeV}^2)$	Upper Error(GeV^2)	$\chi^2_{d.o.f.}$
2.06	0.372	0.217	1.90
2.30	0.376	0.217	1.93
2.52	0.377	0.219	2.01
2.67	0.376	0.222	2.11
2.79	0.377	0.225	1.94
2.91	0.376	0.230	1.99
3.04	0.378	0.233	2.01
3.22	0.366	0.242	1.99
3.53	0.359	0.250	2.04
3.81	0.348	0.261	2.11
4.07	0.336	0.271	2.12
4.20	0.337	0.287	2.28
4.39	0.313	0.301	1.81

Table 4.2: Fits of c/p^2 to the non-perturbative data in Fig 4.4. The perturbative estimate is from Eq 4.18 (the points marked with a $\circ$). Fits are performed with varying initial points to check for stability. Here, the fit for every fourth initial momentum is shown.

Initial Momentum(GeV)	$c(\mathrm{GeV}^2)$	Upper Error(GeV^2)	$\chi^2_{d.o.f.}$
2.06	0.620	0.175	1.61
2.30	0.623	0.177	1.64
2.52	0.625	0.180	1.71
2.67	0.625	0.183	1.79
2.79	0.627	0.188	1.59
2.91	0.628	0.194	1.63
3.04	0.631	0.197	1.60
3.22	0.625	0.207	1.63
3.53	0.623	0.216	1.71
3.81	0.619	0.227	1.82
4.07	0.613	0.237	1.89
4.20	0.624	0.253	1.97
4.39	0.611	0.268	1.67

Table 4.3: Fits of c/p^2 to the non-perturbative data in Fig 4.4. The perturbative estimate is from the numerical inversion of Eq 4.15 (the points marked with a $\square$). Fits are performed with varying initial points to check for stability. Here, the fit for every fourth initial momentum is shown.

uncertainties in the perturbative estimate.

4.8.2 Determination of Λ From one Parameter Fits

It may be suggested that the power correction term is just mimicking the effect of a higher loop perturbative analysis. This seems unlikely since we have shown in Figs 4.2 and 4.4 that the three loop estimate of the perturbative part is quite sound. Also, Fig 4.5 shows that a c/p^2 term matches the non-perturbative data very well.

Nevertheless we can check this suggestion to some extent by allowing Λ to vary to fit the data. Λ has a log dependence, so a slight variation will mimic to some extent a higher loop analysis.

For the formula and numerical inversion we obtain Tables 4.4 and 4.5 respectively. It is clear that the $\chi^2_{d.o.f.}$ on these fits are unacceptable and that the data clearly has a significant non-perturbative contribution.

4.8.3 Determination of Λ and c from two Parameter Fits

Clearly, the best approach is to allow a fit for a free Λ and c. Here the hope is that the variation in Λ will account to some extent for the higher perturbative orders. This would then lessen the discrepancy between Eq 4.18 and the numerical inversion of Eq 4.15. If our ansatz Eq 4.3 is correct, there should be less discrepancy between the values for c.

For the formula and numerical inversion we obtain Tables 4.6and 4.7 respec-

Initial Momentum(GeV)	$\Lambda_{\bar{ms}}$(GeV)	$\chi^2_{d.o.f.}$
2.06	0.2682	4.58
2.30	0.2684	4.77
2.52	0.2682	4.97
2.67	0.2677	5.13
2.79	0.2671	5.03
2.91	0.2662	5.04
3.04	0.2660	5.24
3.22	0.2641	4.71
3.53	0.2627	4.47
3.81	0.2610	4.14
4.07	0.2595	3.79
4.20	0.2583	3.84
4.39	0.2563	2.79

Table 4.4: Fits of Eq 4.18 to the running coupling data in Fig 4.3. Here, the fit for every fourth initial momentum is shown.

Initial Momentum(GeV)	$\Lambda_{\overline{ms}}$(GeV)	$\chi^2_{d.o.f.}$
2.06	0.2986	7.51
2.30	0.2975	8.72
2.52	0.2957	9.76
2.67	0.2935	10.55
2.79	0.2912	10.92
2.91	0.2886	11.11
3.04	0.2872	11.96
3.22	0.2837	10.59
3.53	0.2810	9.88
3.81	0.2784	8.84
4.07	0.2762	7.85
4.20	0.2742	7.35
4.39	0.2723	5.35

Table 4.5: Fits of the numerical inversion of Eq 4.15 to the running coupling data in Fig 4.3. Here, the fit for every fourth initial momentum is shown.

tively.

4.9 Conclusions

Comparing Tables 4.2 and 4.3 with Tables 4.6 and 4.7, we see that the two parameter fits have brought the two correction terms closer together (the difference is about 0.13GeV^2 instead of 0.25GeV^2) as we had hoped, giving support to our ansatz. The best quality and most stable fits we have obtained are for the two parameter numerical inversion.

The values of Λ in Table 4.7 do not differ much from the value in Eq 3.38. On the other hand, the values returned by the two parameter fits using the three loop formula (Table table6) differ more. The results in both Table 4.6 and Table 4.7 are within the error bounds of Eq 3.38.

It is pleasing to see that our two parameter numerical inversion has returned a Λ which is the same as the independent estimate Eq 3.38 which was obtained[29] from a numerical inversion for quenched lattice data at a much higher energy ($\sim 100\text{GeV}$) than we are using.

For the numerical inversion with a correction, we calculated the $\chi^2_{d.o.f.}$ for a range of Λ and c on the whole data set (corresponding to the first row on Table 4.7). The results are plotted in Fig 4.6 where we have imposed $\chi^2_{d.o.f.} < 10$. Fig 4.7 is the profile along the Λ axis with $\chi^2_{d.o.f.} < 3$, and Fig 4.8 is the profile along the c axis with $\chi^2_{d.o.f.} < 3$. The minima are clear in both Figs 4.7 and 4.8.

Initial Momentum(GeV)	$\Lambda_{\bar{m}s}$(GeV)	c(GeV^2)	$\chi^2_{d.o.f.}$
2.06	0.2271	0.491	1.69
2.30	0.2265	0.501	1.69
2.52	0.2260	0.510	1.74
2.67	0.2258	0.514	1.83
2.79	0.2249	0.527	1.61
2.91	0.2245	0.535	1.64
3.04	0.2236	0.549	1.59
3.22	0.2246	0.534	1.65
3.53	0.2247	0.531	1.73
3.81	0.2254	0.519	1.86
4.07	0.2266	0.497	1.93
4.20	0.2236	0.553	2.01
4.39	0.2274	0.480	1.71

Table 4.6: Two parameter fits of Eq 4.3 to the running coupling data in Fig 4.3. α_P is given by Eq 4.18. Here, the fit for every fourth initial momentum is shown.

Initial Momentum(GeV)	$\Lambda_{\bar{m}s}$(GeV)	c(GeV^2)	$\chi^2_{d.o.f.}$
2.06	0.2377	0.623	1.63
2.30	0.2374	0.629	1.66
2.52	0.2372	0.632	1.73
2.67	0.2372	0.632	1.82
2.79	0.2368	0.639	1.61
2.91	0.2367	0.642	1.65
3.04	0.2363	0.650	1.61
3.22	0.2372	0.634	1.66
3.53	0.2376	0.629	1.74
3.81	0.2382	0.617	1.86
4.07	0.2391	0.600	1.93
4.20	0.2372	0.637	2.02
4.39	0.2398	0.585	1.71

Table 4.7: Two parameter fits of Eq 4.3 to the running coupling data in Fig 4.3. α_P is given by the numerical inversion of Eq 4.15. Here, the fit for every fourth initial momentum is shown.

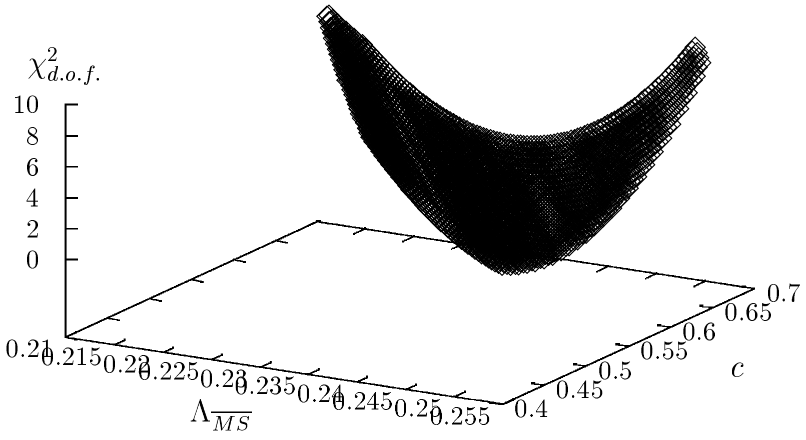

Figure 4.6: Plot of $\chi^2_{d.o.f.}$ against $\Lambda_{\overline{MS}}$ and c with the restriction $\chi^2_{d.o.f.} < 10$. The fits are of the numerical inversion with a correction term to the whole of the running coupling data in Fig 4.3.

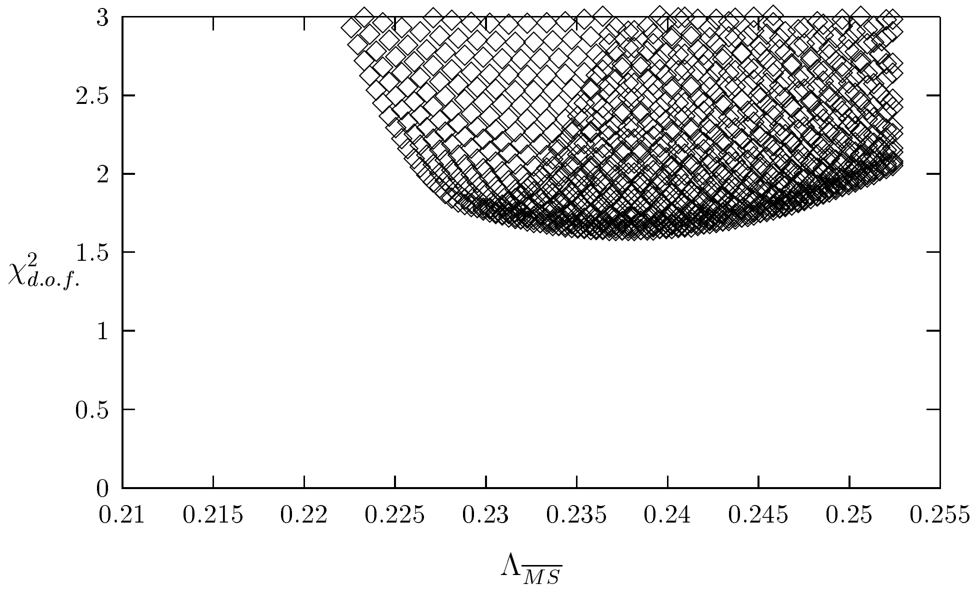

Figure 4.7: View of Fig 4.6 along the Λ axis with $\chi^2_{d.o.f.} < 3$.

We quote as our final result the two parameter fit using the numerical inversion of Eq 4.15:

$$\Lambda_{\overline{MS}} = 0.237^{3\ 0}_{3\ 10}\mathrm{GeV}$$

$$c = 0.63^{3\ 0}_{3\ 10}\mathrm{GeV}^2 \tag{4.20}$$

The first error is the fit error and the second is a systematic error due to our lack of knowledge of the perturbative part. The systematic error is obtained from the difference between the numerical inversion and the fit to Eq 4.18, ie the difference between Table 4.7 and Table 4.6.

The necessity of such a power correction is brought out in Figs 4.9 and 4.10. Fig 4.9 is the fit with the parameters in Eq 4.20. Fig 4.9 also gives the perturbative part by itself for comparison. Fig 4.10 shows the value of lambda when

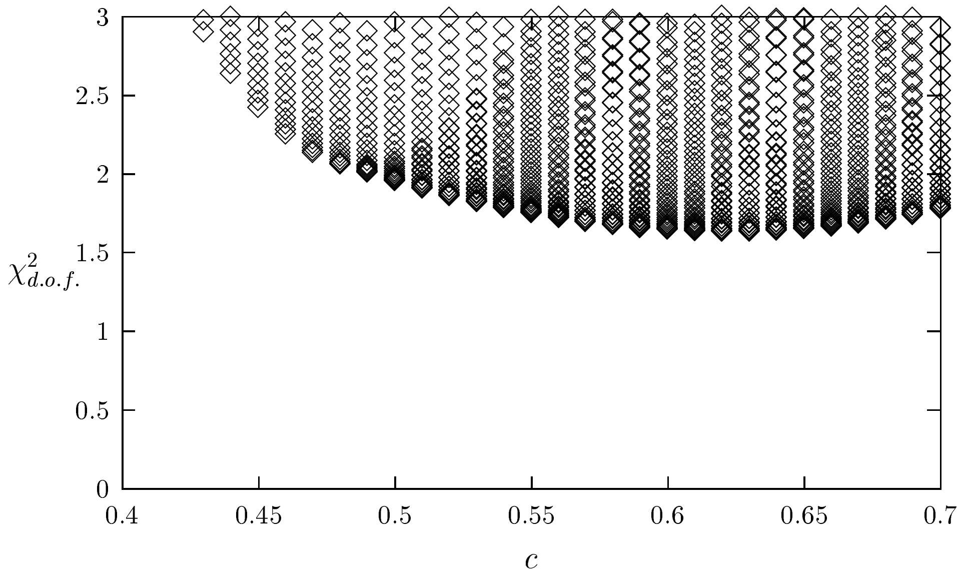

Figure 4.8: View of Fig 4.6 along the c axis with $\chi^2_{d.o.f.} < 3$.

determined via a numerical inversion directly from the data. It is clear that Λ is not a constant. However, when we subtract $0.63/p^2$ from the data, we obtain quite a data set which is consistent with being a constant.

We should add some qualifying remarks here. In particular, the errors quoted in Eq 4.20 are by no means the true error on the quantity. A significant further error comes from the determination of the physical scale for the data which we outlined in section 2.10. Further to this, our fits were on a particular size of lattice and the effects of finite volume were probably not analysed as well as they should be. Also, the data we fitted to was selected on the basis that we obtain a good fit to our ansatz. These further points mean that the errors on Eq 4.20 should be much greater.

Nevertheless it is quite compelling to conclude that there is a large power

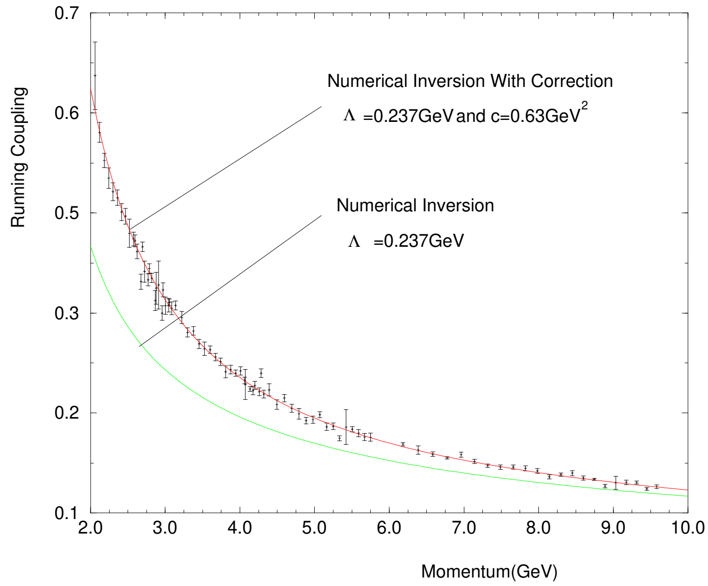

Figure 4.9: This is the best fit of our ansatz with the numerical inversion to the running coupling data in Fig 4.3. The parameters are given in Eq 4.20, ie $\Lambda_{\overline{MS}} = 0.237\text{GeV}$ and $c = 0.63\text{GeV}^2$. Also plotted is the perturbative part on its own with $\Lambda = 0.237\text{GeV}$.

correction to the running coupling when calculated in the $\widetilde{MOM}$ scheme. It is also surprising that the correction term is significant even at momenta as high as 10GeV.

We may wish to compare the result in Eq 4.20 with the world average for results for α_s at the m_{Z^0} scale[43, 44]. This is $\alpha_S(m_{Z^0} = 91.2\text{GeV}) = 0.1181 \pm 0.0031$. If we calculate using a numerical inversion of Eq 4.15 using the input for Λ from Eq 4.20, we obtain $\alpha_S(m_{Z^0} = 91.2\text{GeV}) = 0.0970^{2}_{10}$. The fact that this is significantly smaller than the world average is not a concern to us because we have not included sea quark effects in our lattice simulation[13].

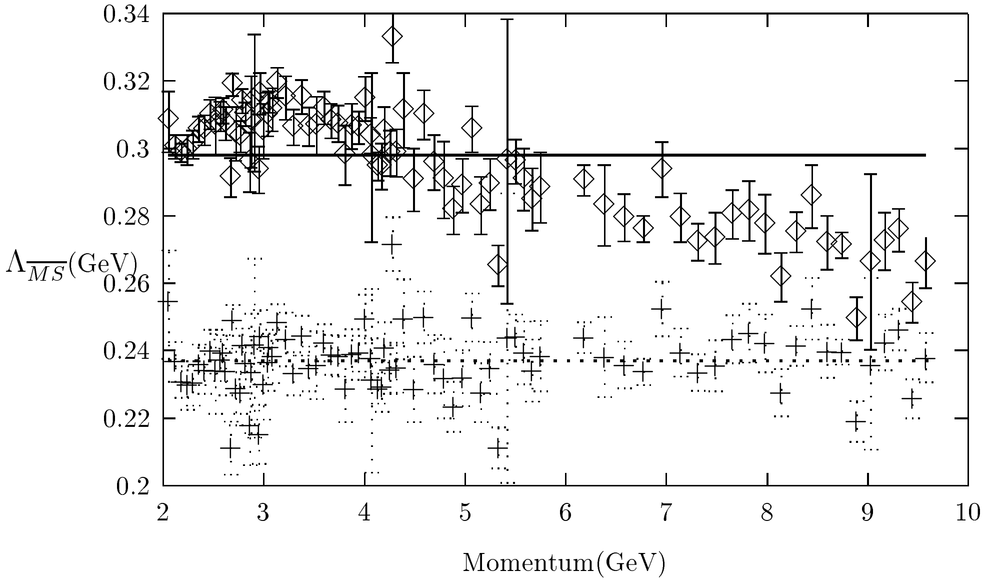

Figure 4.10: Plot (symbol "$\diamond$") of $\Lambda_{\overline{MS}}$ from the numerical inversion of Eq 4.15 applied to the data in Fig 4.3. Also plotted (symbol "+")is $\Lambda_{\overline{MS}}$ calculated from the numerical inversion of Eq 4.15 applied to the data in after the term c/p^2 with $c = 0.63$ has been subtracted (as in Fig 4.3). A fit of $\Lambda_{\overline{MS}}$ to this data over the whole range gives for the original data $\Lambda_{\overline{MS}} = 0.299$GeV with $\chi^2_{d.o.f.} = 7.75$ (continuous line). For the data with c/p^2 subtracted we have $\Lambda_{\overline{MS}} = 0.237$GeV with $\chi^2_{d.o.f.} = 1.61$ (dotted line).

Chapter 5

Mesons on the Lattice

5.1 Introduction

"Meson" is the name given to any bosonic colour singlet state of QCD. A meson is specified by its mass and the quantum numbers J for rotation P for parity and C for charge conjugation. We write this as J^{PC}. We also need to specify isospin which I discuss in section 5.7.

The mass spectrum for a given J^{PC} is very complicated. In general it consists of several meson states with an unknown amount of mixing of various quarks and gluons.

On the lattice the situation can be made simpler than the real world because we can restrict the types of quarks that go into the simulation. Mixing cannot then occur with quark flavours that are not included in the simulation.

In this chapter, we define meson propagators on the lattice and discuss how ground state meson masses can be determined using a lattice calculation.

5.2 Local Operators

A simple way of creating a meson on the lattice is to bind two quarks together to form a quark-antiquark. The particular binding used will dictate the J^{PC} numbers of the meson.

There are many operators that can be constructed to bind a quark-antiquark together. While each operator is designed to produce the same J^{PC} numbers, they will not necessarily produce the same proportions of mesons in the mass spectrum. For example, some operators may produce more ground state mesons than others. These operators would clearly be more useful for studying the ground state mass.

There are two sorts of operator I wish to consider. These are "local" operators and "fuzzed" operators. The generic local operator is:

$$\bar{q}_i(x)\Gamma_{ij}q_j(x) \tag{5.1}$$

where $q(x)$ denotes quark fields.

We call these operators "local" because we define the two quark fields to be in the same place. The Dirac spinor indices are summed via a Dirac matrix Γ.

Γ can be any matrix obtained by multiplying the four Dirac spinor matrices together. There exists a total of sixteen linearly independent Γ matrices (see appendix). From the Γ matrices, we can derive the spin parity and charge quantum numbers of the meson[45]. By comparing the calculated quantum numbers with those of observed mesons, we can identify the Γ matrices with

SPIN 0			**SPIN 1**		
MESON	Γ	J^{PC}	MESON	Γ	J^{PC}
SCALAR(a_0)	I	0^{++}	AXIAL(a_1)	$-i\gamma_5\gamma_i$	1^{++}
EXOTIC	γ_4	0^{+-}	BAXIAL(b_1)	$-i\gamma_5\gamma_4\gamma_i$	1^{+-}
PION(π)	γ_5	0^{-+}	RHO(ρ)	γ_i	1^{--}
PION$'$(π')	$-i\gamma_4\gamma_5$	0^{-+}	RHO$'$(ρ')	$-i\gamma_4\gamma_i$	1^{--}

Table 5.1: J^{PC} numbers of local operators in continuum QCD, $i = 1, 2, 3$. Here I have defined the names by which I shall refer to the mesons in what follows.

observed ground state mesons.

The sixteen Γ matrices give us four spin zero mesons and the spin components of four spin one mesons. These are defined in Table 5.1 where I have defined the names by which I shall refer to the particles in following sections.[1]

A meson with the quantum numbers of the exotic has never been found. We therefore do not expect to find a bound ground state meson corresponding to $\Gamma = \gamma_4$. QCD calculations on the lattice using the γ_4 matrix are consistent with this observation since they show no signal. Exotic mesons are so named because they correspond to states which do not exist in the quark model[47].

We also note that the quantum numbers of the pion and the rho occur twice

[1]Table 5.1 is only valid in the continuum. On the lattice, the local operators not only generate the mesons in the table, but also generate other mesons with higher J numbers[46]. These other meson states are much more massive and so do not mix with the states in Table 5.1. Table 5.1 is therefore valid on the lattice for our purposes.

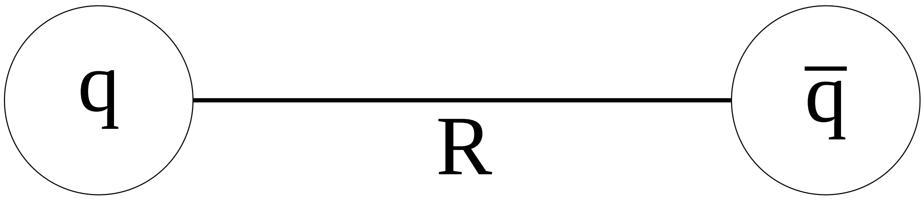

Figure 5.1: A quark-antiquark pair spatially separated by a distance R.

in the local operators. I have distinguished these in Table 5.1 by a prime. We can therefore generate five distinct mesons with local operators. These are the pion, scalar, axial, baxial, and the rho.

5.3 Fuzzed Operators

We now consider another class of operators called "fuzzed" operators[48]. The advantage of using fuzzed operators over local operators is that in practice they are found to generate a bigger signal of ground state masses[48]. This should make the task of obtaining the ground state mass from a lattice simulation easier.

Another advantage of using fuzzed operators is that it is possible to generate J^{PC} numbers that are not available to us from using local operators[46]. However, here we shall only redo the same five J^{PC}'s with fuzzed operators that we can calculate using local operators.

We consider a meson made of quarks separated by a distance R as shown in Fig 5.1. Naively, we would write the analogue of Eq 5.1 as:

$$\bar{q}(x + R_i)\Gamma M(x, t; R_i)q(x) \tag{5.2}$$

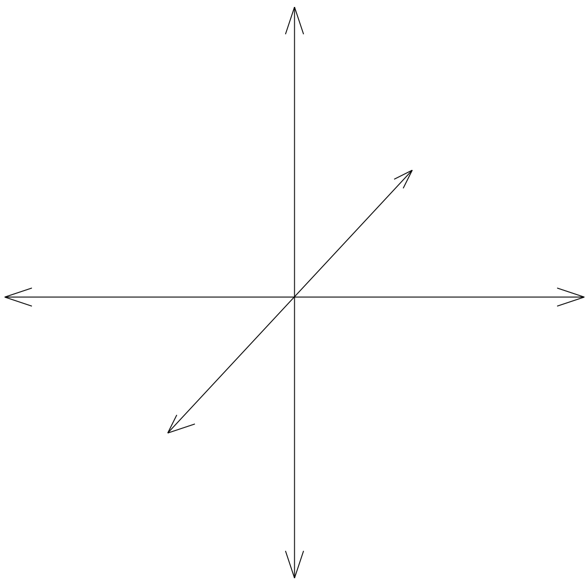

Figure 5.2: The six spatial directions available from a given point on a lattice. By summing over the directions we can construct a more spatially symmetric operator.

where M is the straight line link operator between the two quarks. However, unlike the local meson operator, this is not symmetrical in space so it will give different J^{PC} numbers. This problem can be solved by summing over spatial directions to create the spatially symmetric operator:

$$\frac{1}{6}\sum_{i=1}^{6}\bar{q}(x+R_i)\Gamma M(x,t;R_i)q(x) \tag{5.3}$$

where the i index runs over the six spatial directions allowed at a given point on a lattice as in Fig 5.2.

A "fuzzed" operator is a variant on this operator where, instead of having just a straight line link for the operator M, we consider other links. For example to go from one lattice point to a neighbouring point, we may also consider the links shown in Fig 5.3b.

a.Straight Link

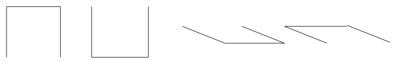

b.U-Bend Links

Figure 5.3: The links between two quarks separated by a distance R. Not only can we consider the straight line link operator in Fig 5.3a, we can also consider the four "U-Bend" links in Fig 5.3b.

We define the fuzzed version of M as:

$$M_{\text{Fuzzed}} = P_{SU(3)}\left(cM(\text{Straight}) + \sum_{1}^{4} M(\text{U-Bends})\right) \tag{5.4}$$

where the c allows us to give a different weight to the straight line link and P makes the operator unitary.

This is the first level of fuzzing. We note that for each of the links in Fig 5.3, we can apply fuzzing again which gives us the second level. We can iterate this fuzzing process to whatever level we wish. The coefficient c and level of fuzzing are ideally tuned to give an operator which maximises ground state meson production.

5.4 Quarks

We have considered some ways in which two quarks can be bound together to make mesons, but have said nothing about the flavour of the quarks. In reality, the flavour of the quarks in a given meson state can be ambiguous since a meson is often a mixture of states containing different quarks and gluons. On the lattice, we can make things simpler by specifying which quarks we want to make up the meson.

There are six different flavours of quark: up(u), down(d), strange(s), charm(c), bottom(b), top(t). These tend to have their own peculiar problems when it comes to putting them on the lattice. The biggest computational problem is to evaluate the fermion determinant. The computational time required is significantly reduced by using the "quenched" approximation in which the fermion determinant is set to a constant. Typically, the errors resulting from this approximation are about 10%.

As well as the problem of computational time, we also run into further problems dependent on the quark we are trying to simulate. I have summarised some of these below:

- It is difficult to study charm quarks on the lattice using the Wilson action because the lattice spacings that are currently used are about the same size as its Compton wavelength. This causes significant technical difficulties, and alternatives to the Wilson action are used[49].
- There are several ways of studying bottom quarks on the lattice[49, 50]. One way is to make the approximation that they don't propagate in space. This is reasonable because they are very heavy so propagating effects can be neglected.

- Mesons made of an s and an $\bar{s}$ can be studied on the lattice. Unfortunately, it is not possible to compare the results directly with experiment because of mixing with $u\bar{u}$ and $d\bar{d}$ states[51].

- Experimentally, the best studied mesons are those made of up and down quarks. However, up and down quarks cannot be computed on the lattice because they are too light. The basic problem is that the computational procedure for inverting the fermion matrix to obtain the quark propagator takes up a rapidly increasing amount of computer time with decreasing quark mass[52]. Further to this, we would need much bigger lattices than we currently work with to reduce finite volume effects to an acceptable level.

Physically, the up and down quarks are approximately degenerate in mass. This means that we can get interesting results which should correspond to good approximation to reality by treating the up and down quarks as exactly degenerate in mass. On the lattice, we make the quarks heavier so that we do not run into the problems with very light quarks mentioned above.

From lattice simulations involving "heavy" up and down quarks, we should be able to obtain at least qualitative information about the real world. With a suitable extrapolation procedure down to real quark masses, quantitative predictions should become possible. This is the basis for this lattice study.

5.5 Determination of Mass from the Lattice

From quantum mechanics we know that a mass eigenstate of a system at rest evolves as e^{imt} where m is the rest mass of the state. We make use of this fact to determine meson masses on the lattice.

If we create a meson with an up and a down quark at time $t = 0$ using one of the operators discussed in sections 5.2 and 5.3 (call it O), and propagate it through time, then we form the Greens function:

$$\langle \overset{t=t}{\bar{u}Od} \mid \overset{t=0}{\bar{u}Od} \rangle \tag{5.5}$$

As we have noted, the particular operator that we use to create the meson is not important, it just gives rise to a different distribution of masses. Therefore, we could as easily destroy the meson with a different operator (O_d) to that which created it (O_c). So:

$$\langle \overset{t=t}{\bar{u}O_d d} \mid \overset{t=0}{\bar{u}O_c d} \rangle \tag{5.6}$$

is equally a Greens function describing the propagation of a meson state.

When we create a meson, we do not generate a single eigen-state, but rather a whole spectrum of meson excitations.

$$\langle \overset{t=t}{\bar{u}O_d d} \mid \overset{t=0}{\bar{u}O_c d} \rangle = \int_{m=0}^{\infty} C(m) e^{imt} \mathrm{d}m \tag{5.7}$$

where $C(m)$ is the distribution function which tells us how many meson states are generated at a given mass. In general, we can expect a mass function C to look qualitatively like Fig 5.4.

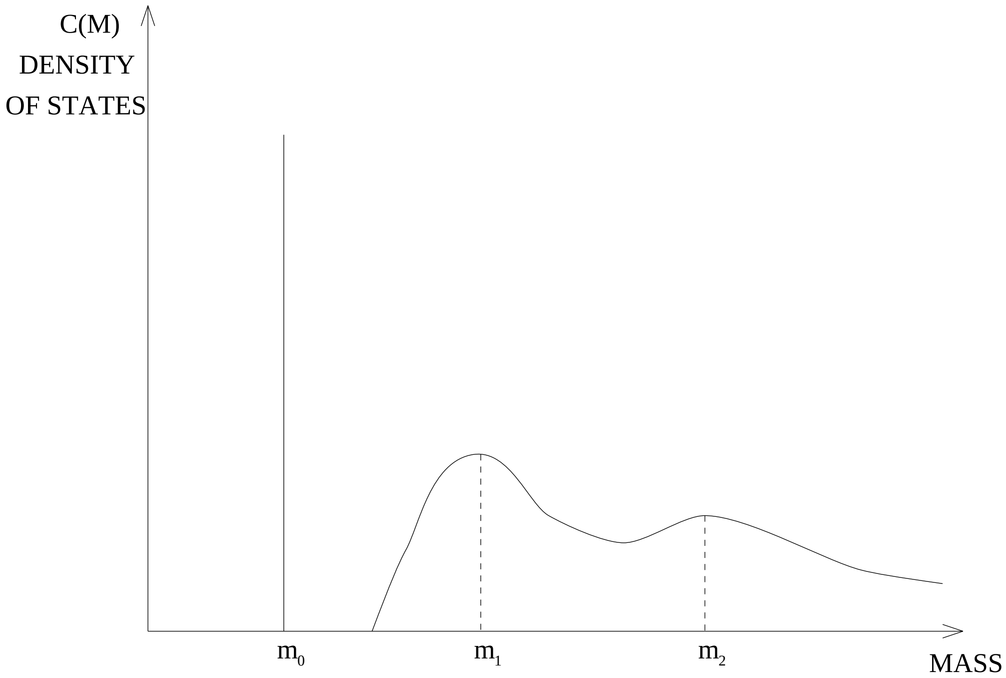

Figure 5.4: Qualitative representation of the density of meson states for a given J^{PC} in a lattice simulation and in the real world.

The lowest mass state m_0 we call the ground state. In the case of the pion, the ground state is a proper eigenstate of the system and therefore has a genuine delta function. This is because the pion is the lightest meson and so cannot decay.

For other particles such as the rho, the ground state is very nearly a delta function. The rho can have some small decay width due to the decay $\rho \to \pi\pi$. This can occur provided that the ground states satisfy $m_\pi/m_\rho < \frac{1}{2}$, but in our simulations, this condition is not satisfied and so the rho has a precise delta function. Nevertheless to approximate the ground state of a meson as a delta function is very accurate.

The general procedure for calculating ground state masses is firstly to evaluate the left hand side (LHS) of Eq 5.7 on the lattice for various values of t. We then obtain m_0 by fitting the spectral function on the right hand side (RHS) to the lattice data. Of course, the lattice exists in Euclidean space, so if we evaluate the Greens function $\langle \bar{u}\Gamma d | \bar{u}\Gamma d \rangle$ on the lattice, then we must apply a Wick rotation ($t \to it$) to the RHS of Eq 5.7. The lattice version of this equation is then:

$$\langle \bar{u}\overset{t=t}{O_d}d \mid \bar{u}\overset{t=0}{O_c}d \rangle = \int_{m=0}^{\infty} C(m)e^{-mt}\mathrm{d}m \tag{5.8}$$

where now the Dirac brackets are taken to mean an averaging over lattice gauge configurations. I shall discuss some details of the lattice evaluation of the Greens function in sections 5.6 and 5.8.

It is important to note that for large enough time t, the contribution to the integral from large mass states is removed by the exponential function. For large enough t, it will suffice to represent the complicated distribution function of Fig 5.4 by the simple function composed of low mass delta functions in Fig 5.5.

As we have already noted, a delta function is an accurate representation of the ground state, and we expect that the value we get from the fit for m_0 to be the real ground state mass. The excited state delta functions are only effective representations of the true picture. The effective masses m_1,m_2,.... will not necessarily coincide very well with the real excited mass peaks.

If we just include the ground state m_0 and first excited state m_1, and assume that all other states have been damped by the exponential function, then we

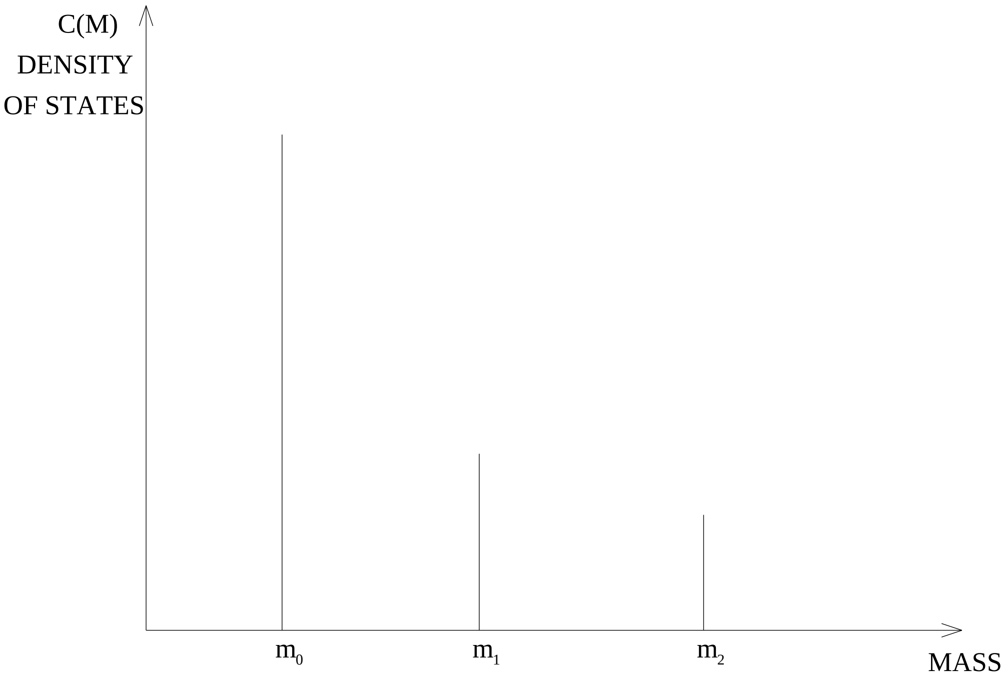

Figure 5.5: For the purposes of fitting to the ground state, we choose to represent the spectral function of Fig 5.4 by this simple function.

get a two exponential function to fit the data to:

$$\langle \bar{u}O_d d | \bar{u}O_c d \rangle = ae^{-m_0 t} + be^{-m_1 t} \tag{5.9}$$

where the coefficients a and b represent the relative amounts of ground and excited states produced. This is an effective representation of the distribution function $C(m)$.

This equation is valid provided that t is large enough for the exponential function to remove contributions from higher mass states. In fact, if t is large enough, we can also ignore the contribution from the first excited state m_1 and do a one exponential fit for the ground state:

$$\langle \bar{u}O_d d | \bar{u}O_c d \rangle = a^{1\,\mathrm{exp}} e^{-m_0 t} \tag{5.10}$$

In section 5.2 we defined local operators which we shall denote by L and in section 5.3 we defined fuzzed operators which we shall denote by F. We noted that among the local operators, there were two operators corresponding to the pion and the rho. This potentially gives us a cross term where for example we could create a pion with the pion operator and destroy it with the pion$'$ operator. This becomes important in the calculation of f_π in chapter 8. For the scalar, baxial and axial mesons, we consider a single fuzzed and a single local binding operator.

For a given meson, the Greens functions that we consider are obtained from implementing fuzzing at the source (t=0) or at the sink (t=t) or at both ends or not at all. This gives us four possibilities which we term FL,LF,FF,LL respectively:

$$
\begin{aligned}
LL &\equiv \langle \bar{u}Ld|\bar{u}Ld\rangle && (5.11)\\
LF &\equiv \langle \bar{u}Fd|\bar{u}Ld\rangle \\
FL &\equiv \langle \bar{u}Ld|\bar{u}Fd\rangle && (5.12)\\
FF &\equiv \langle \bar{u}Fd|\bar{u}Fd\rangle && (5.13)
\end{aligned}
$$

where, for example, FL means that we use a fuzzed source and a local sink operator.

We choose to ignore the LF because the sum over x at the sink which is performed when calculating a Greens function on a lattice seems to duplicate to some extent the effect of fuzzing at the sink and so we get better statistics with the FL. For each of the mesons we study, we therefore have three sets of data.

5.6 Flavour

In the previous section, we considered creating a meson, propagating it through time and then destroying it. We now examine this more closely.

To expand the ket on the LHS of Eq 5.9 requires more than just taking the hermitian conjugate since it contains Grassmann variables. The Euclidean space generalisation of hermitian conjugation to include Grassmann variables is known as "reflection positivity"[10]. When applied to the LHS of Eq 5.9 we get:

$$\langle \bar{u} O_d d \; \bar{d} \gamma_4 O_c^\dagger \gamma_4 u \rangle = a e^{-m_0 t} + b e^{-m_1 t} \tag{5.14}$$

where $\dagger$ denotes the hermitian conjugate. Reflection positivity in Euclidean spacetime implies that this Greens function is positive definite for $t > 1$.

We can now expand the LHS using Wick's Theorem. This requires us to pair fields together.

This pairing of fields is dependent on the type of meson. Specifically it depends on whether the meson is a flavour singlet or nonsinglet. We first consider the flavour nonsinglet.

5.6.1 Flavour Nonsinglet

Flavour nonsinglet means that there is a net flavour in the meson. The meson propagated in Eq 5.14 is a flavour nonsinglet because it is made with an up quark and a down quark. In this case, the only pairings that we are allowed give us the u and d quark propagators G_{uu} and G_{dd} respectively, ie:

$$\begin{aligned} \langle u\bar{u}\rangle &= G_{uu} \\ \langle d\bar{d}\rangle &= G_{dd} \end{aligned} \tag{5.15}$$

but the pairings:

$$\begin{aligned} \langle u\bar{d}\rangle &= 0 \\ \langle d\bar{u}\rangle &= 0 \end{aligned} \tag{5.16}$$

are not allowed because the u and d quarks are different flavours and we cannot change one into the other.

With these allowed pairings, Wicks theorem gives us just one term:

$$\langle \bar{u}O_d d\ \bar{d}\gamma_4 O_c^\dagger \gamma_4 u\rangle = -r\langle G_{uu}O_d G_{dd} O_c\rangle = C \tag{5.17}$$

where:

$$rO\gamma_4 = \gamma_4 O \tag{5.18}$$

and we have assumed a hermitian representation for the operators: $O^\dagger = O$ (see appendix for the local operator case). The minus sign comes from commuting

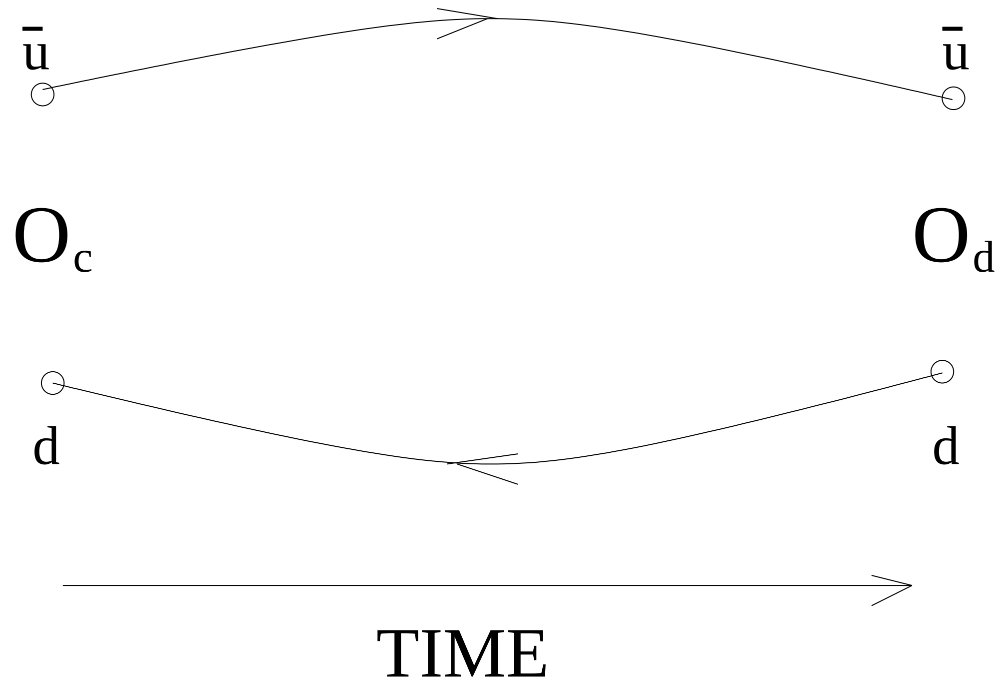

Figure 5.6: The connected part of a meson propagating in time. This quarks in this figure are different, so this corresponds to a flavour nonsinglet meson.

the u field past the other fermionic fields to produce the G_{uu} propagator.

We can represent the Greens function of Eq 5.17 by a spacetime diagram. See Fig 5.6. I call these Greens functions "C" or "Connected" as a descriptive term for this diagram.

We see that propagating a nonsinglet meson in time is equivalent to propagating the two quarks independently and binding the propagators together at $t = 0$ and at $t = t$.

5.6.2 Flavour Singlet

We now apply Wicks theorem to the flavour singlet case. For the flavour nonsinglet we had just two field pairings (Eq 5.15). Now we have two more as

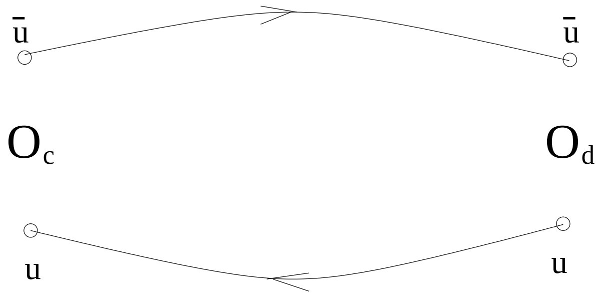

a.Connected Part

b.Disconnected Part

Figure 5.7: For flavour singlet mesons we need to add to the connected part C of Fig 5.6 a disconnected part D.

shown:

$$\langle \bar{u} \overbrace{O_d}^{G_{uu}} u\bar{u} \underbrace{\gamma_4 O_c^\dagger \gamma_4}_{G_{uu}} u\rangle \tag{5.19}$$

So applying Wicks theorem to the flavour singlet version of Eq 5.14 gives:

$$\langle \bar{u} O_d u \bar{u} \gamma_4 O_c^\dagger \gamma_4 u\rangle = -r\langle G_{uu} O_d G_{uu} O_c\rangle + r\langle G_{uu} O_d\rangle\langle G_{uu} O_c\rangle = C + D \tag{5.20}$$

where r is defined in Eq 5.18. We obtain a similar result for d quarks. We can represent these terms on a spacetime diagram as in Fig 5.7.

When the up and down quark masses are set to be the same, the first term in Eq 5.20 is the same as the connected term C of the flavour nonsinglet Eq 5.17.

The second term we denote by "D" for "Disconnected".

Eq 5.20 does not describe the propagation of a flavour singlet meson because $u\bar{u}$ and $d\bar{d}$ are not mass eigenstates of the flavour singlet. To evaluate mass eigenstate propagators we need to consider isospin.

5.7 Isospin

In QCD, there is an approximate symmetry connected with the small mass difference between the up and down quarks. If we assume that the up and down quark masses are the same, then in so far as the QCD Lagrangian is concerned, there is no difference between u and d quarks. This approximate flavour symmetry of QCD is known as isospin.

If we invoke isospin to make the u and d quarks the same mass, then the connected parts will be the same in Eq 5.17 and Eq 5.20. Also the disconnected parts of the singlet will not be dependent on whether we make them with u quarks or d quarks.

So for the flavour singlet we write the four possible Greens functions:

$$\begin{aligned} C + D &= \langle u O_d \bar{u} | u O_c \bar{u} \rangle \\ C + D &= \langle d O_d \bar{d} | d O_c \bar{d} \rangle \end{aligned} \tag{5.21}$$

and:

$$D = \langle u O_d \bar{u} | d O_c \bar{d} \rangle$$

$$D = \langle dO_d\bar{d}|uO_c\bar{u}\rangle \tag{5.22}$$

We can obtain the flavour nonsinglet Greens functions by putting $D = 0$.

Eq's 5.21 and 5.22 are represented by the matrix:

$$\begin{array}{cc} & \begin{array}{cc} u\bar{u} & d\bar{d} \end{array} \\ \begin{array}{c} u\bar{u} \\ d\bar{d} \end{array} & \begin{pmatrix} C+D & D \\ D & C+D \end{pmatrix} \end{array} \tag{5.23}$$

This has eigenvalues C and $C + 2D$ with eigenvectors $1/\sqrt{2}(u\bar{u} - d\bar{d})$ and $1/\sqrt{2}(u\bar{u} + d\bar{d})$ respectively.

For the $u\bar{d}$ and $d\bar{u}$ nonsinglet mesons, $D = 0$ so the correlation is given by C as discussed above.

The $1/\sqrt{2}(u\bar{u} - d\bar{d})$ eigenstate has the same eigenvalue as the nonsinglet. The particles therefore have the same mass. They are distinguished by the isospin quantum number I. The flavour singlet particle has $I = 0$. The flavour nonsinglet has $I = 1$.

In conclusion, we construct the flavour nonsinglet mesons on the lattice by calculating the connected correlators C. By adding to C the disconnected part $2D$, we construct the $1/\sqrt{2}(u\bar{u} + d\bar{d})$ flavour singlet correlators:

$$\langle \text{Nonsinglet} \rangle = C \tag{5.24}$$

$$\langle \text{Singlet} \rangle = C + 2D \tag{5.25}$$

5.8 Technicalities of the Lattice Calculation

The Greens function $\langle G_{uu}O_dG_{dd}O_c\rangle$ has been calculated[2][53] in full (unquenched) QCD. This was done on a $12^3 \times 24$ lattice at $\beta = 5.2$ using fuzzed and local operators. When fuzzed operators were used, $R = 2$, $c = 2.5$ and the level of fuzzing used is 5 (see section 5.3).

The action used was a Wilson action with the clover term added to remove $\mathcal{O}(a)$ ambiguities. This action is discussed in section 1.4. The clover coefficient used was $C_{SW} = 1.76$. This value of the clover coefficient comes from a lattice calculation of the clover term such that $\mathcal{O}(a)$ corrections are removed from the fermionic sector. This coefficient was later improved by the ALPHA collaboration to $C_{SW} = 2.02$[54]. It follows that, we do not have full non-perturbative $\mathcal{O}(a)$ improvement in our simulation.

The number of flavours (N_f) used in the simulation was 2 (representing the up and down quarks). The masses of the up and down quarks were set equal to the sea quark mass:

$$m_u = m_d = m_{sea} \tag{5.26}$$

The Greens function was evaluated for five values of κ from $0.1370 \rightarrow 0.1398$. κ is related to the quark mass in Eq 1.18. In the simulation, r in Eq 1.18 was set equal to 1.

[2]In practice, it was found easier to calculate the quantity $\langle O_d^* G_{uu}^* O_c G_{dd}\rangle$. This was then related to the Greens function via factors of γ_5 derived using the relation $\gamma_5 G^\dagger \gamma_5 = G$. This relationship can be derived from the definition of the fermion matrix $M = G^{-1}$ in lattice gauge theory.

κ	Number of Configurations
0.1370	151
0.1380	151
0.1390	151
0.1395	121
0.1398	98

Table 5.2: The number of configurations calculated at each κ (see [53]).

These values of κ roughly correspond to a quark mass between m_s and $2m_s$ where m_s is the mass of the strange quark.

The number of configurations calculated are low due to the amount of computation required for the unquenched calculation. They are given in Table 5.2.

The lattice calculation gives us the Greens functions (correlators) evaluated for time $0 \leq t \leq 11$ in lattice spacing units.

The results obtained were multiplied by the factor $-r$ of Eq 5.17 and found to be positive for $t > 1$ as we expected from reflection positivity.

5.9 Summary

In this chapter we have defined some meson correlators. In the following two chapters we shall use a fitting analysis on the correlators to determine what can be said the ground state masses of the mesons defined here.

Chapter 6

Flavour Nonsinglet Mesons

6.1 Introduction

In this chapter we shall focus on the flavour nonsinglet mesons. This means that we need only consider the connected type of correlator described in section 5.6.1.

Of the five mesons we defined in chapter 5, the flavour nonsinglet pion and flavour nonsinglet rho have been studied quite extensively on the lattice[53]. I shall therefore consider the flavour nonsinglet baxial, axial and scalar mesons from an unquenched lattice simulation[53]. The objective is to see what can be said about the mass ordering of the ground states of these mesons from the lattice results. Previous studies from quenched simulations[46] have failed to conclusively determine a definite ordering.

MESON	J^{PC}	MASS(GeV)	WIDTH(GeV)
SCALAR	0^{++}	0.9848(14)	$0.050 \to 0.100$
B	1^{+-}	1.2295(32)	0.142(9)
AXIAL	1^{++}	1.230(40)	$0.250 \to 0.600$

Table 6.1: Experimental masses for the lightest state scalar, baxial and axial mesons.

6.2 Experimental Results

The experimentally obtained masses for the lightest states of the particles are given in Table 6.1[55]. These results correspond to $u\bar{d}$ or $d\bar{u}$ ground state mesons.

If we assume that the uncertainty in the particle's mass coming from the decay width is about a tenth of the total width, we might conclude that while we cannot see any mass difference between the baxial and the axial mesons, the scalar is clearly lighter than both.

Unfortunately, the experimental identification of the scalar meson is ambiguous. The $K\bar{K}$ bound state provides a relevant description of the 985MeV state. The $K\bar{K}$ state does not occur in our simulation, so a comparison of our simulation with experiment is difficult.

6.3 Types of Fits

6.3.1 Simultaneous Fits

For a given meson, we have defined three Greens functions: Eq's 5.11,5.12 and 5.13. These represent the time evolution of the same meson, so we expect that they will give rise to the same ground state mass. We therefore define a simultaneous one exponential fit[1]:

$$\mathrm{Data}_{ab}(t) \leftrightarrow a_{ab} e^{-m_0 t} \tag{6.1}$$

where the symbol $\leftrightarrow$ denotes a fit of the expression on the right of Eq 6.1 to the lattice on the left. The index ab runs over LL, FL, FF. There are four fit parameters (m_0,a_{ab}) to be found.

We also expect the excited state masses to be independent of the choice of source and sink operators (although not perhaps to the same extent as the ground state mass since they are only effective masses). We therefore define a simultaneous two exponential fit:

$$\mathrm{Data}_{ab}(t) \leftrightarrow a_{ab} e^{-m_0 t} + b_{ab} e^{-m_1 t} \tag{6.2}$$

This equation has eight fit parameters (m_0,m_1,a_{ab},b_{ab}).

[1]In fact, we fit to the formula $a_{ab}\left(e^{-m_0 t} + e^{-m_0(T-t)}\right)$ where $T = 24$ is the total time length. This accounts for propagation around the back of the lattice.

6.3.2 Factorizing Fits

We now proceed to define what we call a factorizing fit which is a way of reducing the number of fit parameters.

We introduce a complete set of mass eigenstates $|m_i\rangle$ of the meson into each of the correlators:

$$\langle M_a|M_b\rangle = \sum_i \langle M_a|m_i\rangle e^{-m_i t}\langle m_i|M_b\rangle = \sum_i A_a^i e^{-m_i t} A_b^i \tag{6.3}$$

where M represents the meson's initial and final states, and the indices a, b can be either L or F. The product $A_a^i A_b^i$ must be real, so we can define the A's to be real.

Making a one and two exponential approximation to this as we did in Eq's 6.1 and 6.2 we get:

$$\text{Data}_{ab}(t) \leftrightarrow A_a A_b e^{-m_0 t} \tag{6.4}$$

and:

$$\text{Data}_{ab}(t) \leftrightarrow A_a A_b e^{-m_0 t} + B_a B_b e^{-m_1 t} \tag{6.5}$$

where we have replaced the first excited state coefficients A_L^1, A_F^1 with B_L, B_F respectively.

We now have the three fit parameters (m_0,A_L,A_F) for the one exponential fits and the six fit parameters (m_0,m_1,A_L,A_F,B_L,B_F) for the two exponential fits. We can of course choose all of the fitting parameters to be real numbers. This is clearly an improvement over the simultaneous fits.

6.3.3 Correlated Fits

The data from the lattice calculation are not statistically independent. This means that if a fit to the data goes through the upper end of an error bar at time t, then it would be more likely to pass the neighbouring points in t at the upper ends of their error bars. Due to this, a standard minimisation of χ^2 analysis which ignores this correlation will indicate a better fit than it should do. Our analysis should therefore account for the correlation in the data. To do this we make use of what we call a correlated fit [11, 56, 57].

In practice, it is found from studying errors on known quantities[56] that while the correlated fits give good results for the $\chi^2_{d.o.f.}$, the fit parameters are better determined by a standard (uncorrelated) fit. The uncorrelated fits are also found to be more stable than the correlated ones. We obtain the fit parameters from uncorrelated fits and the $\chi^2_{d.o.f.}$ from correlated fits while making sure that the fit parameters returned by the two are approximately the same.

6.4 Results

The low t values from the lattice data are likely to be problematic because excited states greater than the first become important. Our two exponential analysis then becomes unrealistic. Large t values can be well approximated be a two or even a one exponential fit, but the signal is weak which makes it difficult to pin down a fit. We therefore need to strike some sort of balance between the two.

I performed two exponential fits to the data for various initial and final points (t_1,t_2). The regions of acceptable $\chi^2_{d.o.f.}$ are $3 \leq t_1,t_2 \leq 11$. The lower value of t_1 is determined as when the value of χ^2 increases notably. The lower value of t_1 could run up to 4 or 5 before the signal was significantly weakened. The last point ($t_2 = 11$) made very little difference to the fits.

Two exponential fits are six parameter fits as in Eq 6.5. The χ^2 for this is a complicated function and may have several minima. The fitting procedure is somewhat prone to finding minima of χ^2 that are of no interest to us. To check that the two exponential fits were giving sensible results for the meson masses, I compared the results to some one exponential fits. The one exponential fits are very stable. They have reasonable χ^2 around $t_1 = 4$ or 5.

The results from the two exponential fits are given in Table 6.2. The errors given are systematic errors due to variation in the fits with initial and final points within a region where the fits are relatively stable.

The statistical errors on the data are given in Table 6.3. They were obtained from a bootstrap analysis (see section 6.5). To save time, the fit range used in determining the statistical errors was the same for all three mesons, and so does not necessarily correspond precisely to the best fit given in Table 6.2.

Taking the values of r_0/a in [53] reproduced in Table 6.4 with $r_0^{-1} = (0.49\text{fm})^{-1} = 0.4028\text{GeV}$, we can convert the mass values in Table 6.2 into MeV. The results

κ	$m_A a$	$m_B a$	$m_S a$	Comment
0.1370	1.85^{1}_{1}	1.79^{2}_{2}	1.63^{3}_{3}	$m_S < m_B < m_A$
0.1380	1.61^{1}_{1}	1.50^{2}_{2}	1.50^{1}_{1}	m_S,$m_B < m_A$
0.1390	1.41^{2}_{1}	1.38^{1}_{1}	1.17^{2}_{2}	$m_S < m_B < m_A$
0.1395	1.11^{6}_{6}	1.17^{1}_{12}	1.28^{10}_{5}	m_A,$m_B < m_S$
0.1398	0.75^{15}_{5}	1.06^{4}_{3}	1.00^{2}_{2}	$m_A < m_S < m_B$

Table 6.2: Ground state masses from two exponential fits for axial (m_A), baxial (m_B) and scalar (m_S) mesons in lattice units. Here, a is the lattice spacing. The errors are fit errors taken from the variation of the fit within a region of stability.

κ	$m_A a$	$m_B a$	$m_S a$	Fit
0.1370	1.84^{6}_{33}	1.77^{6}_{7}	1.64^{12}_{14}	[3-9]
0.1380	1.60^{4}_{7}	1.51^{9}_{13}	1.51^{9}_{22}	[3-9]
0.1390	1.41^{3}_{3}	1.39^{3}_{3}	1.19^{6}_{9}	[2-9]
0.1395	1.12^{10}_{26}	1.10^{29}_{38}	1.28^{9}_{8}	[3-9]
0.1398	0.76^{16}_{16}	1.07^{16}_{34}	1.00^{13}_{24}	[3-9]

Table 6.3: Statistical errors on the results of Table 6.2 in lattice units. Some values differ from those in Table 6.2 because a fit range was chosen so as to determine the errors on all three mesons at the same time.

κ	r_0/a
0.1370	2.294^{27}_{25}
0.1380	2.568^{68}_{118}
0.1390	3.046^{100}_{59}
0.1395	3.435^{90}_{47}
0.1398	3.652^{36}_{38}

Table 6.4: Values of r_0/a for different κ reproduced from [53]

are given in Table 6.5, where we have accounted for the errors in r_0/a in Table 6.4. The first set of errors are the fitting errors of Table 6.2. The second set are the statistical errors in Table 6.3.

Table 6.6 gives the masses for the pseudoscalar meson taken from [53].

Fig 6.1 is the plot of the meson masses against the square of the pseudoscalar mass (m^2_{PS}). In principle we should be able to make a linear extrapolation down to the chiral limit $m^2_{PS} = 0$. Clearly the data is not accurate enough to make such an extrapolation meaningful. However, we note that such an extrapolation would be consistent with the experimental values for the axial and baxial mesons which are 1.230GeV and 1.235GeV respectively (see Table 6.1). A direct comparison with the experimental scalar meson is more complicated.

It is clear that the fits do not give any real indication of the mass ordering of the mesons.

κ	m_A	m_B	m_S
0.1370	$1.708\,^{29}_{28}\,^{76}_{324}$	$1.655\,^{38}_{37}\,^{75}_{83}$	$1.506\,^{45}_{44}\,^{129}_{146}$
0.1380	$1.663\,^{54}_{87}\,^{85}_{148}$	$1.551\,^{62}_{92}\,^{134}_{206}$	$1.551\,^{51}_{82}\,^{134}_{299}$
0.1390	$1.728\,^{81}_{46}\,^{94}_{70}$	$1.692\,^{68}_{45}\,^{93}_{70}$	$1.434\,^{72}_{52}\,^{122}_{139}$
0.1395	$1.535\,^{123}_{104}\,^{179}_{381}$	$1.619\,^{56}_{188}\,^{444}_{548}$	$1.772\,^{185}_{93}\,^{171}_{135}$
0.1398	$1.104\,^{232}_{85}\,^{246}_{247}$	$1.559\,^{74}_{60}\,^{251}_{516}$	$1.470\,^{44}_{45}\,^{206}_{368}$

Table 6.5: Meson masses in GeV. The first set of errors are fitting errors (from Table 6.2). The second are statistical errors from a bootstrap analysis (Table 6.3).

κ	Pseudoscalar Mass (GeV)	Pseudoscalar Mass Squared (GeV^2)
0.1370	1.024^{9}_{11}	1.048^{19}_{21}
0.1380	0.968^{13}_{12}	0.938^{26}_{23}
0.1390	0.868^{18}_{15}	0.754^{31}_{27}
0.1395	0.772^{15}_{14}	0.596^{24}_{22}
0.1398	0.700^{7}_{25}	0.490^{10}_{34}

Table 6.6: Masses of the Pseudoscalar meson in GeV taken from [53].

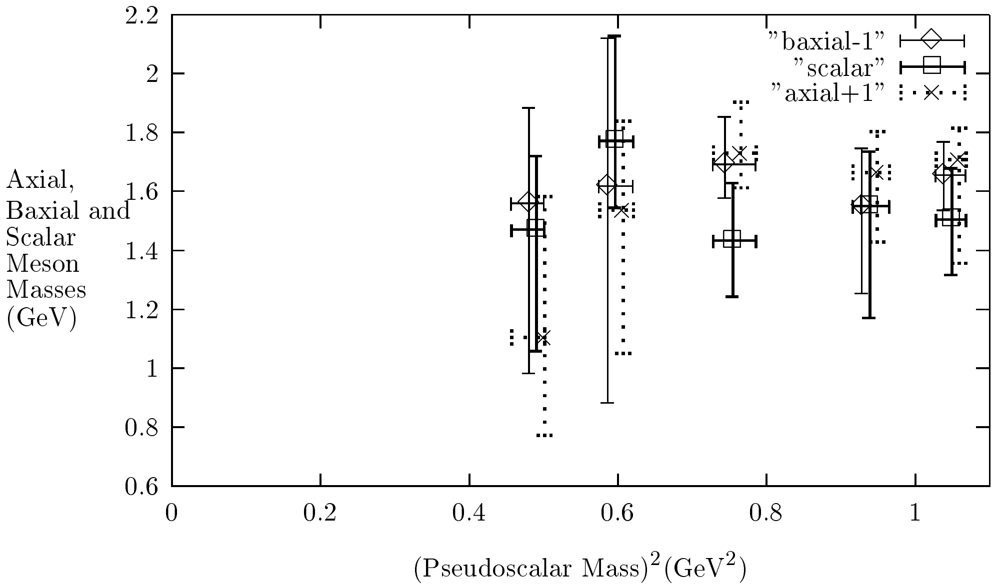

Figure 6.1: Plot of the masses of the Scalar, Axial, and Baxial mesons in GeV against the square of the pseudoscalar mass at values of κ between 0.1370 and 0.1398.

6.5 Bootstrap Analysis

The statistical errors of Table 6.3 were evaluated by a bootstrap analysis. We now describe how this works.

If we have say 151 configurations, then the bootstrap analysis will take at random 151 configurations from the original 151. This means that some configurations will be duplicated and some will not be selected at all. This gives us a random sample. If this is repeated say 100 times, then we have 100 sets of 151 configurations selected randomly from the original 151. We then perform fits to each of the 100 samples. This gives us 100 values of the ground state mass m_0. From the standard deviation of this distribution, we obtain the statistical error.

It may turn out that the distribution is asymmetrical, in which case we would wish to quote asymmetrical errors as in Table 6.3. To determine the upper error on a quantity, we take the set of bootstrap samples that return fit values greater than the mean value. We then create a perfectly symmetrical distribution by matching these point for point with contrived fit values less than the mean. From the standard deviation of this distribution, the upper statistical error is obtained. We do a similar exercise to determine the lower error, but this time creating a symmetrical distribution from the points which are lower than the mean value.

We can use the bootstrap analysis directly to determine whether the original sample had any statistically significant signal for the mass difference. We do this by performing fits for say the axial and the baxial mesons for each of the 100 samples. We then find the difference $m_A - m_B$. This gives us 100 numbers from which we can determine the mean and the statistical error. We do this for the three mass differences. The results are given in Table 6.7.

It is clear that the data contains no statistically significant mass ordering.

6.6 Conclusions

In this chapter we made a determination of the masses of the flavour nonsinglet axial, baxial and scalar mesons. The errors on the results were too great to make a chiral extrapolation meaningful, however we noted that in the cases of the axial and baxial, the masses were consistent with the experimentally

κ	$m_A - m_B$	$m_A - m_S$	$m_B - m_S$	Fit
0.1370	$0.20\,^{16}_{23}$	$0.07\,^{6}_{28}$	$0.13\,^{16}_{12}$	[3-9]
0.1380	$0.10\,^{19}_{9}$	$0.10\,^{15}_{7}$	$0.00\,^{15}_{18}$	[3-9]
0.1390	$0.21\,^{10}_{7}$	$0.02\,^{3}_{3}$	$0.19\,^{9}_{8}$	[2-9]
0.1395	$-0.16\,^{12}_{28}$	$0.02\,^{48}_{19}$	$-0.17\,^{19}_{46}$	[3-9]
0.1398	$-0.24\,^{23}_{25}$	$-0.31\,^{21}_{31}$	$0.07\,^{18}_{24}$	[3-9]

Table 6.7: Bootstrap analysis on the mass differences

determined masses.

We hoped to find some prediction for the mass ordering of the axial, baxial and scalar mesons. We found via a bootstrap analysis that the data was too noisy to give a signal. With better statistics, future lattice calculations may be able to gain a signal.

Chapter 7

Flavour Singlet and Nonsinglet Mesons

7.1 Introduction

In this chapter, we attempt to calculate the mass difference between the flavour singlet and nonsinglet mesons. To do this, we need to look more closely at the differences between the two.

7.2 Determining Mass Difference between Singlet and Nonsinglet States

Using Eq's 6.5 and 5.17 we fit the nonsinglet Greens function to:

$$\langle \mathrm{NONSINGLET} \rangle_{ab} = C_{ab} = A_a^N A_b^N e^{-m_0^N t} + B_a^N B_b^N e^{-m_1^N t} \tag{7.1}$$

Whereas the nonsinglet only has a connected part, the singlet Greens function is made up of the connected part of Eq 7.1 and a disconnected part as in Eq 5.25. Using a one exponential approximation to Eq 7.1, we have for the flavour singlet:

$$\langle \text{SINGLET} \rangle_{ab} = C_{ab} + 2D_{ab} = A_a^N A_b^N e^{-m_0^N t} + 2D_{ab} = A^S A^S e^{-m_0^S t} \qquad (7.2)$$

Here, the superscripts N,S differentiate the parameters of the singlet and the nonsinglet.

We may be tempted to reason that for flavour singlet and nonsinglet mesons created and destroyed with the same operator, the relative amount of ground and excited state in each should be the same. We would therefore put $A_a^S = A_a^N$ and $B_a^S = B_a^N$. This has previously been assumed elsewhere[58]. We have not assumed this here since it turns out not to be generally true as we shall now demonstrate[59].

7.2.1 Single Exponential Case

Let us consider the disconnected contribution to the flavour singlet in more detail.

Consider the disconnected diagram in Fig 7.1. Up to some arbitrary time t_1 and after some arbitrary time t_2, the diagram behaves like the connected diagrams of a nonsinglet meson propagating through time(Figs 5.6 and 5.7a). The piece marked on the diagram with an "X" is composed of some unknown mess of disconnected quark loop diagrams. Therefore, to a one exponential

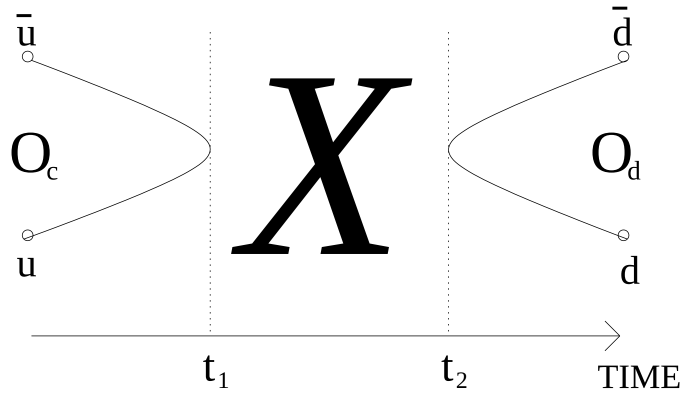

Figure 7.1: Spacetime diagram of disconnected meson correlators. "X" represents an unknown collection of quark loop diagrams.

approximation, we can write the time evolution of the disconnected part:

$$2D_{ab} = A_a^N A_b^N \sum_{t_1,t_2} e^{-m_0^N t_1} X(m_0^N, t_1, t_2) e^{-m_0^N (t-t_2)} \tag{7.3}$$

The sum over t_1, t_2 follows from the summation over time in the Feynman path integral. X denotes an unknown time evolution between t_1 and t_2 which is dependent on the particles mass.

We choose to model X by writing it as an expansion in quark loops (see Fig 7.2). By adding the bubble diagrams together we obtain:

$$\begin{aligned} 2D_{ab} = \quad & A_a^N A_b^N \left(\sum_{t_1} e^{-m_0^N t_1} x e^{-m_0^N (t-t_1)} \right. \\ & \left. + \sum_{t_1,t_2} e^{-m_0^N t_1} x e^{-m_0^N (t_2-t_1)} x e^{-m_0^N (t-t_2)} + ... \right) \end{aligned} \tag{7.4}$$

where now x represents the unknown factor joining two disconnected diagrams at given time and we assume that it is the same factor for each join (see Fig 7.2).

If we add to Eq 7.4 the contribution from the connected correlator we get

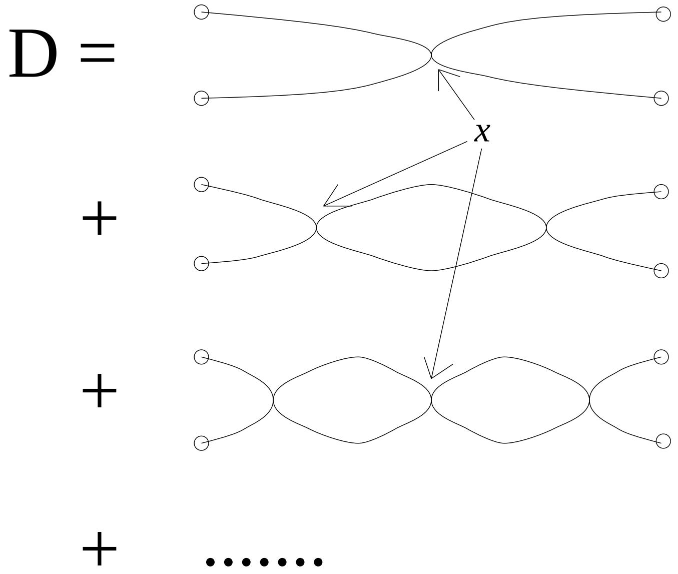

Figure 7.2: We choose to represent the "X" of Fig 7.1 as an expansion in bubble diagrams. The joins correspond to an unknown factor "x" which we assume to be the same for each join.

the full flavour singlet correlator:

$$\begin{aligned}\langle\text{SINGLET}\rangle_{ab} = \quad & A_a^N A_b^N \Bigg(e^{-m_0^N t} + \sum_{t_1} e^{-m_0^N t_1} x e^{-m_0^N (t-t_1)} \\ & + \sum_{t_1,t_2} e^{-m_0^N t_1} x e^{-m_0^N (t_2-t_1)} x e^{-m_0^N (t-t_2)} + ... \Bigg)\end{aligned} \tag{7.5}$$

By doing the sums over $t_1, t_2, ...$ we obtain:

$$\langle\text{SINGLET}\rangle_{ab} = A_a^N A_b^N e^{-m_0^N t} \left(1 + xt + x^2t^2/2 + ...\right) = A_a^N A_b^N e^{-(m_0^N - x)t} \tag{7.6}$$

Comparing with Eq 7.2 we get:

$$\langle\text{SINGLET}\rangle_{ab} = C_{ab} + 2D_{ab} = A_a^N A_b^N e^{-(m_0^N - x)t} = A_a^N A_b^N e^{-m_0^S t} \tag{7.7}$$

So we see that the factor x is the difference in mass between the singlet and nonsinglet. Further, the A coefficients are the same for the singlet and nonsinglet for our one exponential assumption.

From Eq's 7.1 and 7.7 we have:

$$\frac{\langle\text{SINGLET}\rangle_{ab}}{\langle\text{NONSINGLET}\rangle_{ab}} = 1 + \frac{2D_{ab}}{C_{ab}} = e^{(m_0^N - m_0^S)t} \approx 1 + \Delta m t \tag{7.8}$$

where:

$$\Delta m = m_0^N - m_0^S \tag{7.9}$$

So:

$$\frac{2D_{ab}}{C_{ab}} \approx \Delta m t \tag{7.10}$$

So the slope of $2D/C$ with t gives us Δm which in turn tells us whether the singlet meson is heavier or lighter than the nonsinglet meson. We get three attempts at calculating $2D/C$ since the indices ab run over LL,FL,FF.

As an aside to the one exponential case, we consider quenched QCD. Here there are no quark loops, so we retain only the first term in Eq 7.5. Eq 7.6 is then:

$$\langle\text{QUENCHED SINGLET}\rangle_{ab} = A_a^N A_b^N e^{-m_0^N t}(1 + xt) \tag{7.11}$$

This then gives us in the quenched approximation:

$$\frac{2D_{ab}}{C_{ab}} = xt = \Delta m t \tag{7.12}$$

We see that the approximation to the exponential in Eq 7.8 is the quenched approximation.

7.2.2 Two Exponentials (Quenched)

The above argument goes through provided that our one exponential assumption is valid. We now determine what changes are to be made if there is an excited state m_1. For now we restrict ourselves to the quenched case where we ignore the bubble diagrams in Fig 7.2.

The two exponential version of Eq 7.3 is:

$$\begin{aligned} 2D_{ab} = \quad & \sum_{t_1,t_2} \Big(A_a^N A_b^N e^{-m_0^N t_1} X e^{-m_0^N (t-t_2)} + B_a^N B_b^N e^{-m_1^N t_1} X'' e^{-m_1^N (t-t_2)} \\ & + B_a^N A_b^N e^{-m_1^N t_1} X' e^{-m_0^N (t-t_2)} + A_a^N B_b^N e^{-m_0^N t_1} X' e^{-m_1^N (t-t_2)} \Big) \end{aligned} \tag{7.13}$$

This is quite different from the one exponential version since not only does it have an excited state term, it also contains two cross terms. There are now three factors like X corresponding to different spacetime diagrams like Fig 7.1. We have X as before for connecting the two ground state mesons. We also have X'' for when the mesons in Fig 7.1 are excited state mesons. X' is for the cross terms when there is a ground state meson at $t = 0$ and an excited state at $t = 1$ and vice-versa. Corresponding to the x in Fig 7.2 we also introduce x' and x'' corresponding to X' and X'' respectively.

In a two exponential analysis, the equivalent of Eq 7.5 now has four times as many terms due to Eq 7.13. Let us look at the cross terms in the quenched case. These give us:

$$\sum_{t_1} B_a^N e^{-m_1^N t_1} x' e^{-m_0^N (t-t_1)} A_b^N + \sum_{t_1} A_a^N e^{-m_0^N t_1} x' e^{-m_1^N (t-t_1)} B_b^N \tag{7.14}$$

If $m_1 \gg m_0$, then in the sum over t_1, the first term is dominated by terms around $t_1 = 0$ and the second is dominated by terms around $t_1 = t$. We therefore approximate this by:

$$(B_a^N x' A_b^N + A_a^N x' B_b^N) e^{-m_0^N t} = A_a^N A_b^N (f_a + f_b) e^{-m_0^N t} \tag{7.15}$$

where we have defined $f_a = B_a x'/A_a$.

In quenched QCD we can write the two exponential version of Eq 7.11:

$$\begin{aligned} \langle \text{QUENCHED SINGLET} \rangle_{ab} &= A_a^N A_b^N \left(1 + xt + f_a + f_b\right) e^{-m_0^N t} + B_a^N B_b^N e^{-m_1^N t} \\ &= A_a^S A_b^S e^{-m_0^S t} + B_a^N B_b^N e^{-m_1^N t} \end{aligned} \tag{7.16}$$

Notice that now that the A coefficients are no longer the same for the singlet and nonsinglet. For the quenched approximation with an excited state, we have:

$$\frac{2D_{ab}}{C_{ab}} = xt + f_a + f_b \tag{7.17}$$

7.2.3 Two Exponentials (Unquenched)

In unquenched QCD we obtain more cross terms from higher order contributions. The ground state exponential becomes:

$$\begin{aligned} & A_a^N A_b^N e^{-m_0^S} \left(e^{-(m_0^N - x)} + f_a + f_b + f_a X t + X t f_b + f_a f_b + ...\right) \\ & = (1 + f_a)(1 + f_b) e^{-(m-x)} = A_a^S A_b^S e^{-m_0^S t} \end{aligned} \tag{7.18}$$

This gives us:

$$\frac{2D_{ab}}{C_{ab}} = (1+f_a)(1+f_b)e^{xt}-1 \approx (1+f_a)(1+f_b)\Delta mt+(1+f_a)(1+f_b)-1 \quad (7.19)$$

Or:

$$\frac{2D_{ab}}{C_{ab}} \approx K_{ab} - 1 + K_{ab}\Delta mt \quad (7.20)$$

where:

$$K_{ab} = \frac{A_a^S A_b^S}{A_a^N A_b^N} = (1+f_a)(1+f_b) \quad (7.21)$$

The assumption that $A^S = A^N$ and $B^S = B^N$ is equivalent to putting $K = 1$ in Eq 7.20. We have shown that that this is not necessarily a generally valid assumption to make. Looking ahead to the results, it is evident from Fig 7.3 that the $2D/C$ data for the pseudoscalar require $K_{ab} \neq 1$ because a straight line cannot be drawn through the data that also passes through the origin.

7.3 Procedure for determining $2D/C$

Of the five meson types defined in section 5.2, the pseudoscalar and scalar have already been studied in this context[60]. The scalar mesons present additional problems because of glueball mixing[59]. I shall not consider these here.

The data for the disconnected correlators is calculated[60] with $N_f = 2$ $\beta = 5.2$ and $C_{SW} = 1.76$ which is the same as for the connected correlators[53] used in chapter 6.

The values of D were calculated for three values of κ (0.1390, 0.1395, 0.1398). Unfortunately, when we calculate disconnected Greens functions on the lattice, their error remains essentially constant in time while the magnitude of the correlator decreases. This means that the signal decreases rapidly with increasing time. This was not so in the case of the connected Greens functions where the error tended to decrease with time, so there was still a signal even at large t. Nevertheless, some analysis of $2D/C$ could be carried out using low values of t.

Ignoring the details of the factorizing process described in section 6.3, fits from $t_1 = 3$ to $t_2 = 6$ were performed on the nonsinglet or connected data. This gave the parameters in the following equation:

$$C = A^N e^{-m_0^N t} + B^N e^{-m_1^N t} \tag{7.22}$$

To this equation we add the disconnected data to give the flavour singlet. Since the disconnected data is very noisy, it is found that only one exponential fits can be reliably performed. We fit to:

$$C + 2D = A^S e^{-m_0^S t} \tag{7.23}$$

for the t range $t_1 = 2$ to $t_2 = 6$.

Dividing the results of the two fits, we can obtain $2D/C$.

The FF,FL, and LL data should give differing amounts of excited states. Therefore, referring to Eq 7.20, we expect Δm to be the same for each, but the value of K might be different because this depends on the relative amounts of ground state for the singlet and nonsinglet. From the fit parameters in Eq's 7.22 and 7.23, we can determine Δm and K_{ab} as defined in Eq's 7.9

KAPPA	0.1390	0.1395	0.1395 (IMPROVED)	0.1398
PSEUDOSCALAR	-0.046^{24}_{35}	-0.057^{33}_{25}	-0.135^{48}_{47}	-0.122^{55}_{66}
VECTOR	-0.0051^{51}_{71}	-0.0037^{72}_{55}	-0.0051^{23}_{32}	-0.0037^{107}_{82}
VECTOR′	0.0070^{163}_{193}	0.0042^{215}_{168}	-0.0002^{75}_{56}	0.0035^{220}_{203}
AXIAL	0.0283^{389}_{344}	-0.0266^{444}_{322}	-0.0091^{239}_{274}	-0.0462^{349}_{264}
BAXIAL	0.0434^{602}_{690}	-0.0025^{645}_{682}	0.0039^{258}_{294}	0.0495^{524}_{451}

Table 7.1: Values of Δm in lattice units from fits to $2D/C$. The values of r_0/a are given in Table 6.4 ($r_0 = 0.49 fm$).

and 7.21 respectively. A bootstrap analysis returns the statistical errors. The results for Δm are given in Table 7.1.

Initialy the disconnected part was calculated using 24 source samples for each gauge configuration. This has proved sufficient to determine the disconnected part of the pion and scalar mesons to within their variance[60]. However, it was noted that in the case of the vector and to a lesser extent the axial and baxial, that the statistical errors were still bigger than the variance. We therefore recalculated the disconnected part in the $\kappa = 0.1395$ case with 96 samples. The others κ values were not redone due to constraints on computing time. The results of the fits to this data set are also in Table 7.1. It is seen that there is a notable improvement in the bootstrap errors.

The data for $2D/C$ is given in Figs 7.3 to 7.6 for the improved data at $\kappa = 0.1395$.

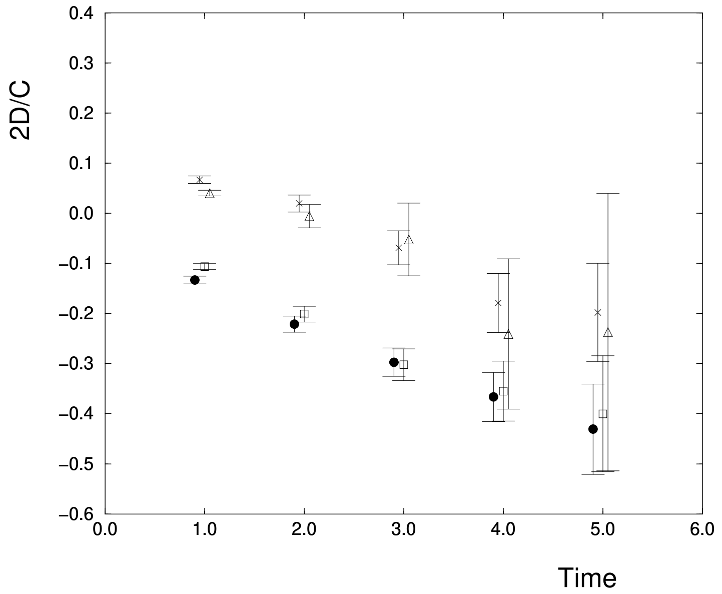

Figure 7.3: $2D/C$ data for pseudoscalar mesons as a function of time at $\kappa = 0.1395$. The points with $\Box$ are for the pseudoscalar with a LL correlator. The points with $\bullet$ are for the pseudoscalar with FF correlator. The points with $\triangle$ are for the pseudoscalar' with LL correlator, and those with $\times$ are for the pseudoscalar' with FF correlator.

7.4 Conclusions and Experimental Results

It is unfortunate that the fits in Table 7.1 have not yielded any definite conclusions about the sign of Δm except for the pseudoscalar. In the case of the vector, there is a two sigma signal with the improved data. When taken with the consistent negative bias for the other values of κ, it is suggestive that Δm is negative for the vector meson.

In spite of the lack of a definite sign for Δm, the data provide a limit on its size. Taking the values with the improved statistics at $\kappa = 0.1395$ the bounds are given in Table 7.2 where the results are converted into MeV using the values

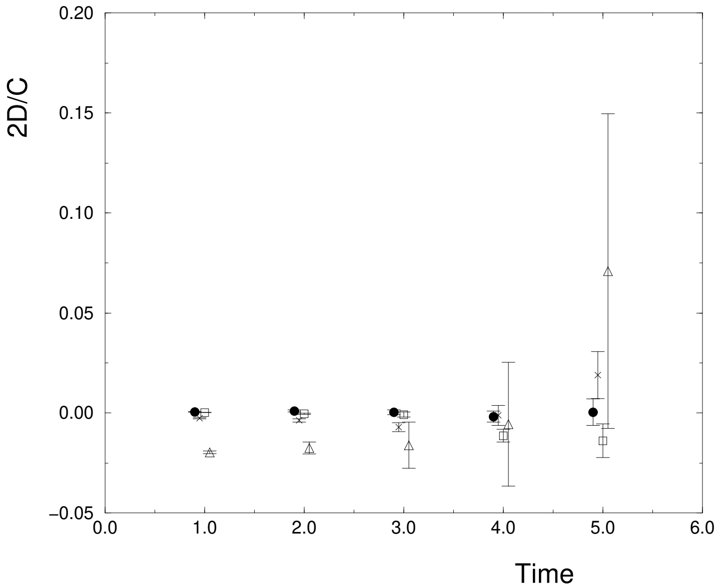

Figure 7.4: $2D/C$ data for pseudoscalar mesons as a function of time at $\kappa = 0.1395$. The points with $\square$ are for the vector with a LL correlator. The points with $\bullet$ are for the vector with FF correlator. The points with $\triangle$ are for the vector' with LL correlator, and those with $\times$ are for the vector' with FF correlator.

of r_0/a in Table 6.4. The bounds are determined by adding a two sigma error to the quantity.

Table 7.2 also gives a comparison with present experimental values given in [55]. The order of magnitude of Δm from experiment suggests that without a very significant improvement in accuracy, we may be able to determine the sign of Δm on the lattice.

There are a few points to be made about the comparison with experiment in Table 7.2.

- We have ignored the width of the measured states. Therefore, the errors

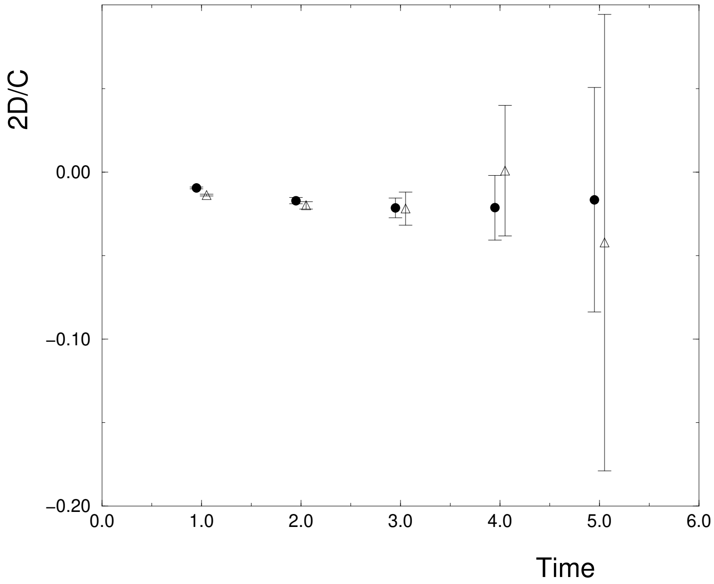

Figure 7.5: $2D/C$ data for axial mesons as a function of time at $\kappa = 0.1395$. The points with $\triangle$ are for the LL correlator. The points with $\bullet$ are for the FF correlator.

on the measurements are actually bigger than the quoted ones.

- For our lattice calculation we have assumed that there is no strange quark. We can compare this to the real world provided that we assume that the mixing with the strange quark is small. This is usually a valid assumption since the strange quark mass is significantly bigger than the up, down quark masses. However, in the case of the pion it is not valid to ignore strange quark mixing[61]. For the pseudoscalar, we cannot compare the singlet and nonsinglet masses directly with our two quark lattice simulation.

- Our lattice simulation with two quarks should be valid for determining

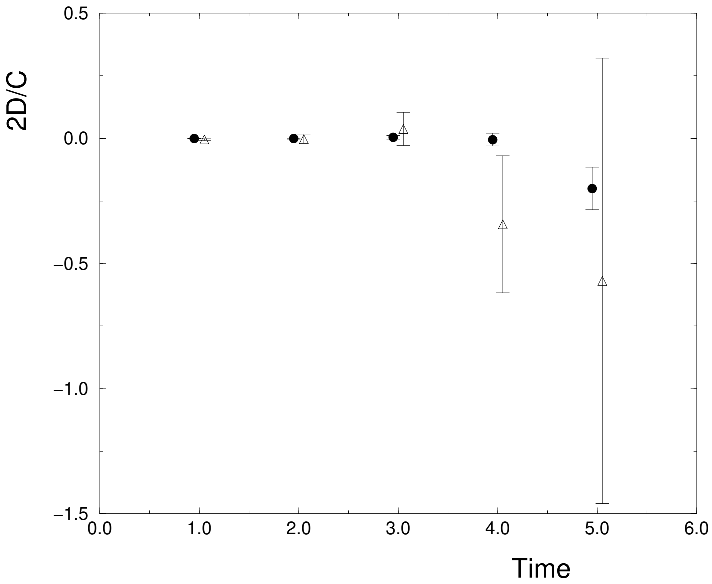

Figure 7.6: $2D/C$ data for baxial mesons as a function of time at $\kappa = 0.1395$. The points with $\triangle$ are for the LL correlator. The points with $\bullet$ are for the FF correlator.

the ground state mass of the vector rho, axial and baxial mesons since the amount of strange quark mixing is small. Further, there are no peculiar ground states as there are in the case of the scalar[59].

Meson	m_0^N	m_0^S	Δm Exp	Δm Theory
PSEUDOSCALAR	134.9766(6)	547.30(12)	-412	$-317 < \Delta m < -54$
VECTOR RHO	769.3(8)	782.57(12)	-13	$-17 < \Delta m - 1$
AXIAL	1230(40)	1281.9(6)	-52	$-89 < \Delta m < 54$
B AXIAL	1229.5(32)	1170(20)	60	$-76 < \Delta m < 77$

Table 7.2: Mass ordering of mesons from experiment (masses in MeV). Δm is determined from the experimental results to give an idea of its order of magnitude. A comparison is made with theoretical bounds determined from the lattice results in Table 7.1. The ranges for the theoretical Δm are given in MeV, obtained using the the values of r_0/a in Table 6.4.

Chapter 8

Lattice Determination of f_π

8.1 Introduction

In this chapter, we determine the pion decay constant f_π from meson correlators. To do this, we first review the theoretical basis for this number. We then discuss the fits performed to determine its value from the meson correlators. The meson correlators we use here are different from those used in the last two chapters. We outline details of the data used in section 8.6.

8.2 Noether's Theorem

Consider a Lagrangian which is dependent on the fields $\phi_i(x)$ and their derivatives $\partial_\mu \phi_i(x)$:

$$L = \int d^3x \mathcal{L}(\phi_i(x), \partial_\mu \phi_i(x)) \tag{8.1}$$

where $\mathcal{L}$ is the Lagrangian density.

Now consider a transformation of the fields under a group G:

$$\phi_i(x) \to \phi_i'(x) = \phi_i(x) + \delta\phi_i(x) \tag{8.2}$$

where

$$\delta\phi_i(x) = i\epsilon^a t^a_{ij}\phi_j(x) \tag{8.3}$$

Here the ϵ^a's are small and x independent and the t^a's are matrices satisfying the algebra:

$$[t^a, t^b] = iC^{abc}t^c \tag{8.4}$$

C^{abc} are the structure constants of the group G.

It is easily seen that under this transformation, the change in the Lagrangian density $\delta\mathcal{L}$ is given by:

$$\delta\mathcal{L} = \epsilon^a \delta_\mu \left[\frac{\delta\mathcal{L}}{\delta(\partial_\mu\phi_i)} it^a_{ij}\phi_j \right] \tag{8.5}$$

By definition, $\delta\mathcal{L}$ is zero if G is a symmetry of the Lagrangian. We can therefore use this to define a conserved current:

$$J^a_\mu = \frac{\delta\mathcal{L}}{\delta(\partial_\mu\phi_i)} it^a_{ij}\phi_j \tag{8.6}$$

with divergence:

$$\partial^\mu J^a_\mu = 0 \tag{8.7}$$

We can now define a charge which is independent of time:

$$Q^a = \int J^a_0(x) d^3x \tag{8.8}$$

Now suppose that we have a Lagrangian which has an approximate symmetry. This can be regarded as a small perturbation $\mathcal{L}_1$ on a Lagrangian $\mathcal{L}_0$

which has the exact symmetry. We write:

$$\mathcal{L} = \mathcal{L}_0 + \mathcal{L}_1 \tag{8.9}$$

where $\mathcal{L}_0$ is symmetric under a group G whereas $\mathcal{L}_1$ is not.

The current can still be defined as in Eq 8.6, but it is no longer conserved so Eq 8.7 is no longer valid. We can also define charges as in Eq 8.8, but they will no longer be time independent.

For a symmetry which is only slightly broken, we expect Eq 8.7 to be approximately true. We also expect the charges defined by Eq 8.8 to be approximately conserved. A situation like this arises in QCD which we shall now consider.

8.3 Chiral Symmetry

In QCD, the different flavours of quarks are identical except for differing masses. We therefore note that if the quark masses were the same, then QCD would have a $U(N)$ flavour symmetry where N is the number of quarks.

In reality, the masses of the three lightest quarks up(u) down(d) and strange(s) are very similar (approximately zero). In the case when $m_u = m_d = m_s$, we have an exact $U(3)$ symmetry. The fact that QCD almost has this flavour symmetry shows up in the hadron spectrum since the quantum numbers of the hadrons can be associated with the representations of $U(3)$. The only thing which prevents $U(3)$ from being a perfect symmetry of QCD and the hadron spectrum is the particles' masses.

The $U(3)$ symmetry group can be broken down into subgroups $U(1)$ and $SU(3)$:

$$U(3) = U(1) \otimes SU(3) \tag{8.10}$$

For reasons that we shall return to briefly in section 8.4, I shall refer only to the $SU(3)$ part of the symmetry.

To conclude, if we put $m_u = m_d = m_s$, QCD has an exact $SU(3)$ flavour symmetry:

$$q \to \exp(i\lambda^a \theta^a)q \tag{8.11}$$

where the λ^as are the Gell-Mann matrices. I shall call this $SU(3)_F$.

Now, in the case where $m_u = m_d = m_s = 0$, the QCD Lagrangian Eq 1.4 reduces to:

$$\mathcal{L} = i\bar{q}\gamma^\mu \partial_\mu q \tag{8.12}$$

where we have ignored the gluonic or gauge terms since they are not relevant to symmetries in the quark fields. Eq 8.12 is clearly invariant under a chiral transformation defined by:

$$q \to \gamma_5 q \tag{8.13}$$

Applying this to the symmetry Eq 8.11, We pick up another $SU(3)$ symmetry:

$$q \to \exp(i\gamma_5 \lambda^a \psi^a)q \tag{8.14}$$

I denote this by $SU(3)_C$.

The Lagrangian Eq 8.12 is therefore symmetric under $SU(3)_F \times SU(3)_C$.

We note that since the three lightest quark masses are close to zero, the real QCD Lagrangian almost has this symmetry.

To a better approximation $m_u = m_d = 0$ which gives us an even closer symmetry of the QCD Lagrangian: $U(2)_F \times U(2)_C$. We already considered the $U(2)_F$ symmetry in section 5.7.

8.4 Spontaneous Symmetry Breaking

We have noted that the hadronic spectrum has an $SU(3)$ symmetry. We might also expect to see the $SU(3)_F \times SU(3)_C$ symmetry. This is not seen. The picture we now have of this comes from spontaneous symmetry breaking.

Spontaneous symmetry breaking occurs when the ground state of the system does not have the symmetry that the Lagrangian has. We suppose that while the QCD Lagrangian has the $SU(3)_C$ symmetry, the vacuum has not, so to attain the lowest energy state, the symmetry must be broken. If I_C^a are the generators of the group $SU(3)_C$, then:

$$I_C^a|0\rangle \neq 0 \tag{8.15}$$

We suppose that $SU(3)_F$ is not spontaneously broken by the vacuum, so if I_F are its generators, then:

$$I_F^a|0\rangle = 0 \tag{8.16}$$

Goldstone's theorem tells us that the spontaneously broken $SU(3)_C$ symmetry will give rise to eight massless Goldstone bosons with the quantum numbers of the states $I_C|0\rangle$, i.e. spin zero, negative parity and $I = 1$. In fact the eight lightest bound states ($\pi^+, \pi^0, \pi^-, K^+, K^0, \bar{K}^0, K^-, \eta$) have the necessary quantum numbers. The only problem with this picture is that they are not massless states as is required by Goldstone's theorem. However, $SU(3)_C$ was only an approximate symmetry of QCD, so the fact that the Goldstone bosons are light, but not massless should be regarded as reflecting the fact that in real QCD, $m_u = m_d = m_s \neq 0$.

The picture that seems to have emerged is to regard the eight lightest ground states as the Goldstone bosons of the broken approximate $SU(3)$ chiral symmetry of QCD. We must assume from Goldstone's theorem that in the massless limit of QCD where $SU(3)_C$ becomes exact, the eight ground states would be genuine massless Goldstone bosons.

At the beginning of this section, we chose to ignore the fact that the Lagrangian Eq 8.12 actually has the symmetry $U(3)_F \otimes U(3)_C$. When the chiral part of this symmetry is broken, we would expect nine light Goldstone bosons. We should have the eight that we had before from $SU(3)_C$ and also a light degenerate flavour singlet from the broken $U(1)_C$ symmetry. Unfortunately this particle is not observed in the hadronic spectrum.

This problem was solved when it was realised the flavour singlet of $U(3)$ has special interactions with the vacuum. It has the same quantum numbers as the vacuum, which leads to it being much heavier than the other eight particles[62]. So while the underlying symmetry is $U(3)$, we only observe the $SU(3)$ part in the light hadronic spectrum.

8.5 Partially Conserved Axial Current(PCAC)

We now use Eq 8.6 and the Lagrangian Eq 8.12 to derive the following conserved currents:

- For the $SU(3)_F$ symmetry we define the "vector" current:

$$V_\mu^a(x) = \bar{q}(x)\gamma_\mu\lambda^a q(x) \tag{8.17}$$

- For the $SU(3)_C$ symmetry we define the "axial vector" current:

$$A_\mu^a(x) = \bar{q}(x)\gamma_\mu\gamma_5\lambda^a q(x) \tag{8.18}$$

Since the axial current is not annihilated by the vacuum (Eq 8.15), we can consider the probability of a pion coupling to the vacuum via the axial current:

$$\langle\pi^b(p)|A_\mu^a(0)|0\rangle = if^{ab}p_\mu \tag{8.19}$$

where p is the pion momentum.

The R.H.S of Eq 8.19 comes from the need to factor out the colour symmetry and to have matching Lorentz symmetry. As the L.H.S. is a bosonic quantity, we cannot have any non-summed Dirac matrices, so the Lorentz index must come from a ∂_μ (or p_μ), and the only momentum is the pion momentum. Also, f^{ab} may have some momentum dependence, but to first approximation and at low momenta we treat it as a constant.

Taking the divergence of Eq 8.19 gives:

$$\langle \pi^b(p)|\partial^\mu A^a_\mu(0)|0\rangle = f^{ab}m_\pi^2 \tag{8.20}$$

Provided that we use the normalisation:

$$\langle 0|\phi^a(0)|\pi^b(p)\rangle = \delta^{ab} \tag{8.21}$$

where ϕ is the pion field operator, then we can put $f^{ab} = f_\pi \delta^{ab}$ where f_π is the pion decay constant. When the pion is at rest, we have $p_\mu = (m_\pi, 0, 0, 0)$. So, ignoring the colour factor, we have:

$$\langle \pi|m_\pi A_0(0)|0\rangle = f_\pi m_\pi^2 \tag{8.22}$$

and

$$A_0 = \bar{\psi}\gamma_0\gamma_5\psi \tag{8.23}$$

so:

$$f_\pi m_\pi = \langle \pi|\bar{\psi}\gamma_0\gamma_5\psi|0\rangle \tag{8.24}$$

8.6 Determining f_π from a Lattice Calculation

When we calculate the decay constant of the pion on the lattice, we need to take care of normalisation factors.

In particular, if we fit to the correlator in Eq 8.24, we introduce a complete set of pion states $|\pi_i\rangle$. If we destroy the pion at time t with the local operator

$\bar{\psi}\gamma_5\psi$, we have (to two exponentials):

$$C_{AP} = \sum_{i=0}^{\infty} \frac{1}{2m_\pi^i} \langle \bar{\psi}\gamma_5\psi|\pi_i\rangle e^{-m_\pi^i t} \langle \pi_i|\bar{\psi}\gamma_4\gamma_5\psi|0\rangle = c_P c_A e^{-m_\pi^0 t} + d_P d_A e^{-m_\pi^1 t} \quad (8.25)$$

where the factor $\frac{1}{2m_\pi}$ comes from the need to normalise the intermediate set of pion states. We have made the change $\gamma_0 \to \gamma_4$ to indicate that we are now considering Euclidean space on the lattice.

Now consider the local pion-pion correlator (to two exponentials) with the pions at rest:

$$C_{PP} = \sum_{i=0}^{\infty} \frac{1}{2m_\pi^i} \langle \bar{\psi}\gamma_5\psi|\pi_i\rangle e^{-m_\pi^i t} \langle \pi_i|\bar{\psi}\gamma_5\psi\rangle = c_P^2 e^{-m_\pi^0 t} + d_P^2 e^{-m_\pi^1 t} \quad (8.26)$$

c_P^2 and $c_A c_P$ can therefore be determined directly from fits to the pion-pion and axial-pion correlators respectively. m_π is determined by the same factorizing fits that determine the values of c_A and c_P.

Taking the one exponential part of Eq 8.25 at $t = 0$ and using Eq 8.24 we have:

$$c_P c_A = \frac{Z_P f_\pi m_\pi}{2m_\pi} \quad (8.27)$$

where

$$Z_P = \langle \bar{\psi}\gamma_5\psi|\pi_i\rangle \quad (8.28)$$

Using Eq 8.26 we have:

$$c_P^2 = \frac{Z_P^2}{2m_\pi} \quad (8.29)$$

so:

$$c_A = \frac{f_\pi m_\pi}{\sqrt{2m_\pi}} \quad (8.30)$$

So by performing fits to Eq's 8.25 and 8.26 we can obtain f_π from Eq 8.30.

8.7 Details of the Lattice Simulation

The correlators discussed in the last section were evaluated[63] for a 208 configurations using a clover improved Wilson action (see section 1.4). Unlike the dynamical configurations discussed in section 5.8, we have full $\mathcal{O}(a)$ improvement with $C_{SW} = 2.02$[54]. As before, we have $\beta = 5.2$. We only consider the data with the lightest sea quark mass: $\kappa_{sea} = 0.1355$.

We also use correlators from a quenched simulation for comparison. In quenched QCD, the fermionic determinant is set equal to a constant (see section 1.5). The quenched data[63] was calculated using a clover improved Wilson action for 524 configurations with $\beta = 5.93$, $C_{SW} = 1.82$.

8.8 Fit Results and Conclusions

Fits were performed both on the dynamical fermion data set and also on the quenched data set. Both sets of fits were two exponential fits between $t_1 = 4$ and $t_2 = 15$. For the dynamical fermion sets, the excited state mass was fixed at $1.15a$ where a is the lattice spacing.

The results for the dynamical fermion fits are given in Table 8.1. The results of the quenched fits are in Table 8.2.

The values of f_π are plotted against m_π^2 with error bars on f_π in Fig 8.1.

The values plotted in Fig 8.1 are in MeV, obtained from the values of a given in the captions to Tables 8.1 and 8.2. The values of a are taken from [63].

A chiral extrapolation to $m_{pi}^2 = 0$ gives $f_\pi = 201$MeV for the quenched data and $f_\pi = 190$MeV for the dynamical data. These extrapolations are indicated in Fig 8.1.

The extrapolations given here should not be compared directly with the experimental determination $f_\pi = 137.7(5)$[55] because we have not accounted for the perturbative matching of the lattice clover improved action to the continuum in the chiral limit[64, 65]. Further, we have not made an extrapolation down to zero lattice spacing ($a = 0$) because we only had data from one lattice.

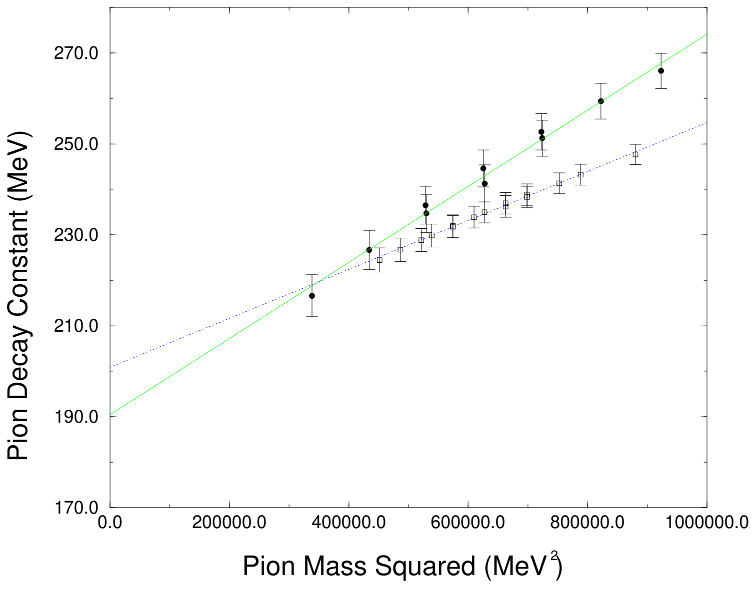

Figure 8.1: f_π plotted against m_π^2. The the Quenched data set correspond to points with a $\square$. The dynamical data correspond to points with a $\bullet$. A chiral extrapolation is made down to $m_\pi^2 = 0$ in both cases.

$\kappa 1$	$\kappa 2$	$m_\pi a$	$m_\pi a c_p / c_a$	$f_\pi a$
0.1355	0.1355	0.2869^{41}_{41}	1.772^{46}_{54}	0.1068^{23}_{25}
0.1350	0.1355	0.3249^{35}_{35}	1.762^{39}_{45}	0.1118^{23}_{23}
0.1345	0.1355	0.3591^{30}_{32}	1.759^{34}_{35}	0.1158^{24}_{21}
0.1340	0.1355	0.3908^{27}_{28}	1.760^{32}_{28}	0.1190^{25}_{21}
0.1350	0.1350	0.3585^{25}_{30}	1.754^{30}_{33}	0.1166^{25}_{20}
0.1345	0.1350	0.3900^{22}_{26}	1.754^{26}_{27}	0.1206^{23}_{21}
0.1340	0.1350	0.4196^{23}_{24}	1.758^{24}_{25}	0.1239^{22}_{21}
0.1345	0.1345	0.4192^{21}_{24}	1.755^{23}_{25}	0.1246^{22}_{22}
0.1340	0.1345	0.4473^{18}_{23}	1.760^{21}_{24}	0.1279^{21}_{23}
0.1340	0.1340	0.4739^{18}_{19}	1.765^{20}_{23}	0.1312^{20}_{22}

Table 8.1: Fit results for the pion mass and the decay constant f_π on the dynamical fermion gauges at $\kappa^{sea} = 0.1355$ and $\beta = 5.2$. The results are given in lattice units ($a = 0.0973(8)$fm).

$\kappa 1$	$\kappa 2$	$m_\pi a$	$m_\pi a c_p/c_a$	$f_\pi a$
0.1327	0.1327	0.4945^{17}_{16}	1.672^{12}_{13}	0.1306^{12}_{14}
0.1327	0.1332	0.4681^{18}_{16}	1.664^{13}_{13}	0.1282^{12}_{15}
0.1327	0.1334	0.4572^{18}_{17}	1.661^{13}_{13}	0.1272^{12}_{15}
0.1327	0.1337	0.4406^{19}_{17}	1.659^{13}_{14}	0.1256^{12}_{15}
0.1327	0.1339	0.4292^{19}_{19}	1.658^{14}_{14}	0.1245^{12}_{15}
0.1332	0.1332	0.4406^{19}_{17}	1.657^{13}_{14}	0.1259^{12}_{14}
0.1332	0.1334	0.4292^{20}_{17}	1.655^{13}_{15}	0.1249^{13}_{14}
0.1332	0.1337	0.4116^{20}_{19}	1.653^{14}_{15}	0.1233^{13}_{15}
0.1332	0.1339	0.3995^{19}_{20}	1.652^{15}_{15}	0.1222^{13}_{14}
0.1334	0.1334	0.4175^{20}_{19}	1.653^{14}_{15}	0.1239^{13}_{14}
0.1334	0.1337	0.3995^{21}_{20}	1.651^{15}_{15}	0.1223^{13}_{14}
0.1334	0.1339	0.3870^{21}_{20}	1.651^{15}_{17}	0.1211^{13}_{14}
0.1337	0.1337	0.3807^{20}_{20}	1.650^{16}_{17}	0.1206^{13}_{14}
0.1337	0.1339	0.3676^{19}_{22}	1.651^{16}_{17}	0.1195^{13}_{14}
0.1339	0.1339	0.3541^{23}_{21}	1.652^{17}_{18}	0.1183^{14}_{14}

Table 8.2: Fit results for the pion mass and the pion decay constant f_π on quenched gauges at $\beta = 5.93$. The results are given in lattice units ($a = 0.1040(3)$fm).

Chapter 9

Summary of Conclusions

9.1 The QCD Coupling

In chapter 4 the objective was to determine a correction term of the form c/p^2 to the perturbative running coupling. After an unsuccessful attempt to fit to the individual lattice data, we formed an aggregated data set on a 24^4 lattice comprising data from lattices with different values of β. By fitting to this data set, we found that the data did want a correction term of the type postulated, and with $c = 0.63^{3}_{13}\text{GeV}^2$. The value of $\Lambda_{\bar{ms}}$ determined from the fit was 0.237^{3}_{13}GeV (with other errors which were not quantified in the work). We concluded that there is a large power correction to the running coupling when calculated in the $\widetilde{MOM}$ scheme.

Since we lack any theoretical matching procedure to other schemes, we cannot claim that the power correction is a universal property of the running coupling. Its existence and magnitude should be determined independently in any scheme in which it is needed.

9.2 Meson Masses

In chapter 6 we attempted to determine a mass ordering of the axial(a_1), baxial(b_1) and scalar(a_0) mesons from a dynamical fermion lattice simulation. No statistically significant mass ordering was determined. We noted that in the case of the axial and baxial mesons, a chiral extrapolation would be consistent with the experimental determination.

In chapter 7 we tried to find a mass ordering of the singlet and nonsinglet mesons for the pseudoscalar, vector rho, axial and baxial mesons. The results were inconclusive except in the case of the pseudoscalar. For the other particles, bounds were determined on the mass differences. We noted that with a relatively small increase in statistics, the question of meson mass ordering could probably be answered on the lattice.

In chapter 8 we made a lattice determination of the pion decay constant f_π. This was done for both a quenched and an unquenched simulation. The statistics were good, but the chiral limit could not be trusted because we had not accounted for the perturbative matching of the clover improved lattice gauge theory to continuum QCD.

Appendix

Hermitian Representation of the Local Γ matrices

$$\begin{pmatrix} 0 & 0 & 1 & 0 \\ 0 & 0 & 0 & 1 \\ 1 & 0 & 0 & 0 \\ 0 & 1 & 0 & 0 \end{pmatrix} \quad \begin{pmatrix} 0 & 0 & 0 & i \\ 0 & 0 & i & 0 \\ 0 & -i & 0 & 0 \\ -i & 0 & 0 & 0 \end{pmatrix} \quad \begin{pmatrix} 0 & 0 & 0 & 1 \\ 0 & 0 & -1 & 0 \\ 0 & -1 & 0 & 0 \\ 1 & 0 & 0 & 0 \end{pmatrix} \quad \begin{pmatrix} 0 & 0 & i & 0 \\ 0 & 0 & 0 & -i \\ -i & 0 & 0 & 0 \\ 0 & i & 0 & 0 \end{pmatrix}$$

$$\begin{pmatrix} 0 & 0 & -i & 0 \\ 0 & 0 & 0 & -i \\ i & 0 & 0 & 0 \\ 0 & i & 0 & 0 \end{pmatrix} \quad \begin{pmatrix} 0 & 0 & 0 & 1 \\ 0 & 0 & 1 & 0 \\ 0 & 1 & 0 & 0 \\ 1 & 0 & 0 & 0 \end{pmatrix} \quad \begin{pmatrix} 0 & 0 & 0 & -i \\ 0 & 0 & i & 0 \\ 0 & -i & 0 & 0 \\ i & 0 & 0 & 0 \end{pmatrix} \quad \begin{pmatrix} 0 & 0 & 1 & 0 \\ 0 & 0 & 0 & -1 \\ 1 & 0 & 0 & 0 \\ 0 & -1 & 0 & 0 \end{pmatrix}$$

$$\begin{pmatrix} 1 & 0 & 0 & 0 \\ 0 & 1 & 0 & 0 \\ 0 & 0 & 1 & 0 \\ 0 & 0 & 0 & 1 \end{pmatrix} \quad \begin{pmatrix} 0 & -1 & 0 & 0 \\ -1 & 0 & 0 & 0 \\ 0 & 0 & 0 & 1 \\ 0 & 0 & 1 & 0 \end{pmatrix} \quad \begin{pmatrix} 0 & i & 0 & 0 \\ -i & 0 & 0 & 0 \\ 0 & 0 & 0 & -i \\ 0 & 0 & i & 0 \end{pmatrix} \quad \begin{pmatrix} -1 & 0 & 0 & 0 \\ 0 & 1 & 0 & 0 \\ 0 & 0 & 1 & 0 \\ 0 & 0 & 0 & -1 \end{pmatrix}$$

$$\begin{pmatrix} 1 & 0 & 0 & 0 \\ 0 & 1 & 0 & 0 \\ 0 & 0 & -1 & 0 \\ 0 & 0 & 0 & -1 \end{pmatrix} \quad \begin{pmatrix} 0 & 1 & 0 & 0 \\ 1 & 0 & 0 & 0 \\ 0 & 0 & 0 & 1 \\ 0 & 0 & 1 & 0 \end{pmatrix} \quad \begin{pmatrix} 0 & -i & 0 & 0 \\ i & 0 & 0 & 0 \\ 0 & 0 & 0 & -i \\ 0 & 0 & i & 0 \end{pmatrix} \quad \begin{pmatrix} 1 & 0 & 0 & 0 \\ 0 & -1 & 0 & 0 \\ 0 & 0 & 1 & 0 \\ 0 & 0 & 0 & -1 \end{pmatrix}$$

Bibliography

[1] D. Espriu. hep-ph/9410287.

[2] D. B. Lichtenberg and S. P. Rosen,*eds.Developments in the Quark Theory of Hadrons* Nonantum: Hadronic Press, (1980).

[3] D. Balin and A. Love. *Introduction to Gauge Field Theory* J W Arrowsmith Ltd, (1996).

[4] K. G. Wilson. Phys. Rev. D 14 (1974) 2455.

[5] R. Gupta. hep-lat/9807028.

[6] B. Sheikholesalami and R. Wohlert. Nucl. Phys. B 259 (1985) 572.

[7] D. G. Richards. hep-lat/0006020.

[8] R. P. Feynman and A. R. Hibbs. *Quantum Mechanics and Path Integrals*, New York: McGraw-Hill (1965).

[9] M. Di Pierro. hep-lat/0009001.

[10] I. Montvay and G. Münster. *Quantum Fields on a Lattice* Cambridge University Press, (1994).

[11] D. Toussaint. *From Actions to Answers*, World Scientific, (1990).

[12] M. Creutz. *Quarks. Gluons and Lattices*, Cambridge University Press, (1983).

[13] M. Luscher. hep-lat/9802029.

[14] D. J. Gross and F. Wilczek. Phys. Rev. D8 (1973) 3497.

[15] D. R. T. Jones. Nucl. Phys. B 75 (1974) 531.

[16] J. S. Ball and T. Chiu. Phys. Rev. D 22 (1980) 2550.

[17] S. K. Kim and M. Baker. Nucl. Phys. B 164 (1980) 152.

[18] C. Parrinello. Phys. Rev. D 50 (1994) 4247.

[19] B. All*é*s *et al.* Nucl. Phys B 502 (1997) 325.

[20] P. Boucaud *et al.* J. High Energy Phys. 12 (1998) 004.

[21] P. Boucaud *et al.* J. High Energy Phys. 10 (1998) 017.

[22] A. Hasenfratz and P. Hasenfratz. Phys. Lett. B 93 (1980) 165.

[23] W. Celmaster and R. J. Gonsalves. Phys. Rev. D 20 (1979) 1420.

[24] D. Becirevic *et al.*hep-lat/9809129.

[25] G. S. Bali and K. Schilling. Phys. Rev. D 47 (1993) 661.

[26] P. Boucaud *et al.* JHEP 0004 (2000) 006

[27] A. I. Davydychev, P. Osland and O. V. Tarasov. Phys. Rev. D 54 (1996) 4087.

[28] A. I. Davydychev, P. Osland and O. V. Tarasov. Phys. Rev. D 58 (1998) 036007.

[29] S. Capitani *et al.*Nucl. Phys. B 544 (1999) 669.

[30] R. Akhoury and V. I. Zakharov. Phys. Lett. B 438 (1998) 165.

[31] G. S. Bali. Phys. Lett. B 460 (1999) 170.

[32] C. Michael. Nucl. Phys. Proc. Suppl. 42 (1995) 147.

[33] K. G. Wilson. Phys. Rev. 179 (1969) 1499.

[34] M. A. Shifman, A. I. Vainshtein and V. I. Zakharov. Nucl. Phys. B147 (1979) 385.

[35] G. Burgio *et al.*Phys. Lett. B422 (1998) 219.

[36] M. Beneke. Phys. Rept. 317 (1999) 1.

[37] F. DiRenzo. hep-lat/0009020.

[38] G. Grunberg. hep-ph/9705290.

[39] V. A. Novikov *et al.*Nucl. Phys. B249 (1985) 445.

[40] D. V. Shirkov and I. L. Solovstov. Phys. Rev. Lett 79 (1997) 1209.

[41] R. Akhoury and V. I. Zakharov. hep-ph/9705318.

[42] M. Beneke, V. M. Braun and N. Kivel. Phys. Lett. B 443 (1998) 308.

[43] Y. L. Dokshitzer. hep-ph/9812252.

[44] S. Bethke. J. Phys. G26 (2000) R27.

[45] Y. V. Novozhilov. *Introduction to Elementary Particle Theory* Pergamon Press, (1975).

[46] P. Lacock *et al.*Phys. Rev. D 54 (1996) 6997.

[47] F. E. Close. *An Introduction to Quarks and Partons* Academic Press, (1979).

[48] P. Lacock *et al.*Phys. Rev. D 51 (1995) 6403.

[49] C. T. H. Davies. hep-ph/9710394.

[50] J. M. Flynn, C. T. Sachrajda. hep-ph/9710057.

[51] C. McNeile, C. Michael. hep-lat/0006020.

[52] C. T. Sachrajda. Nucl. Phys. Proc. Suppl 83 (2000) 93.

[53] C. R. Allton *et al.*Phys. Rev. D 60 (1999) 034507.

[54] K. Jansen, R. Sommer. Nucl Phys. B530 (1998) 185.

[55] The European Physical Journal. C Vol 15 (2000) 1.

[56] C. Michael, A. McKerrel. Phys. Rev. D 51 (1995) 3745.

[57] C. Chatfield. *Statistics for Technology* J. W. Arrowsmith, (1983).

[58] Y. Kuramashi *et al.*Phys. Rev. Lett. 72 (1994) 3348.

[59] C. McNeile, C. Michael. hep-lat/0010019.

[60] C. Michael, M.S. Foster, C. McNeile. Nucl.Phys. Proc. Suppl 73 (1999) 198.

[61] C. McNeile, C. Michael. hep-lat/0006020.

[62] G. 'tHooft. Phys. Rev. D14 (1976) 3432.

[63] A. C. Irving. hep-lat/0010012

[64] S. Sint, P. Weisz. Nucl. Phys. Proc. Suppl. 63 (1998) 856.

[65] S. Sint, P. Weisz, Nucl. Phys. B502 (1997) 251.